- -

First measurement of the ratio of branching fractions
$B(\Lambda_b^0 \to \Lambda_c^+ \mu^- \nu_\mu)/B(\Lambda_b^0 \to \Lambda_c^+ \pi^-)$

- -

Collaborators: Clark, Allan Geoffrey; Garcia Navarro, Jose Enrique; Vallecorsa, Sofia; Wu, Xin

First measurement of the ratio of branching fractions $\mathcal{B}(\Lambda_b^0 \to \Lambda_c^+ \mu^- \bar{\nu}_\mu)/\mathcal{B}(\Lambda_b^0 \to \Lambda_c^+ \pi^-)$

T. Aaltonen,[24] J. Adelman,[14] T. Akimoto,[56] M. G. Albrow,[18] B. Álvarez González,[12] S. Amerio,[44b,44a] D. Amidei,[35] A. Anastassov,[39] A. Annovi,[20] J. Antos,[15] G. Apollinari,[18] A. Apresyan,[49] T. Arisawa,[58] A. Artikov,[16] W. Ashmanskas,[18] A. Attal,[4] A. Aurisano,[54] F. Azfar,[43] P. Azzurri,[47d,47a] W. Badgett,[18] A. Barbaro-Galtieri,[29] V. E. Barnes,[49] B. A. Barnett,[26] V. Bartsch,[31] G. Bauer,[33] P.-H. Beauchemin,[34] F. Bedeschi,[47a] D. Beecher,[31] S. Behari,[26] G. Bellettini,[47b,47a] J. Bellinger,[60] D. Benjamin,[17] A. Beretvas,[18] J. Beringer,[29] A. Bhatti,[51] M. Binkley,[18] D. Bisello,[44b,44a] I. Bizjak,[31,w] R. E. Blair,[2] C. Blocker,[7] B. Blumenfeld,[26] A. Bocci,[17] A. Bodek,[50] V. Boisvert,[50] G. Bolla,[49] D. Bortoletto,[49] J. Boudreau,[48] A. Boveia,[11] B. Brau,[11,b] A. Bridgeman,[25] L. Brigliadori,[44a] C. Bromberg,[36] E. Brubaker,[14] J. Budagov,[16] H. S. Budd,[50] S. Budd,[25] S. Burke,[18] K. Burkett,[18] G. Busetto,[44b,44a] P. Bussey,[22,l] A. Buzatu,[34] K. L. Byrum,[2] S. Cabrera,[17,v] C. Calancha,[32] M. Campanelli,[36] M. Campbell,[35] F. Canelli,[18] A. Canepa,[46] B. Carls,[25] D. Carlsmith,[60] R. Carosi,[47a] S. Carrillo,[19,n] S. Carron,[34] B. Casal,[12] M. Casarsa,[18] A. Castro,[6b,6a] P. Catastini,[47c,47a] D. Cauz,[55b,55a] V. Cavaliere,[47c,47a] M. Cavalli-Sforza,[4] A. Cerri,[29] L. Cerrito,[31,o] S. H. Chang,[28] Y. C. Chen,[1] M. Chertok,[8] G. Chiarelli,[47a] G. Chlachidze,[18] F. Chlebana,[18] K. Cho,[28] D. Chokheli,[16] J. P. Chou,[23] G. Choudalakis,[33] S. H. Chuang,[53] K. Chung,[13] W. H. Chung,[60] Y. S. Chung,[50] T. Chwalek,[27] C. I. Ciobanu,[45] M. A. Ciocci,[47c,47a] A. Clark,[21] D. Clark,[7] G. Compostella,[44a] M. E. Convery,[18] J. Conway,[8] M. Cordelli,[20] G. Cortiana,[44b,44a] C. A. Cox,[8] D. J. Cox,[8] F. Crescioli,[47b,47a] C. Cuenca Almenar,[8,v] J. Cuevas,[12,s] R. Culbertson,[18] J. C. Cully,[35] D. Dagenhart,[18] M. Datta,[18] T. Davies,[22] P. de Barbaro,[50] S. De Cecco,[52a] A. Deisher,[29] G. De Lorenzo,[4] M. Dell'Orso,[47b,47a] C. Deluca,[4] L. Demortier,[51] J. Deng,[17] M. Deninno,[6a] P. F. Derwent,[18] G. P. di Giovanni,[45] C. Dionisi,[52b,52a] B. Di Ruzza,[55b,55a] J. R. Dittmann,[5] M. D'Onofrio,[4] S. Donati,[47b,47a] P. Dong,[9] J. Donini,[44a] T. Dorigo,[44a] S. Dube,[53] J. Efron,[40] A. Elagin,[54] R. Erbacher,[8] D. Errede,[25] S. Errede,[25] R. Eusebi,[18] H. C. Fang,[29] S. Farrington,[43] W. T. Fedorko,[14] R. G. Feild,[61] M. Feindt,[27] J. P. Fernandez,[32] C. Ferrazza,[47d,47a] R. Field,[19] G. Flanagan,[49] R. Forrest,[8] M. J. Frank,[5] M. Franklin,[23] J. C. Freeman,[18] I. Furic,[19] M. Gallinaro,[52a] J. Galyardt,[13] F. Garberson,[11] J. E. Garcia,[21] A. F. Garfinkel,[49] K. Genser,[18] H. Gerberich,[25] D. Gerdes,[35] A. Gessler,[27] S. Giagu,[52b,52a] V. Giakoumopoulou,[3] P. Giannetti,[47a] K. Gibson,[48] J. L. Gimmell,[50] C. M. Ginsburg,[18] N. Giokaris,[3] M. Giordani,[55b,55a] P. Giromini,[20] M. Giunta,[47b,47a] G. Giurgiu,[26] V. Glagolev,[16] D. Glenzinski,[18] M. Gold,[38] N. Goldschmidt,[19] A. Golossanov,[18] G. Gomez,[12] G. Gomez-Ceballos,[33] M. Goncharov,[54] O. González,[32] I. Gorelov,[38] A. T. Goshaw,[17] K. Goulianos,[51] A. Gresele,[44b,44a] S. Grinstein,[23] C. Grosso-Pilcher,[14] R. C. Group,[18] U. Grundler,[25] J. Guimaraes da Costa,[23] Z. Gunay-Unalan,[36] C. Haber,[29] K. Hahn,[33] S. R. Hahn,[18] E. Halkiadakis,[53] B.-Y. Han,[50] J. Y. Han,[50] F. Happacher,[20] K. Hara,[56] D. Hare,[53] M. Hare,[57] S. Harper,[43] R. F. Harr,[59] R. M. Harris,[18] M. Hartz,[48] K. Hatakeyama,[51] C. Hays,[43] M. Heck,[27] A. Heijboer,[46] J. Heinrich,[46] C. Henderson,[33] M. Herndon,[60] J. Heuser,[27] S. Hewamanage,[5] D. Hidas,[17] C. S. Hill,[11,d] D. Hirschbuehl,[27] A. Hocker,[18] S. Hou,[1] M. Houlden,[30] S.-C. Hsu,[29] B. T. Huffman,[43] R. E. Hughes,[40] U. Husemann,[36] M. Hussein,[36] U. Husemann,[61] J. Huston,[36] J. Incandela,[11] G. Introzzi,[47a] M. Iori,[52b,52a] A. Ivanov,[8] E. James,[18] B. Jayatilaka,[17] E. J. Jeon,[28] M. K. Jha,[6a] S. Jindariani,[18] W. Johnson,[8] M. Jones,[49] K. K. Joo,[28] S. Y. Jun,[13] J. E. Jung,[28] T. R. Junk,[18] T. Kamon,[54] D. Kar,[19] P. E. Karchin,[59] Y. Kato,[42] R. Kephart,[18] J. Keung,[46] V. Khotilovich,[54] B. Kilminster,[18] D. H. Kim,[28] H. S. Kim,[28] H. W. Kim,[28] J. E. Kim,[28] M. J. Kim,[20] S. B. Kim,[28] S. H. Kim,[56] Y. K. Kim,[14] N. Kimura,[56] L. Kirsch,[7] S. Klimenko,[19] B. Knuteson,[33] B. R. Ko,[17] K. Kondo,[58] D. J. Kong,[28] J. Konigsberg,[19] A. Korytov,[19] A. V. Kotwal,[17] M. Kreps,[27] J. Kroll,[46] D. Krop,[14] N. Krumnack,[5] M. Kruse,[17] V. Krutelyov,[11] T. Kubo,[56] T. Kuhr,[27] N. P. Kulkarni,[59] M. Kurata,[56] Y. Kusakabe,[58] S. Kwang,[14] A. T. Laasanen,[49] S. Lami,[47a] S. Lammel,[18] M. Lancaster,[31] R. L. Lander,[8] K. Lannon,[40,r] A. Lath,[53] G. Latino,[47c,47a] I. Lazzizzera,[44b,44a] T. LeCompte,[2] E. Lee,[54,u] H. S. Lee,[14] S. W. Lee,[54,t] S. Leone,[47a] J. D. Lewis,[18] C.-S. Lin,[29] J. Linacre,[43] M. Lindgren,[18] E. Lipeles,[46] A. Lister,[8] D. O. Litvintsev,[18] C. Liu,[48] T. Liu,[18] N. S. Lockyer,[46] A. Loginov,[61] M. Loreti,[44b,44a] L. Lovas,[15] D. Lucchesi,[44b,44a] C. Luci,[52b,52a] J. Lueck,[27] P. Lujan,[29] P. Lukens,[18] G. Lungu,[51] L. Lyons,[43] J. Lys,[29] R. Lysak,[15] D. MacQueen,[34] R. Madrak,[18] K. Maeshima,[18] K. Makhoul,[33] T. Maki,[24] P. Maksimovic,[26] S. Malde,[43] S. Malik,[31] G. Manca,[30,f] A. Manousakis-Katsikakis,[3] F. Margaroli,[49] C. Marino,[27] C. P. Marino,[25] A. Martin,[61] V. Martin,[22,m] M. Martínez,[4] R. Martínez-Ballarín,[32] T. Maruyama,[56] P. Mastrandrea,[52a] T. Masubuchi,[56] M. Mathis,[26] M. E. Mattson,[59] P. Mazzanti,[6a] K. S. McFarland,[50] P. McIntyre,[54] R. McNulty,[30,k] A. Mehta,[30] P. Mehtala,[24] A. Menzione,[47a] P. Merkel,[49] C. Mesropian,[51] T. Miao,[18] N. Miladinovic,[7] R. Miller,[36] C. Mills,[23] M. Milnik,[27] A. Mitra,[1] G. Mitselmakher,[19] H. Miyake,[56] N. Moggi,[6a] C. S. Moon,[28] R. Moore,[18] M. J. Morello,[47b,47a] J. Morlok,[27] P. Movilla Fernandez,[18] J. Mülmenstädt,[29] A. Mukherjee,[18] Th. Muller,[27] R. Mumford,[26] P. Murat,[18] M. Mussini,[6b,6a] J. Nachtman,[18] Y. Nagai,[56] A. Nagano,[56] J. Naganoma,[56] K. Nakamura,[56] I. Nakano,[41] A. Napier,[57] V. Necula,[17] J. Nett,[60] C. Neu,[46,w] M. S. Neubauer,[25] S. Neubauer,[27] J. Nielsen,[29,h] L. Nodulman,[2] M. Norman,[10] O. Norniella,[25] E. Nurse,[31]

L. Oakes,[43] S. H. Oh,[17] Y. D. Oh,[28] I. Oksuzian,[19] T. Okusawa,[42] R. Orava,[24] S. Pagan Griso,[44b,44a] E. Palencia,[18] V. Papadimitriou,[18] A. Papaikonomou,[27] A. A. Paramonov,[14] B. Parks,[40] S. Pashapour,[34] J. Patrick,[18] G. Pauletta,[55b,55a] M. Paulini,[13] C. Paus,[33] T. Peiffer,[27] D. E. Pellett,[8] A. Penzo,[55a] T. J. Phillips,[17] G. Piacentino,[47a] E. Pianori,[46] L. Pinera,[19] K. Pitts,[25] C. Plager,[9] L. Pondrom,[60] O. Poukhov,[16,a] N. Pounder,[43] F. Prakoshyn,[16] A. Pronko,[18] J. Proudfoot,[2] F. Ptohos,[18,j] E. Pueschel,[13] G. Punzi,[47b,47a] J. Pursley,[60] J. Rademacker,[43,d] A. Rahaman,[48] V. Ramakrishnan,[60] N. Ranjan,[49] I. Redondo,[32] P. Renton,[43] M. Renz,[27] M. Rescigno,[52a] S. Richter,[27] F. Rimondi,[6b,6a] L. Ristori,[47a] A. Robson,[22] T. Rodrigo,[12] T. Rodriguez,[46] E. Rogers,[25] S. Rolli,[57] R. Roser,[18] M. Rossi,[55a] R. Rossin,[11] P. Roy,[34] A. Ruiz,[12] J. Russ,[13] V. Rusu,[18] A. Safonov,[54] W. K. Sakumoto,[50] O. Saltó,[4] L. Santi,[55b,55a] S. Sarkar,[52b,52a] L. Sartori,[47a] K. Sato,[18] A. Savoy-Navarro,[45] P. Schlabach,[18] A. Schmidt,[27] E. E. Schmidt,[18] M. A. Schmidt,[14] M. P. Schmidt,[61,a] M. Schmitt,[39] T. Schwarz,[8] L. Scodellaro,[12] A. Scribano,[47c,47a] F. Scuri,[47a] A. Sedov,[49] S. Seidel,[38] Y. Seiya,[42] A. Semenov,[16] L. Sexton-Kennedy,[18] F. Sforza,[47a] A. Sfyrla,[25] S. Z. Shalhout,[59] T. Shears,[30] P. F. Shepard,[48] M. Shimojima,[56,q] S. Shiraishi,[14] M. Shochet,[14] Y. Shon,[60] I. Shreyber,[37] A. Sidoti,[47a] P. Sinervo,[34] A. Sisakyan,[16] A. J. Slaughter,[18] J. Slaunwhite,[40] K. Sliwa,[57] J. R. Smith,[8] F. D. Snider,[18] R. Snihur,[34] A. Soha,[8] S. Somalwar,[53] V. Sorin,[36] J. Spalding,[18] T. Spreitzer,[34] P. Squillacioti,[47c,47a] M. Stanitzki,[61] R. St. Denis,[22] B. Stelzer,[34] O. Stelzer-Chilton,[34] D. Stentz,[39] J. Strologas,[38] G. L. Strycker,[35] D. Stuart,[11] J. S. Suh,[28] A. Sukhanov,[19] I. Suslov,[16] T. Suzuki,[56] A. Taffard,[25,g] R. Takashima,[41] Y. Takeuchi,[56] R. Tanaka,[41] M. Tecchio,[35] P. K. Teng,[1] K. Terashi,[51] R. J. Tesarek,[18] J. Thom,[18,i] A. S. Thompson,[22] G. A. Thompson,[25] E. Thomson,[46] P. Tipton,[61] P. Ttito-Guzmán,[32] S. Tkaczyk,[18] D. Toback,[54] S. Tokar,[15] K. Tollefson,[36] T. Tomura,[56] D. Tonelli,[18] S. Torre,[20] D. Torretta,[18] P. Totaro,[55b,55a] S. Tourneur,[45] M. Trovato,[47a] S.-Y. Tsai,[1] Y. Tu,[46] N. Turini,[47c,47a] F. Ukegawa,[56] S. Vallecorsa,[21] N. van Remortel,[24,c] A. Varganov,[35] E. Vataga,[47d,47a] F. Vázquez,[19,n] G. Velev,[18] C. Vellidis,[3] V. Veszpremi,[49] M. Vidal,[32] R. Vidal,[18] I. Vila,[12] R. Vilar,[12] T. Vine,[31] M. Vogel,[38] I. Volobouev,[29,t] G. Volpi,[47b,47a] P. Wagner,[46] R. G. Wagner,[2] R. L. Wagner,[18] W. Wagner,[27] J. Wagner-Kuhr,[27] T. Wakisaka,[42] R. Wallny,[9] S. M. Wang,[1] A. Warburton,[34] D. Waters,[31] M. Weinberger,[54] J. Weinelt,[27] W. C. Wester III,[18] B. Whitehouse,[57] D. Whiteson,[46,g] A. B. Wicklund,[2] E. Wicklund,[18] S. Wilbur,[14] G. Williams,[34] H. H. Williams,[46] P. Wilson,[18] B. L. Winer,[40] P. Wittich,[18,i] S. Wolbers,[18] C. Wolfe,[14] T. Wright,[35] X. Wu,[21] F. Würthwein,[10] S. M. Wynne,[30] S. Xie,[33] A. Yagil,[10] K. Yamamoto,[42] J. Yamaoka,[53] U. K. Yang,[14,p] Y. C. Yang,[28] W. M. Yao,[29] G. P. Yeh,[18] J. Yoh,[18] K. Yorita,[14] T. Yoshida,[42] G. B. Yu,[50] I. Yu,[28] S. S. Yu,[18] J. C. Yun,[18] L. Zanello,[52b,52a] A. Zanetti,[55a] X. Zhang,[25] Y. Zheng,[9,e] and S. Zucchelli[6b,6a]

(CDF Collaboration)

[1]*Institute of Physics, Academia Sinica, Taipei, Taiwan 11529, Republic of China*

[2]*Argonne National Laboratory, Argonne, Illinois 60439, USA*

[3]*University of Athens, 157 71 Athens, Greece*

[4]*Institut de Fisica d'Altes Energies, Universitat Autonoma de Barcelona, E-08193, Bellaterra (Barcelona), Spain*

[5]*Baylor University, Waco, Texas 76798 USA*

[6a]*Istituto Nazionale di Fisica Nucleare Bologna, I-40127 Bologna, Italy*

[6b]*University of Bologna, I-40127 Bologna, Italy*

[7]*Brandeis University, Waltham, Massachusetts 02254, USA*

[8]*University of California, Davis, Davis, California 95616, USA*

[9]*University of California, Los Angeles, Los Angeles, California 90024, USA*

[10]*University of California, San Diego, La Jolla, California 92093, USA*

[11]*University of California, Santa Barbara, Santa Barbara, California 93106, USA*

[12]*Instituto de Fisica de Cantabria, CSIC-University of Cantabria, 39005 Santander, Spain*

[13]*Carnegie Mellon University, Pittsburgh, Pennsylvania 15213, USA*

[14]*Enrico Fermi Institute, University of Chicago, Chicago, Illinois 60637, USA*

[15]*Comenius University, 842 48 Bratislava, Slovakia, Institute of Experimental Physics, 040 01 Kosice, Slovakia*

[16]*Joint Institute for Nuclear Research, RU-141980 Dubna, Russia*

[17]*Duke University, Durham, North Carolina 27708, USA*

[18]*Fermi National Accelerator Laboratory, Batavia, Illinois 60510, USA*

[19]*University of Florida, Gainesville, Florida 32611, USA*

[20]*Laboratori Nazionali di Frascati, Istituto Nazionale di Fisica Nucleare, I-00044 Frascati, Italy*

[21]*University of Geneva, CH-1211 Geneva 4, Switzerland*

[22]*Glasgow University, Glasgow G12 8QQ, United Kingdom*

[23]*Harvard University, Cambridge, Massachusetts 02138, USA*

[24]Division of High Energy Physics, Department of Physics, University of Helsinki and Helsinki Institute of Physics, FIN-00014, Helsinki, Finland

[25]University of Illinois, Urbana, Illinois 61801, USA

[26]The Johns Hopkins University, Baltimore, Maryland 21218, USA

[27]Institut für Experimentelle Kernphysik, Universität Karlsruhe, 76128 Karlsruhe, Germany

[28]Center for High Energy Physics: Kyungpook National University, Daegu 702-701, Korea,
Seoul National University, Seoul 151-742, Korea,
Sungkyunkwan University, Suwon 440-746, Korea,
Korea Institute of Science and Technology Information, Daejeon, 305-806, Korea,
Chonnam National University, Gwangju, 500-757, Korea

[29]Ernest Orlando Lawrence Berkeley National Laboratory, Berkeley, California 94720, USA

[30]University of Liverpool, Liverpool L69 7ZE, United Kingdom

[31]University College London, London WC1E 6BT, United Kingdom

[32]Centro de Investigaciones Energeticas Medioambientales y Tecnologicas, E-28040 Madrid, Spain

[33]Massachusetts Institute of Technology, Cambridge, Massachusetts 02139, USA

[34]Institute of Particle Physics: McGill University, Montréal, Québec, Canada H3A 2T8,
Simon Fraser University, Burnaby, British Columbia, Canada V5A 1S6,
University of Toronto, Toronto, Ontario, Canada M5S 1A7,
TRIUMF, Vancouver, British Columbia, Canada V6T 2A3

[35]University of Michigan, Ann Arbor, Michigan 48109, USA

[36]Michigan State University, East Lansing, Michigan 48824, USA

[37]Institution for Theoretical and Experimental Physics, ITEP, Moscow 117259, Russia

[38]University of New Mexico, Albuquerque, New Mexico 87131, USA

[39]Northwestern University, Evanston, Illinois 60208, USA

[40]The Ohio State University, Columbus, Ohio 43210, USA

[41]Okayama University, Okayama 700-8530, Japan

[42]Osaka City University, Osaka 588, Japan

[43]University of Oxford, Oxford OX1 3RH, United Kingdom

[44a]Istituto Nazionale di Fisica Nucleare, Sezione di Padova-Trento, I-35131 Padova, Italy

[44b]University of Padova, I-35131 Padova, Italy

[45]LPNHE, Universite Pierre et Marie Curie/IN_2P_3-CNRS, UMR7585, Paris, F-75252 France

[46]University of Pennsylvania, Philadelphia, Pennsylvania 19104, USA

[47a]Istituto Nazionale di Fisica Nucleare Pisa, I-56127 Pisa, Italy

[47b]University of Pisa, I-56127 Pisa, Italy

[a]Deceased.

[b]Visitor from the University of Massachusetts Amherst, Amherst, MA 01003, USA.

[c]Visitor from the Universiteit Antwerpen, B-2610 Antwerp, Belgium.

[d]Visitor from the University of Bristol, Bristol BS8 1TL, United Kingdom.

[e]Visitor from the Chinese Academy of Sciences, Beijing 100864, China.

[f]Visitor from the Istituto Nazionale di Fisica Nucleare, Sezione di Cagliari, 09042 Monserrato (Cagliari), Italy.

[g]Visitor from the University of California Irvine, Irvine, CA 92697, USA.

[h]Visitor from the University of California Santa Cruz, Santa Cruz, CA 95064, USA.

[i]Visitor from Cornell University, Ithaca, NY 14853, USA.

[j]Visitor from the University of Cyprus, Nicosia CY-1678, Cyprus.

[k]Visitor from the University College Dublin, Dublin 4, Ireland.

[l]Visitor from the Royal Society of Edinburgh, Edinburgh EH2 2PQ, United Kingdom.

[m]Visitor the from University of Edinburgh, Edinburgh EH9 3JZ, United Kingdom.

[n]Visitor from the Universidad Iberoamericana, Mexico D.F., Mexico

[o]Visitor from Queen Mary, University of London, London, E1 4NS, England.

[p]Visitor from the University of Manchester, Manchester M13 9PL, England

[q]Visitor from Nagasaki Institute of Applied Science, Nagasaki, Japan.

[r]Visitor from the University of Notre Dame, Notre Dame, IN 46556, USA.

[s]Visitor from the University de Oviedo, E-33007 Oviedo, Spain.

[t]Visitor from Texas Tech University, Lubbock, TX 79409, USA.

[u]Visitor from IFIC (CSIC-Universitat de Valencia), 46071 Valencia, Spain.

[v]Visitor from the University of Virginia, Charlottesville, VA 22904, USA.

[w]On leave from J. Stefan Institute, Ljubljana, Slovenia.

^{47c}*University of Siena, I-56127 Pisa, Italy*
^{47d}*Scuola Normale Superiore, I-56127 Pisa, Italy*
^{48}*University of Pittsburgh, Pittsburgh, Pennsylvania 15260, USA*
^{49}*Purdue University, West Lafayette, Indiana 47907 USA*
^{50}*University of Rochester, Rochester, New York 14627, USA*
^{51}*The Rockefeller University, New York, New York 10021, USA*
^{52a}*Istituto Nazionale di Fisica Nucleare, Sezione di Roma 1, I-00185 Roma, Italy*
^{52b}*Sapienza Università di Roma, I-00185 Roma, Italy*
^{53}*Rutgers University, Piscataway, New Jersey 08855, USA*
^{54}*Texas A&M University, College Station, Texas 77843, USA*
^{55a}*Istituto Nazionale di Fisica Nucleare Trieste/Udine, I-34100, Trieste, Italy*
^{55b}*University of Trieste/Udine, I-33100, Udine, Italy*
^{56}*University of Tsukuba, Tsukuba, Ibaraki 305, Japan*
^{57}*Tufts University, Medford, Massachusetts 02155 USA*
^{58}*Waseda University, Tokyo 169, Japan*
^{59}*Wayne State University, Detroit, Michigan 48201, USA*
^{60}*University of Wisconsin, Madison, Wisconsin 53706, USA*
^{61}*Yale University, New Haven, Connecticut 06520, USA*

This article presents the first measurement of the ratio of branching fractions $\mathcal{B}(\Lambda_b^0 \to \Lambda_c^+ \mu^- \bar{\nu}_\mu)/\mathcal{B}(\Lambda_b^0 \to \Lambda_c^+ \pi^-)$. Measurements in two control samples using the same technique $\mathcal{B}(\bar{B}^0 \to D^+ \mu^- \bar{\nu}_\mu)/\mathcal{B}(\bar{B}^0 \to D^+ \pi^-)$ and $\mathcal{B}(\bar{B}^0 \to D^*(2010)^+ \mu^- \bar{\nu}_\mu)/\mathcal{B}(\bar{B}^0 \to D^*(2010)^+ \pi^-)$ are also reported. The analysis uses data from an integrated luminosity of approximately 172 pb^{-1} of $p\bar{p}$ collisions at $\sqrt{s} = 1.96$ TeV, collected with the CDF II detector at the Fermilab Tevatron. The relative branching fractions are measured to be $\frac{\mathcal{B}(\Lambda_b^0 \to \Lambda_c^+ \mu^- \bar{\nu}_\mu)}{\mathcal{B}(\Lambda_b^0 \to \Lambda_c^+ \pi^-)} = 16.6 \pm 3.0(\text{stat}) \pm 1.0(\text{syst})^{+2.6}_{-3.4}(\text{PDG}) \pm 0.3(\text{EBR})$, $\frac{\mathcal{B}(\bar{B}^0 \to D^+ \mu^- \bar{\nu}_\mu)}{\mathcal{B}(\bar{B}^0 \to D^+ \pi^-)} = 9.9 \pm 1.0(\text{stat}) \pm 0.6(\text{syst}) \pm 0.4(\text{PDG}) \pm 0.5(\text{EBR})$, and $\frac{\mathcal{B}(\bar{B}^0 \to D^*(2010)^+ \mu^- \bar{\nu}_\mu)}{\mathcal{B}(\bar{B}^0 \to D^*(2010)^+ \pi^-)} = 16.5 \pm 2.3(\text{stat}) \pm 0.6(\text{syst}) \pm 0.5(\text{PDG}) \pm 0.8(\text{EBR})$. The uncertainties are from statistics (stat), internal systematics (syst), world averages of measurements published by the Particle Data Group or subsidiary measurements in this analysis (PDG), and unmeasured branching fractions estimated from theory (EBR), respectively. This article also presents measurements of the branching fractions of four new Λ_b^0 semileptonic decays: $\Lambda_b^0 \to \Lambda_c(2595)^+ \mu^- \bar{\nu}_\mu$, $\Lambda_b^0 \to \Lambda_c(2625)^+ \mu^- \bar{\nu}_\mu$, $\Lambda_b^0 \to \Sigma_c(2455)^0 \pi^+ \mu^- \bar{\nu}_\mu$, and $\Lambda_b^0 \to \Sigma_c(2455)^{++} \pi^- \mu^- \bar{\nu}_\mu$, relative to the branching fraction of the $\Lambda_b^0 \to \Lambda_c^+ \mu^- \bar{\nu}_\mu$ decay. Finally, the transverse-momentum distribution of Λ_b^0 baryons produced in $p\bar{p}$ collisions is measured and found to be significantly different from that of $\bar{B}^0$ mesons, which results in a modification in the production cross-section ratio $\sigma_{\Lambda_b^0}/\sigma_{\bar{B}^0}$ with respect to the CDF I measurement.

I. INTRODUCTION

Amplitudes for the weak decays of b hadrons are described by the product of Cabibbo-Kobayashi-Maskawa (CKM) matrix elements [1,2] and dynamical factors. The CKM matrix elements represent the coupling strength of the weak decays and are fundamental parameters of the standard model of particle physics. In order to extract values of the CKM elements, knowledge of the dynamical factors is needed either from experiment or theory. Calculation of the dynamical factors, in the case of b-hadron decays, is aided by heavy quark effective theory (HQET) [3–5]. HQET is an approximation relying on the large mass of the b quark ($m_b \approx 4000$ MeV/c^2), as compared with the quantum chromodynamics energy scale ($\Lambda_{\text{QCD}} \approx 200$ MeV), to imply a spin-independent interaction between the b quark and the light degrees of freedom. In baryon spectroscopy, the light degrees of freedom are in a relative spin-0 state for all Λ-type baryons; there is no

spin-related interaction between the b quark and the light degrees of freedom. Therefore, the subleading order corrections to the heavy quark limit are simpler than those mesons which contain a b quark (b mesons) [6]. Measurements of Λ_b^0-baryon branching fractions may be compared with predictions by HQET and test the calculation of dynamical factors to subleading order. However, in contrast to the b mesons, little is known about the Λ_b^0 baryon. At the time of writing this article, only five decay modes of the Λ_b^0 have been observed, with large uncertainties on their branching fraction measurements [7]. On the theoretical side, combining measurements of the CKM matrix element $|V_{cb}|$ and the world average of the Λ_b^0 lifetime [7,8], the branching fraction predicted by HQET for $\Lambda_b^0 \to \Lambda_c^+ \mu^- \bar{\nu}_\mu$ is 7.6% by Huang *et al.* [9], and that for $\Lambda_b^0 \to \Lambda_c^+ \pi^-$ is 0.54% by Leibovich *et al.* [10]. An independent prediction of $\mathcal{B}(\Lambda_b^0 \to \Lambda_c^+ \pi^-)$ by Cheng using the nonrelativistic quark model yields 0.50% [11].
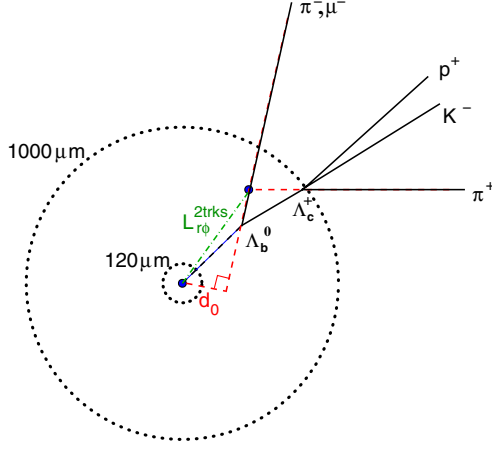
FIG. 1 (color online). An r-ϕ view of a $\Lambda_b^0 \to \Lambda_c^+ \pi^- (\Lambda_b^0 \to \Lambda_c^+ \mu^- \bar{\nu}_\mu)$ decay with a two-prong Λ_b^0 decay vertex and a three-prong Λ_c^+ decay vertex. In this case, the d_0 of each pion (the pion and the muon) and the $L_{r\phi}^{2\mathrm{trks}}$ of the two-pion vertex (pion-muon vertex) satisfy the trigger requirements.

Presented here is the first measurement of the ratio of the Λ_b^0 branching fractions, $\mathcal{B}(\Lambda_b^0 \to \Lambda_c^+ \mu^- \bar{\nu}_\mu)/\mathcal{B}(\Lambda_b^0 \to \Lambda_c^+ \pi^-)$. This measurement is based on data from an integrated luminosity of approximately 172 pb^{-1} of $p\bar{p}$ collisions at $\sqrt{s} = 1.96$ TeV, collected with the CDF II detector at Fermilab. Taking advantage of the relatively long lifetime of b hadrons ($c\tau \approx 400~\mu$m), all b-hadron decays described in this article are reconstructed from data satisfying an online event selection (trigger) which requires two charged tracks forming a vertex displaced from the location of $p\bar{p}$ collisions (two-track trigger). The Λ_c^+ is reconstructed using the three-body decay $\Lambda_c^+ \to pK^-\pi^+$, therefore both the $\Lambda_b^0 \to \Lambda_c^+ \pi^-$ and $\Lambda_b^0 \to \Lambda_c^+ \mu^- \bar{\nu}_\mu$ decays result in four charged particles, which are observable in the detector and have a similar topology (Fig. 1). Since both decays have a similar topology and satisfy the same trigger, most systematic uncertainties from the detector, trigger, and reconstruction efficiencies cancel in the measurement of the ratio of branching fractions. Throughout this article, the inclusion of charge conjugate decays is implied.

The ratio of the branching fraction of the Λ_b^0 exclusive semileptonic decay relative to that of the Λ_b^0 hadronic decay $\mathcal{B}_{\mathrm{exclsemi}}/\mathcal{B}_{\mathrm{had}}$ is extracted from the ratio of signal yields ($N_{\mathrm{exclsemi}}/N_{\mathrm{had}}$) divided by the ratio of acceptance times efficiency ($\epsilon_{\mathrm{exclsemi}}/\epsilon_{\mathrm{had}}$)

$$
\begin{aligned}
\frac{\mathcal{B}(\Lambda_b^0 \to \Lambda_c^+ \mu^- \bar{\nu}_\mu)}{\mathcal{B}(\Lambda_b^0 \to \Lambda_c^+ \pi^-)} &\equiv \frac{\mathcal{B}_{\mathrm{exclsemi}}}{\mathcal{B}_{\mathrm{had}}} \\
&= \left(\frac{N_{\mathrm{exclsemi}}}{N_{\mathrm{had}}}\right) \bigg/ \left(\frac{\epsilon_{\mathrm{exclsemi}}}{\epsilon_{\mathrm{had}}}\right) \\
&= \left(\frac{N_{\mathrm{inclsemi}} - N_{\mathrm{semibg}}}{N_{\mathrm{had}}}\right) \frac{\epsilon_{\mathrm{had}}}{\epsilon_{\mathrm{exclsemi}}}.
\end{aligned}
\tag{1}
$$

The analysis procedure can be summarized in four steps: First, the hadronic ($\Lambda_c^+ \pi^-$) and inclusive semileptonic ($\Lambda_c^+ \mu^- X$) candidates are reconstructed. Second, the yields N_{had} and N_{inclsemi} are determined by fitting the mass distributions. Third, the contribution of backgrounds that produce a $\Lambda_c^+ \mu^-$ in the final state is either measured or estimated and combined into N_{semibg}. The estimate of N_{semibg} requires a modification of the production cross-section ratio, $\sigma_{\Lambda_b^0}/\sigma_{\bar{B}^0}$, with respect to the CDF I measurement [12]. The dominant backgrounds that contribute to N_{semibg}, $\Lambda_b^0 \to \Lambda_c(2595)^+ \mu^- \bar{\nu}_\mu$, $\Lambda_b^0 \to \Lambda_c(2625)^+ \mu^- \bar{\nu}_\mu$, $\Lambda_b^0 \to \Sigma_c(2455)^0 \pi^+ \mu^- \bar{\nu}_\mu$, and $\Lambda_b^0 \to \Sigma_c(2455)^{++} \pi^- \mu^- \bar{\nu}_\mu$ have also been reconstructed in the data for the first time. Measurements of their branching fractions relative to the branching fraction of the $\Lambda_b^0 \to \Lambda_c^+ \mu^- \bar{\nu}_\mu$ decay will be used in the estimate of N_{semibg}. Fourth, the ratio of the products of detector acceptance and reconstruction efficiency, $\epsilon_{\mathrm{had}}/\epsilon_{\mathrm{exclsemi}}$, is estimated from simulation.

The analysis method described above is tested by performing the same measurements in $\bar{B}^0$ decays, which have a similar event topology. Specifically, the following ratios of branching fractions are measured: $\mathcal{B}(\bar{B}^0 \to D^+ \mu^- \bar{\nu}_\mu)/\mathcal{B}(\bar{B}^0 \to D^+ \pi^-)$ where $D^+ \to K^- \pi^+ \pi^+$, and $\mathcal{B}(\bar{B}^0 \to D^*(2010)^+ \mu^- \bar{\nu}_\mu)/\mathcal{B}(\bar{B}^0 \to D^*(2010)^+ \pi^-)$ where $D^*(2010)^+ \to D^0 \pi^+$, $D^0 \to K^- \pi^+$. The results of the $\bar{B}^0$ measurements are compared with previous results from the B factories [7] to check the techniques used in this analysis.

This article is structured as follows: Section II describes the relevant parts of the CDF II detector and trigger. Section III details the event selections for the $\Lambda_c^+ \pi^-$ and $\Lambda_c^+ \mu^- X$ samples. Section IV describes the simulations used in this analysis. Section V gives an account of the determination of the yields N_{had} and N_{inclsemi}. In Sec. VI, N_{semibg} is estimated. Section VII includes measurements and estimates of the branching fractions of other Λ_b^0 semileptonic decays, which may contribute to N_{semibg}, and an estimate of $\mathcal{B}(\Lambda_b^0 \to \Lambda_c^+ \pi^-)$ derived from a modification of the CDF I measurement of $\sigma_{\Lambda_b^0}/\sigma_{\bar{B}^0}$. Section VIII summarizes the systematic uncertainties. Section IX shows the measurements with the $\bar{B}^0$ control samples using the same analysis technique. Section X compares the results of the Λ_b^0 and $\bar{B}^0$ relative branching fractions with the predictions from HQET and the world averages, respectively. Finally, Sec. XI gives the conclusion. Unless stated otherwise, branching fractions, fragmentation fractions, and lifetimes are obtained from the Particle Data Group world averages [7]. The symbols "H_c" and "H_b" are used to generically denote hadrons containing charm and bottom quarks, "c hadrons" and "b hadrons," respectively. The symbol "MC," which stands for "Monte Carlo", is used to generically denote simulation.

II. THE CDF II DETECTOR AND TRIGGER

The CDF II detector is a cylindrically symmetric apparatus described in detail elsewhere [13]. Only the parts of the detector relevant for this analysis are summarized here. The crucial features of the detector for this measurement are the tracking and muon systems. The tracking system, which enables reconstruction of the trajectories of charged particles, is contained in a superconducting solenoid, which generates a 1.4 tesla magnetic field in the $-z$ direction [14]. The 96-cm long silicon vertex detector (SVX II) [15] consists of six equal subsections in z and five concentric layers of double-sided silicon sensors from $r = 2.45$ cm to $r = 10.60$ cm. The 310-cm long central outer tracker (COT) [16], an open-cell wire drift chamber, consists of 96 sense wire layers from $r = 40$ cm to $r = 137$ cm which are grouped into alternating axial and $\pm 2°$ stereo superlayers. The SVX II and COT provide both $r - \phi$ and z position measurements in the pseudorapidity region of $|\eta| < 2$ and $|\eta| < 1$ [17], respectively. The 452-cm long central muon detector (CMU) [18], a set of drift chambers mounted outside of the central hadron calorimeter at $r = 347$ cm, contains four sense wire layers, which allow the formation of short track segments (stubs) and identify the muon candidates in the region of $|\eta| < 0.6$.

The data for this analysis are collected with a three-level, two-track trigger that selects events with a displaced vertex. Consequently, data satisfying this trigger are rich in heavy flavor with a low background from the combination of random tracks (combinatorial background). A schematic diagram of the event topology and trigger requirements is shown in Fig. 1. The strategy of the two-track trigger is as follows: at the first trigger level, the extremely fast tracker (XFT) [19] finds two oppositely charged tracks reconstructed in the COT, with a minimum transverse-momentum (p_T) of 2.04 GeV/c for each track. The scalar sum of the p_T from the two tracks is required to exceed 5.5 GeV/c, and the azimuthal angle between the two tracks ($\Delta\phi$) to be less than 135°. At the second trigger level, the silicon vertex trigger (SVT) [20] attaches hits measured with SVX II to the tracks found by XFT. The SVT reapplies the p_T requirements made at level 1 and further requires that each track has a transverse impact parameter (d_0), measured at the point of closest approach with respect to the beam line [21], in the range 120 μm–1000 μm. In addition, $\Delta\phi$ between the two trigger tracks is required to be in the range 2°–90°. The intersection of the two tracks forms a displaced vertex. Finally, the quantity $L_{r\phi}^{2\text{trks}}$ defined as the projection of the vector from the primary vertex to the displaced vertex onto the vector of the total momentum of the two tracks in the $r - \phi$ plane, must be larger than 200 μm. The level 1 and 2 triggers are implemented in hardware, while at the third level, a cluster of computers uses all detector information to perform a full reconstruction of the event [22]. In addition to reinforcing the same requirements as applied at level 2, level 3 requires the difference in z between the two tracks at the point of closest approach to be less than 5 cm. The measurements presented in this article are based on an integrated luminosity of ≈ 172 pb^{-1} collected between February 2002 and September 2003, comprising ≈ 152 million two-track trigger events.

III. EVENT RECONSTRUCTION

The final states $\Lambda_c^+ \pi^-$ and $\Lambda_c^+ \mu^- X$, where $\Lambda_c^+ \to pK^-\pi^+$, are reconstructed in the data collected with the two-track trigger. The selection criteria for the hadronic and the inclusive semileptonic decay modes are kept as similar as possible, which reduces systematic uncertainties on the relative branching fractions.

Both signal decays have a four-track topology. Therefore, events are selected that contain a minimum of four tracks, each with a minimum p_T of 0.5 GeV/c, d_0 less than 5000 μm (measured with the SVX II), a minimum of 20 hits each in the COT axial and stereo layers [23], and a minimum of three axial hits in the SVX II. Each track is also required to be in the fiducial region of the COT and to traverse all 96 wire layers. Making these requirements on each track ensures good quality of the track reconstruction and good momentum resolution. In addition, the maximum requirement on d_0 suppresses background from daughters of K_S^0 and Λ^0 and from particles produced by inelastic collisions of beam products with the detector material.

The reconstruction begins by identifying the Λ_c^+ candidate. Only combinations of three tracks that satisfy the requirements described above are considered. Every combination must have two positively charged tracks and one negatively charged track. At least one of the three tracks must match a displaced track found by the SVT (SVT track [24]). The proton mass is assigned to the positively charged track of higher p_T, the pion mass to the track of lower p_T and the kaon mass to the negatively charged track. Assuming the proton track to be the higher p_T track reduces the combinatorial background by $\approx 50\%$ while keeping $\approx 90\%$ of the Λ_c^+ signal. A three-track kinematic fit determines the Λ_c^+ decay vertex by varying the track parameters of the daughter particles simultaneously, within their uncertainties, so that the χ^2 between the adjusted and the original track parameters is minimized. Only three-track candidates for which the fit converges and the invariant mass ($M_{pK\pi}$) is in the range 2.18–2.38 GeV/c^2 are considered further.

Next, the selected Λ_c^+ candidate is combined with an additional negatively charged track to form a Λ_b^0 candidate. This fourth track must be matched to a SVT track. The combination is considered a Λ_b^0 semileptonic candidate, and a muon mass is assumed for this track if the following two requirements are satisfied. First, a CMU muon stub must be present within 30 cm of the extrapolated track at the CMU radius ($r = 347$ cm) in the $r - \phi$ view. Second, the matching χ^2 between the track and the stub positions

[25] is less than 9. Otherwise, the combination is a Λ_b^0 hadronic candidate, and a pion mass is assumed. Both the muon and the pion tracks from the Λ_b^0 decay must extrapolate to the fiducial region of the CMU. Making the same fiducial requirement for the hadronic and semileptonic modes ensures that the tracking efficiency of both modes cancel in the ratio.

Once all four Λ_b^0-candidate tracks are found, the two tracks which have been matched to SVT tracks (one track from the Λ_c^+ candidate, the other is the fourth track) must pass the two-track trigger requirements as described in Sec. II. Then, a four-track kinematic fit is performed. This fit includes two constraints. First, the daughter tracks of the Λ_c^+ must originate from a common, tertiary vertex. Second, the trajectory of the Λ_c^+ candidate must intersect with that of the remaining Λ_b^0-candidate track, in three dimensions; this intersection is the decay vertex of the Λ_b^0 candidate (defined as the secondary vertex). The secondary and tertiary vertices are determined in the four-track kinematic fit simultaneously. These constraints improve the precision of the Λ_c^+ decay vertex determination and the invariant mass of the Λ_c^+ candidate is recalculated. After the kinematic fit, the values of $M_{pK\pi}$ must be in the range: 2.269–2.302 GeV/c^2 (2σ around the mean) for the hadronic candidates and 2.18–2.38 GeV/c^2 for the inclusive semileptonic candidates (see Fig. 2). The wider Λ_c^+ mass window for the semileptonic candidates allows for the $M_{pK\pi}$ spectrum to be fit to extract the yield N_{inclsemi}. Also for the semileptonic decays, the four-track invariant mass $M_{\Lambda_c\mu}$ must be in the range of 3.7–5.64 GeV/c^2, where the minimum requirement on $M_{\Lambda_c\mu}$ reduces the background from other c-hadron and b-hadron decays. See Sec. VI for more details.

In order to reduce the combinatorial backgrounds further, the selection criteria on the following variables are optimized: p_T of the proton track, p_T of the fourth Λ_b^0-candidate track $[p_T(\pi^-, \mu^-)]$, p_T of Λ_c^+, p_T of the four-track system, $\chi_{r\phi}^2$ of the Λ_c^+ and the four-track kinematic fits, proper decay length (ct) of the Λ_c^+ candidate, and (pseudo) proper decay length (ct^*) of the Λ_b^0 candidate. The $\chi_{r\phi}^2$ is the $r - \phi$ plane contribution to the χ^2 returned by the kinematic fit. The ct is defined as

$$ ct \equiv L_{r\phi}^c \frac{M_{\Lambda_c}}{p_T(\Lambda_c^+)}, \qquad (2) $$

where $L_{r\phi}^c$ is the projection of the vector from the secondary to the tertiary vertex onto the momentum vector of Λ_c^+ in the $r - \phi$ plane, and M_{Λ_c} is the world average of the Λ_c^+ mass [7]. The ct^* has a similar definition:

$$ ct^* \equiv L_{r\phi}^b \frac{M_{\Lambda_b^0}}{p_T(4_{\mathrm{trks}})}, \qquad (3) $$

where $L_{r\phi}^b$ is the projection of the vector from the primary to the secondary vertex onto the total momentum vector of the four tracks in the $r - \phi$ plane, $p_T(4_{\mathrm{trks}})$ is the transverse component of the total momentum of the four tracks, and $M_{\Lambda_b^0}$ is the world average of the Λ_b^0 mass [7]. Here, the primary vertex is estimated from the intersection of the beam line and the trajectory of the Λ_b^0 candidate.

The optimization procedure maximizes the signal significance of the hadronic decays, $S/\sqrt{S + B}$, where S is the number of $\Lambda_b^0 \rightarrow \Lambda_c^+ \pi^-$ events in simulation multiplied by a data-to-MC scaling factor and B is the number of background events estimated from the $\Lambda_c^+ \pi^-$ candidates in the data sideband. The data-to-MC scaling factor for S is obtained by comparing the number of signal events in data and simulation with relaxed requirements. The background B is estimated by fitting the mass sideband region above the Λ_b^0 signal peak with an exponential function and then extrapolating from the sideband region to the 3σ
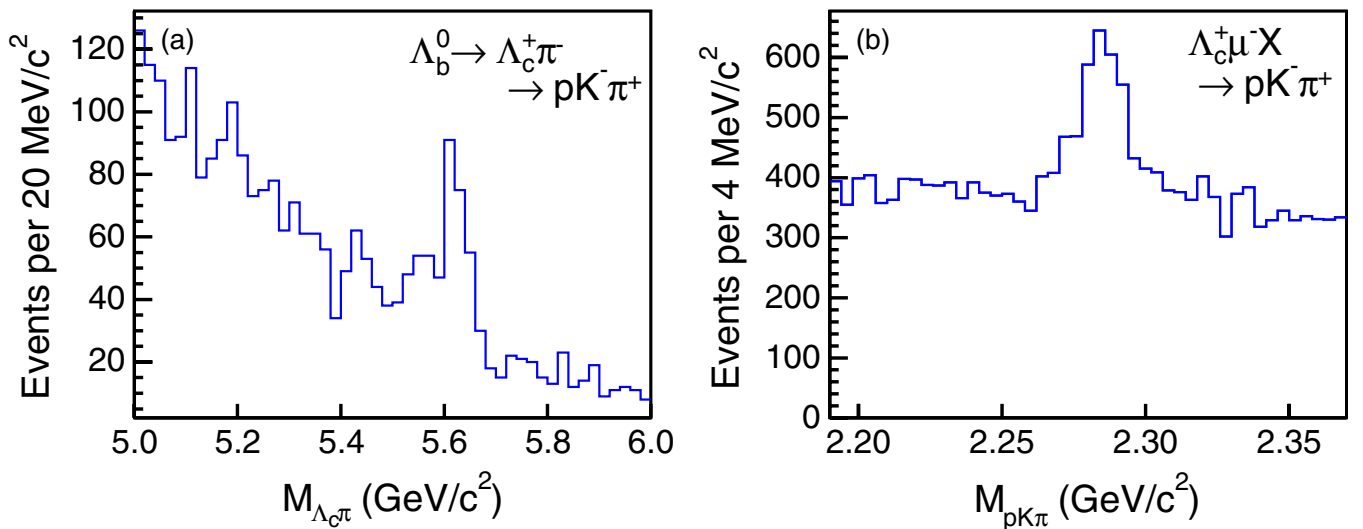

FIG. 2 (color online). The reconstructed invariant mass spectra in data after applying all selection criteria: (a) the $M_{\Lambda_c\pi}$ spectrum of the Λ_b^0 hadronic candidates; (b) the $M_{pK\pi}$ spectrum of the inclusive semileptonic $\Lambda_c^+ \mu^-$ candidates.

TABLE I. Optimized requirements for reconstructing the $\Lambda_b^0 \to \Lambda_c^+ \pi^-$ and $\Lambda_c^+ \mu^- X$ decays.

$\Lambda_b^0 \to \Lambda_c^+ \pi^-$ $\Lambda_c^+ \mu^- X$	
$p_T(p)$	>2 GeV/c
$p_T(\pi^-, \mu^-)$	>2 GeV/c
$p_T(\Lambda_c^+)$	>5 GeV/c
$p_T(4_{\text{trks}})$	>6 GeV/c
$\chi^2_{r\phi}(\Lambda_c^+)$	<14
$\chi^2_{r\phi}(4_{\text{trks}})$	<15
$ct(\Lambda_c^+)$	>-70 μm
$ct^*(\Lambda_b^0)$	>250 μm

signal region around the peak. The optimized selection criteria are listed in Table I. Figure 2(a) shows the reconstructed $M_{\Lambda_c \pi}$ spectrum from the hadronic data and Fig. 2(b) shows the reconstructed $M_{pK\pi}$ spectrum from the inclusive semileptonic data, both after applying the optimized selections. The most significant peaks in Fig. 2 represent the signals for each decay mode. In order to obtain the correct signal yields, a good modeling of the mass spectra, which includes a description of signal and background, is needed. The mass spectrum shapes of backgrounds from partially reconstructed or misidentified b-hadron decays are determined by fitting the mass distributions from simulation. The next section describes details of the simulations used in this analysis.

IV. SIMULATION

In order to determine the mass spectrum shapes close to the signal peaks in Fig. 2 and to estimate the acceptance and efficiency of signal and background, both generator-level and full simulations are used. The generator-level simulation includes only the production and decay of b hadrons, and the analysis requirements are applied to quantities immediately after generation. The full simulation includes simulation of the CDF II detector and trigger, and track reconstruction. It was found that the efficiency ratios $\epsilon_{\text{had}}/\epsilon_{\text{exclsemi}}$ from a generator-level simulation and from a full simulation differ by only $\approx 3\%$. The generator-level simulation is used to estimate the quantities, which are found to be small or already have large uncertainties from other sources [27]: the size of the background contribution where the Λ_c^+ and the μ^- originate from two different heavy-flavor hadrons produced by the fragmentation of $b\bar{b}$ or $c\bar{c}$ pairs (termed $b\bar{b}/c\bar{c}$ background), part of the Λ_b^0 systematic uncertainties (the semileptonic decay model and lifetime of Λ_b^0, Λ_b^0 and Λ_c^+ polarizations, and Λ_c^+ Dalitz structure), and modification of the CDF I $\sigma_{\Lambda_b^0}/\sigma_{\bar{B}^0}$ result. Therefore, this 3% difference has a negligible effect on the final measurement. The following sections describe the key components of the simulations used in this analysis.

A. Production and decay of b hadrons

Two different programs are used to simulate b-hadron production: PYTHIA VERSION 6.2 [28], which simulates all of the strong interaction processes that are involved in b-hadron production, and BGENERATOR [29], which generates a single b hadron in the event. Since PYTHIA simulates all of the products of the $p\bar{p}$ collision, it is computationally intensive to produce a given final state. Therefore, PYTHIA is used to estimate only the $b\bar{b}/c\bar{c}$ backgrounds in the inclusive semileptonic data (Appendix C). The PYTHIA generator simulates physics processes using leading-order matrix elements, supplemented by initial and final state radiation. The program also includes hadronization of the quarks and gluons in the final state and the beam remnants left when a parton undergoes high-momentum scattering. The BGENERATOR program is very efficient at producing a large sample of a specific b-hadron under well-defined kinematic conditions. It is used to determine the acceptance and efficiency for signal and other backgrounds and to model the mass spectra. In the BGENERATOR program, a single b hadron is generated using the measured p_T spectra of b hadrons as inputs. The Λ_b^0 and $\bar{B}^0$ p_T spectra are derived from the fully reconstructed $\Lambda_b^0 \to \Lambda_c^+ \pi^-$ and $\bar{B}^0 \to D^+ \pi^-$ decays in the two-track trigger data, after correcting for acceptance and efficiency.

After the event generation, the decays of the b and c hadrons and their daughters are simulated using the EVTGEN package [30]. For all other particles in the event, this is done by the PYTHIA program. The EVTGEN program uses the dynamics from a full matrix-element calculation and is tuned to measurements, mainly results from experiments at the $\Upsilon(4S)$ resonance [31–34], where the decay models for the $\bar{B}^0$ and the B^- have been demonstrated to match data. As a full theoretical model for Λ_b^0 semileptonic decays is not yet implemented in EVTGEN, a flat phase space (termed PHSP) simulation is used for Λ_b^0 decays. A correction is applied after generation to account for the proper Λ_b^0 semileptonic decay dynamics. Details of this correction are given in Sec. IV C.

B. Detector simulation and comparison of kinematic distributions

After an event has been simulated at the generator level, it is processed with a full simulation of the CDF II detector and trigger. The geometry and response of the active and passive detector components are simulated using the GEANT software package [26]. The events are then processed with a two-track trigger decision program and reconstructed using the same executable as that used to reconstruct the data. The resulting events have the same structure and format as the data and are analyzed in the framework described in Sec. III.

Distributions of kinematic variables from the full simulation with BGENERATOR input are compared with the same
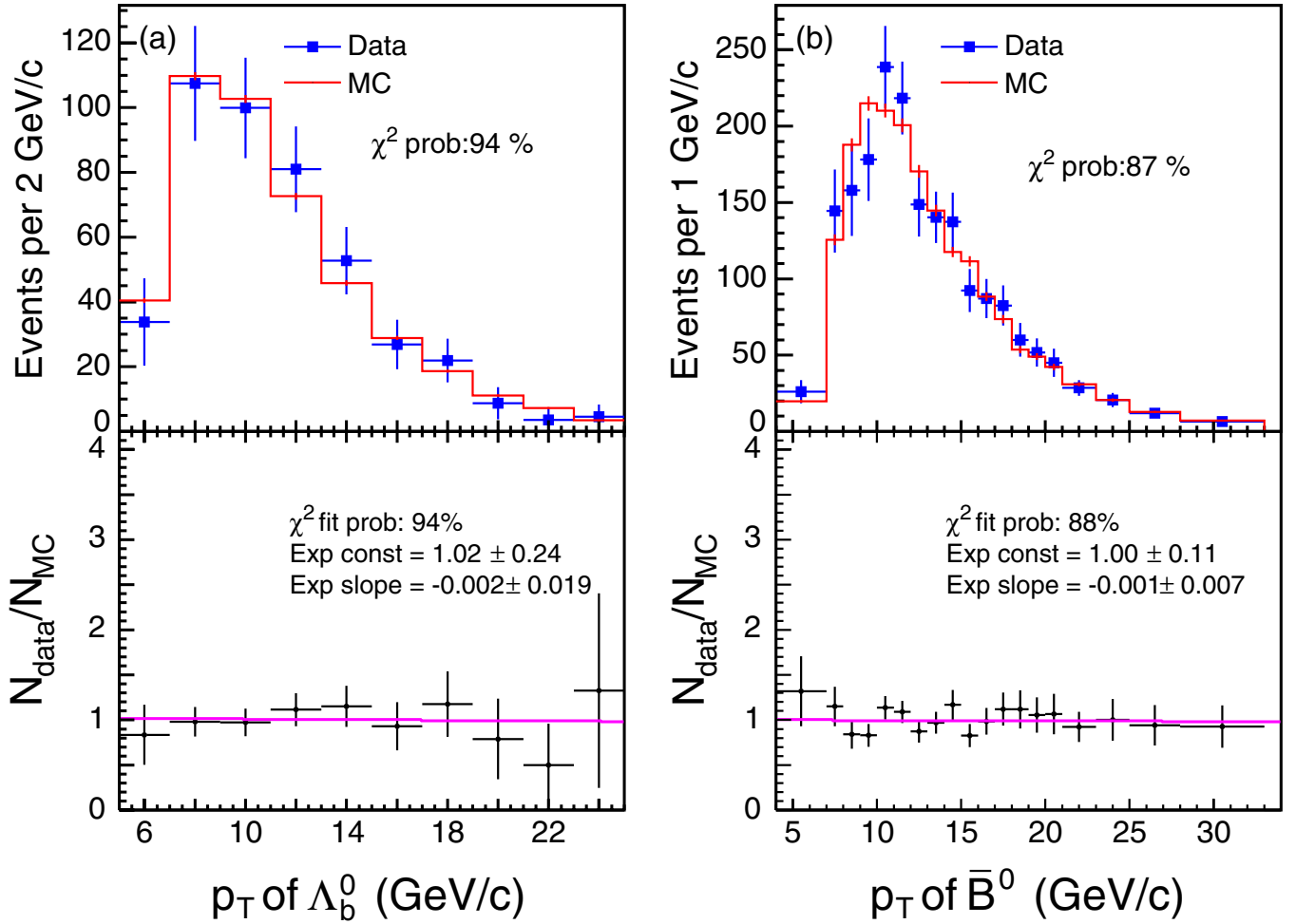
FIG. 3 (color online). Comparison of reconstructed p_T spectra of b hadrons between the data and the full simulation: (a) Λ_b^0 and (b) $\bar{B}^0$. The top figures show the p_T distributions while the bottom figures show the ratio of data to MC. The curves in the bottom figures are the result of an exponential fit of the ratio.

distributions from data. In order to compare the data and the simulation, the data distributions are background subtracted. The agreement between the data and the simulation is quantified by a χ^2 comparison probability and the ratio of spectra produced from the data and the simulation. All relevant distributions agree satisfactorily. Figure 3 shows good agreement between the data and the simulation in the $p_T(\Lambda_b^0)$ and $p_T(\bar{B}^0)$ spectra. The p_T of the b hadron is the most important kinematic variable in this analysis because the b-hadron momentum is distributed among three particles in the final state for the exclusive semileptonic decay and between two particles for the hadronic decay.

C. Acceptance and efficiency scale factors

In order to obtain accurate estimates of the acceptance and efficiency, several scale factors are applied to the number of events selected in simulation and their values are listed in Table II. As mentioned earlier, EVTGEN contains only a phase space simulation of semileptonic Λ_b^0

decays. In order to estimate the effect of decay models on the signal acceptance, a weighting of the flat phase space distribution according to a form factor model from Huang *et al.* [9] for the hadronic current of the Λ_b^0 to Λ_c^+ transition, and a $V - A$ model for the leptonic current, is performed at the generator level. The ratio of the generator-level acceptance after weighting relative to that before weighting, C_{model}, is found to be 0.994 ± 0.025. Since this ratio is consistent with unity, the PHSP full simulation samples are used throughout the Λ_b^0 analysis. The correction factor C_{model}, which accounts for the Λ_b^0 semileptonic decay dynamics, is applied to the efficiencies for semileptonic decays. The shape of the $M_{\Lambda_c \mu}$ distribution is sensitive to the decay dynamics and may be used to cross-check the form factor and $V - A$ models (termed FF). Figure 4 shows the reconstructed $M_{\Lambda_c \mu}$ distributions from the data and from the PHSP full simulation, before and after multiplying the MC histogram with the bin-by-bin ratios, which are derived from the same generator-level simulation samples for C_{model} [35]. The corrected distribu-

TABLE II. Acceptance and efficiency scale factors applied to the number of events selected in simulation. The p_T is the transverse momentum (in GeV/c) of the track that passes the trigger requirements. The uncertainty on C_p is obtained by taking the difference between the p_T-dependent formula below and a constant from an average over the Λ^0 sample, 0.905. The uncertainties on C_K and C_π are below 0.5% and have negligible effect on the final relative branching fractions.

Scale Factor	Value
C_{model}	0.994 ± 0.025
C_{CMU}	0.986 ± 0.003
C_p	$1.06 - \frac{1.3}{p_T} + \frac{3.2}{p_T^2} - \frac{2.2}{p_T^3}$
C_K	$0.969 - \frac{0.094}{p_T}$
C_π	$1.002 - \frac{0.067}{p_T}$

tion has a significantly improved agreement with the data, which confirms the procedure for deriving C_{model}.

In addition, the CMU muon reconstruction efficiency is found to be over estimated in the full simulation; the resulting scale factor, C_{CMU}, is measured using a sample of $J/\psi \rightarrow \mu^+\mu^-$ decays [13]. The dependence of the XFT trigger efficiency on the particle species and p_T is not included in the full simulation. Using a pure proton sample from the $\Lambda^0 \rightarrow p^+\pi^-$ decays, and pure kaon and pion samples from the $D^*(2010)^+ \rightarrow D^0\pi^+$ decays, where $D^0 \rightarrow K^-\pi^+$ [36–38], the data-to-MC scaling factors C_p, C_K, and C_π are derived and applied to the track, which passes the trigger requirements in the reconstruction program.

With a reliable simulation for the modeling of mass spectrum shapes, the numbers of signal events can be determined by fitting the invariant mass spectra in Fig. 2 as described in the following section.

V. DETERMINATION OF THE SIGNAL YIELDS

The numbers of hadronic events (N_{had}) and inclusive semileptonic events (N_{inclsemi}) in Eq. (1) are extracted by fitting the $M_{\Lambda_c\pi}$ and $M_{pK\pi}$ spectra in data, respectively. The fit to the mass spectra is performed using an unbinned, extended likelihood technique [39], where the fit parameters are adjusted to minimize the negative log likelihood ($-\ln\mathcal{L}$). The general unbinned, extended log likelihood is expressed as

$$\ln\mathcal{L} = \sum_i \ln[N_{\text{sig}}S(m_i) + N_{\text{bg}}B(m_i)] - N_{\text{sig}} - N_{\text{bg}}$$
$$+ \sum_j \ln\mathcal{C}_j, \quad (4)$$

where i represents the ith candidate and m represents the reconstructed mass $M_{\Lambda_c\pi}$ or $M_{pK\pi}$. The numbers of signal and background events are denoted as N_{sig} and N_{bg}; $S(m_i)$ and $B(m_i)$ are the normalized functions, which describe the shapes of signal and background mass spectra, respec-
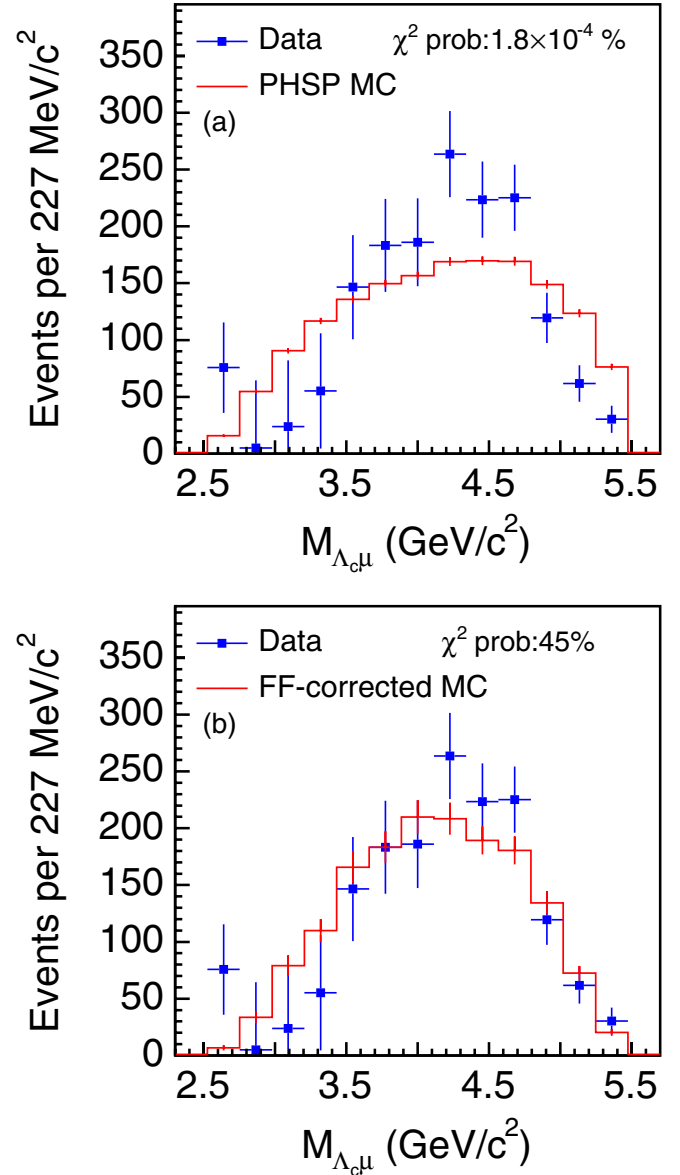

FIG. 4 (color online). Comparison of reconstructed $M_{\Lambda_c\mu}$ between the data and the PHSP full simulation, (a) before and (b) after the MC histogram is corrected to account for the proper Λ_b^0 semileptonic decay dynamics [35]. Note that the feed-in backgrounds that are present in the $\Lambda_c^+\mu^-$ sample are already included in the simulation.

tively. Each $\mathcal{C}_j$ is a Gaussian constraint on a specific fit parameter x_j

$$\mathcal{C}_j = \mathcal{G}(x_j, \mu_j, \sigma_j) = \frac{1}{\sqrt{2\pi}\sigma_j} e^{-(1/2)((x_j-\mu_j)/\sigma_j)^2}, \quad (5)$$

where the parameter x_j has a central value of μ_j and an uncertainty of σ_j. Because the data sample size is not large enough to determine these parameters accurately from the fit, they are constrained to values that are estimated from independent measurements and the full simulation.

Definitions of the constrained parameters (x_j) are given in Sec. VA.

Correct modeling of the mass spectra is crucial in the determination of N_{had} and N_{inclsemi}. Two types of background appear in each mass window of interest. The first is combinatorial background. Combinations of four random tracks contribute to this background in both the hadronic and semileptonic modes. Combinations of a real c hadron and a random track contribute only in the hadronic mode. The mass spectrum of the combinatorial background is determined using data sidebands. The second background is misidentified or partially reconstructed decays of b hadrons. Their mass spectrum shapes are determined using the simulations as described in Sec. IV. The dominant contributing decays are identified with a generator-level simulation of inclusive b-hadron decays, and are categorized according to their mass spectrum shapes. Decay modes with similar shapes are generated together using a full simulation, with the number of generated events for each decay mode proportional to the fragmentation fraction times the branching ratio, and are parameterized by a single function. The functional form for each combined background spectrum is determined empirically to match the shape of simulated mass distribution. The parameter values of each function are obtained by fitting the simulated spectrum. When fitting data, the values of the shape parameters are fixed while the normalization is a free parameter.

A. The $M_{\Lambda_c\pi}$ spectrum for the $\Lambda_b^0 \to \Lambda_c^+ \pi^-$ yield

Figure 5(a) shows the $M_{\Lambda_c\pi}$ spectrum with the fit result superimposed. The likelihood fit is performed in the mass window $M_{\Lambda_c\pi} = 4.6$–7.0 GeV/c^2, whereas Fig. 5(a) shows a more restricted mass range near the signal peak.

The $\Lambda_b^0 \to \Lambda_c^+ \pi^-$ yield returned by the fit is 179 ± 19. The signal peak at $M_{\Lambda_c\pi} \approx 5.6$ GeV/c^2 is described by a Gaussian function. The width of the Gaussian is constrained in the fit to reduce the uncertainty on N_{sig}. The constrained width is the product of a data/MC scale factor and the width of the $M_{\Lambda_c\pi}$ distribution in the full simulation, $(\sigma_{D\pi}^{\text{data}}/\sigma_{D\pi}^{\text{MC}}) \times \sigma_{\Lambda_c\pi}^{\text{MC}}$, which is 0.0231 ± 0.0012 GeV/c^2. The scale factor, $\sigma_{D\pi}^{\text{data}}/\sigma_{D\pi}^{\text{MC}}$, is obtained by comparing the width of the invariant mass distribution in data with that in the simulated events, using the $\bar{B}^0 \to D^+\pi^-$ decay, which has a similar topology and a larger data sample size. The combinatorial background is parameterized by an exponential (light-gray filled region), where the exponential slope is determined by the $\Lambda_c^+\pi^-$ candidates in the mass region above 5.7 GeV/c^2. The functions that describe the mass spectra of backgrounds from the misidentified or partially reconstructed b-hadron decays are determined from the simulated mass distributions.

Details of the background from the misidentified or partially reconstructed b-hadron decays follow. The doubly Cabibbo-suppressed decays $\Lambda_b^0 \to \Lambda_c^+ K^-$, with a pion mass mistakenly assumed for the kaon, are indicated by the black filled region. The ratio of the number of doubly Cabibbo-suppressed decays relative to that of the signal mode, $N_{\Lambda_c K}/N_{\Lambda_c\pi}$, is fixed to 8% in the fit. This value is obtained from the world average of measurements in the $\bar{B}^0$ modes. Fully reconstructed b-meson decays with misidentified daughters produce a distinct peak at $M_{\Lambda_c\pi} \approx 5.5$ GeV/c^2 (wavy-line region). The $\bar{B}^0 \to D^+\pi^-$ decays, where $D^+ \to K^-\pi^+\pi^+$ and one of the pions is reconstructed as a proton, contribute about 50% to this background. The background from the remaining partially reconstructed b-meson decays has a monotonically falling
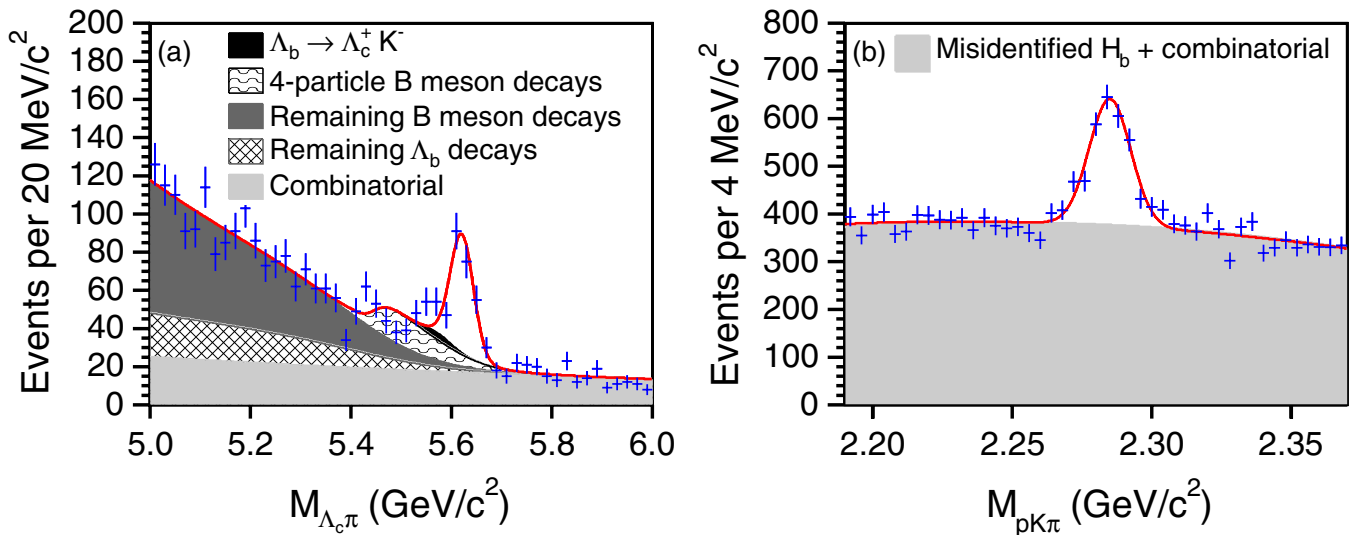

FIG. 5 (color online). Results (curve) of the unbinned, extended likelihood fits for determining the numbers of Λ_b^0 candidates: (a) hadronic and (b) inclusive semileptonic. The filled histograms indicate various backgrounds.

TABLE III. Observed number of events in each Λ_b^0 decay mode determined from the unbinned, extended likelihood fit, χ^2/NDF, and the corresponding probability computed to indicate quality of the fit.

Mode	Yield	χ^2/NDF	Prob (%)
$\Lambda_b^0 \to \Lambda_c^+ \pi^-$	179 ± 19	123/111	20.7
$\Lambda_c^+ \mu^- X$	1237 ± 97	48/38	13.0

mass distribution (dark-gray filled region) dominated by $\bar{B}^0 \to D^+ \mu^- \bar{\nu}_\mu$, $\bar{B}^0 \to D^+ \rho^-$, where $\rho^- \to \pi^0 \pi^-$, and $\bar{B}^0 \to D^*(2010)^+ \pi^-$, where $D^*(2010)^+ \to D^+ \pi^0$ and the π^0's are not reconstructed in the event. The remaining Λ_b^0 decays also have a falling mass spectrum (hatched region) dominated by $\Lambda_b^0 \to \Lambda_c^+ \ell \bar{\nu}_\ell$ and $\Lambda_b^0 \to \Lambda_c^+ \rho^-$, where $\rho^- \to \pi^0 \pi^-$.

B. The $M_{pK\pi}$ spectrum for the $\Lambda_c^+ \mu^- X$ yield

Figure 5(b) shows the $M_{pK\pi}$ spectrum for events with muons, with the fit result superimposed. The inclusive $\Lambda_c^+ \mu^- X$ yield returned by the fit is 1237 ± 97. The fit for the $M_{pK\pi}$ spectrum is less complex than that for the $M_{\Lambda_c \pi}$ spectrum described above. Note that the signal peak includes the backgrounds, which also contain $\Lambda_c^+ \mu^-$ in the final state (see Sec. VI). The signal peak at $M_{pK\pi} \approx$ 2.3 GeV/c^2 is modeled by a Gaussian function. Background from the b-hadron semileptonic decays with a c-hadron daughter misidentified as a Λ_c^+, such as $\bar{B}^0 \to D^+ \mu^- \bar{\nu}_\mu$, where $D^+ \to K^- \pi^+ \pi^+$ and one of the pions is assigned the proton mass, does not produce a peak or distinctive structure and is inseparable from the combinatorial background. These two backgrounds are combined and modeled by a second-order polynomial (light-gray filled region).

C. Summary

Table III summarizes the Λ_b^0 hadronic and inclusive semileptonic yields and the χ^2 probability of corresponding fits. Each model describes the data well, as indicated by the χ^2 probability. In order to obtain the number of exclusive semileptonic signal events N_{exclsemi}, the contributions from backgrounds, which also produce a Λ_c^+ and a μ^- in the final state N_{semibg}, must be subtracted from N_{inclsemi}. Section VI describes the estimation of the composition of the Λ_b^0 inclusive semileptonic data sample. Section VII details observations of four new Λ_b^0 semileptonic decays and the estimates of Λ_b^0 semileptonic and hadronic branching ratios, which are required to determine the sample composition in Sec. VI.

VI. COMPOSITION OF THE INCLUSIVE SEMILEPTONIC DATA

The B factories [31–34] produce b hadrons in $e^+ e^-$ interactions, where the beam energy may be used as a constraint when reconstructing events. This feature is particularly helpful for reconstructing semileptonic decays where a neutrino is missing. At the Tevatron, b hadrons are produced by the interactions between quarks and gluons with a broad parton momentum spectrum. Therefore, beam energy constraints are not available to aid b-hadron reconstruction. Backgrounds that contain a Λ_c^+, a μ^-, and other particles in the final state cannot be separated easily from the exclusive semileptonic signal $\Lambda_b^0 \to \Lambda_c^+ \mu^- \bar{\nu}_\mu$ and will contribute to the inclusive $\Lambda_c^+ \mu^-$ events observed in data. These backgrounds arise from three sources:

(1) false muon: a Λ_c^+ and a hadron track ($\bar{p}$, K^- or π^-) misidentified as a μ^-.

(2) $b\bar{b}/c\bar{c}$: a Λ_c^+ from the decay of a heavy-flavor hadron H_b (H_c) and a μ^- from the decay of the other heavy-flavor hadron $\bar{H}_b$ ($\bar{H}_c$), where the two hadrons are produced by the fragmentation of $b\bar{b}$ ($c\bar{c}$) pairs.

(3) feed in: decays of a single b hadron into a Λ_c^+, a μ^-, and particles not reconstructed in data.

The goal is to measure the branching fraction of the exclusive semileptonic decay relative to that of the hadronic decay. The backgrounds listed above must be subtracted from the observed number of inclusive semileptonic events in data. Equation (1) is then rewritten as follows:

$$\frac{\mathcal{B}_{\text{exclsemi}}}{\mathcal{B}_{\text{had}}} = \left(\frac{N_{\text{inclsemi}} - N_{\text{false}\,\mu} - N_{b\bar{b},c\bar{c}} - N_{\text{feed}}}{N_{\text{had}}}\right) \frac{\epsilon_{\text{had}}}{\epsilon_{\text{exclsemi}}}.$$

(6)

The number of false-muon events ($N_{\text{false}\,\mu}$) is obtained from data containing a Λ_c^+ and a hadron track satisfying reconstruction requirements, with the hadron track weighted by an appropriate muon-misidentification probability. The contributions from the $b\bar{b}/c\bar{c}$ ($N_{b\bar{b},c\bar{c}}$) and the feed-in backgrounds (N_{feed}) are estimated using both data and simulation. Instead of the absolute amount, the ratios $N_{b\bar{b},c\bar{c}}/N_{\text{had}}$ and $N_{\text{feed}}/N_{\text{had}}$ are estimated. Estimating the ratios instead of the absolute amount has one advantage: the majority of the background events are decays of Λ_b^0, so knowledge of the Λ_b^0 production cross section is not necessary. The quantities $N_{b\bar{b},c\bar{c}}/N_{\text{had}}$ and $N_{\text{feed}}/N_{\text{had}}$ are determined from the ratios of the products of branching fractions and efficiencies (times production cross section for non-Λ_b^0 background). The normalization procedure requires measurements or estimates of the branching fractions for the $\Lambda_b^0 \to \Lambda_c^+ \pi^-$ decay and for several semileptonic decays, which contribute to the backgrounds; details of these measurements and estimates are found in Sec. VII. The ratio $N_{b\bar{b},c\bar{c}}/N_{\text{had}}$ has been estimated to be very small and contributes $\leq 1\%$ to the $\Lambda_b^0 \to \Lambda_c^+ \mu^- \bar{\nu}_\mu$ signal. More information on $b\bar{b}$ and $c\bar{c}$ backgrounds may be found in

Appendix C. The following sections describe the estimation of $N_{\text{false}\mu}$ and N_{feed}.

A. False muons

One type of semileptonic background is due to the pairing of a Λ_c^+ with a proton, a kaon, or a pion that is misidentified as a muon. A hadron is misidentified as a muon when it passes through the calorimeter into the muon detector, or when it decays into a muon in flight. The probabilities for a proton, kaon, or pion to be misidentified as a muon ($\mathcal{P}_p$, $\mathcal{P}_K$, and $\mathcal{P}_\pi$, respectively) are measured using a pure proton sample from the $\Lambda^0 \to p^+ \pi^-$ decays, and pure K and π samples from the $D^*(2010)^+ \to D^0 \pi^+$ decays, where $D^0 \to K^- \pi^+$ [40]. The muon-misidentification probability is defined as the fraction of the CMU-fiducial and SVT-matched hadron tracks, which satisfy the muon identification requirement (a track associated with hits in the CMU and with a matching χ^2 less than 9). Figure 6 shows the $\mathcal{P}_p$ (measured in 12 p_T bins) and $\mathcal{P}_\pi$, $\mathcal{P}_K$ (measured in 16 p_T bins) for positively and negatively charged tracks, separately. A difference is observed between $\mathcal{P}_{K^+}$ and $\mathcal{P}_{K^-}$ in the low p_T region, which is not seen for protons and pions. The larger hadronic cross section for the $K^- p$ scattering relative to that for the $K^+ p$ scattering results in a lower rate of K^- being misidentified as muons passing through the calorimeter.

The contribution of the false-muon background to the $\Lambda_b^0 \to \Lambda_c^+ \mu^- \bar{\nu}_\mu$ signal $N_{\text{false}\mu}$ is obtained by weighting data containing a Λ_c^+ and a hadron track (h^-), with the muon-misidentification probability ($\mathcal{P}_{\text{avg}}$) as a function of the momentum of h^-. This hadron track must extrapolate to the fiducial region of the CMU and fail the muon identification requirements in order to remove real muons. The other selection criteria for the $\Lambda_c^+ h^-$ sample are the same as those for the $\Lambda_b^0 \to \Lambda_c^+ \mu^- \bar{\nu}_\mu$ reconstruction. The $N_{\text{false}\mu}$ is then extracted from a χ^2 fit of the $M_{pK\pi}$ distribution produced from the weighted $\Lambda_c^+ h^-$ sample. Figure 7 shows the result of the χ^2 fit.

Since no particle identification requirement is applied, whether h^- is a proton, a kaon, or a pion cannot be determined from data. The muon-misidentification probability, $\mathcal{P}_{\text{avg}}$, is, therefore, an average of $\mathcal{P}_p$, $\mathcal{P}_K$, and $\mathcal{P}_\pi$ weighted by F_p, F_K, and F_π (the fractions of p, K, π in h^-):

$$\mathcal{P}_{\text{avg}} = F_p \mathcal{P}_p + F_K \mathcal{P}_K + F_\pi \mathcal{P}_\pi. \tag{7}$$

In order to determine F_p, F_K, and F_π, physics processes which produce these hadrons must be understood. The principal sources of these hadrons after analysis requirements are the decays $H_b \to \Lambda_c^+ h^- X$, where h^- is a $\bar{p}$, K^-, or π^- misidentified as a muon and X could be nothing (e.g., $\Lambda_b^0 \to \Lambda_c^+ \pi^-$) or any other particles which are not reconstructed (e.g., $B^- \to \Lambda_c^+ \bar{p} \mu^- \bar{\nu}_\mu$). Other sources include fragmentation of a primarily produced quark or
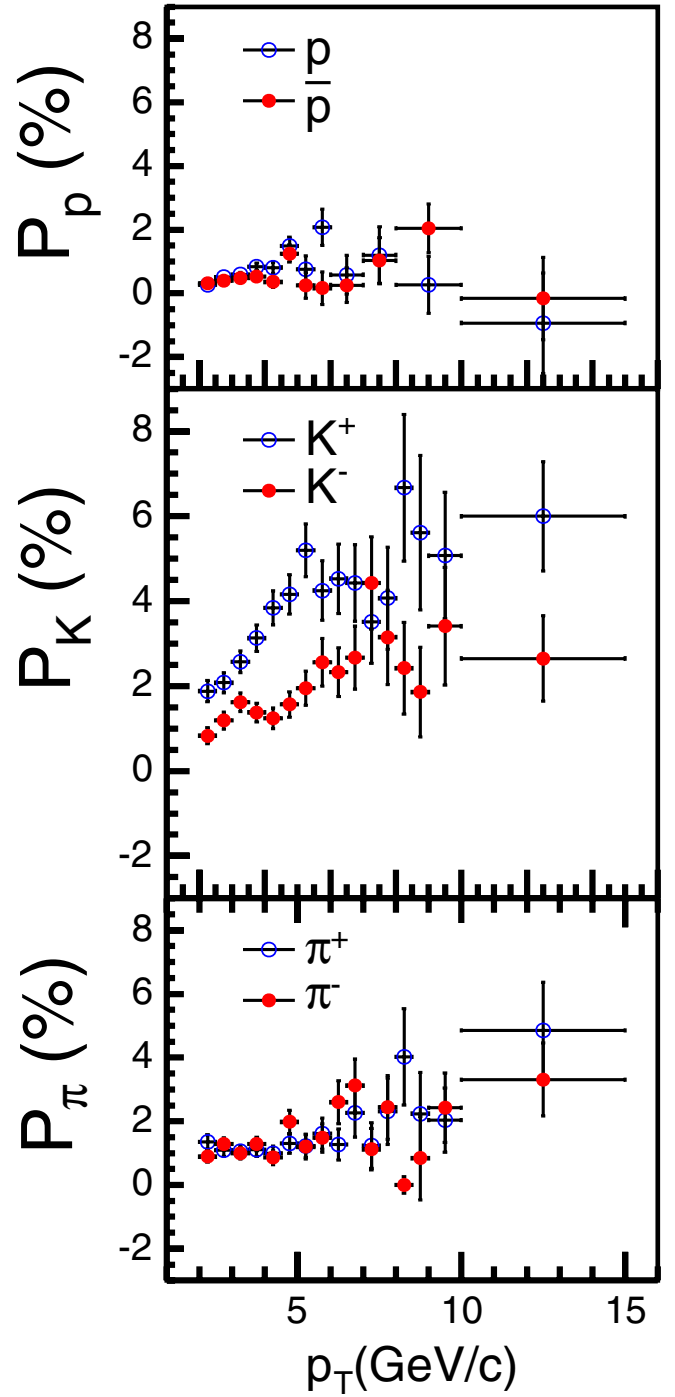

FIG. 6 (color online). The probability for a proton, kaon, or pion to be misidentified as a muon as a function of p_T [40]. Note that for the measurements with negative values, a zero muon-misidentification probability is used to weight the data.

gluon, inelastic collisions of secondary particles with the detector material, and decays of c hadrons. Hadrons that are not from b-hadron decays are suppressed by requiring that the transverse impact parameter (d_0) of the muon candidate is in the range 120 μm–1000 μm, and that the Λ_c^+ and the muon candidates form a vertex significantly
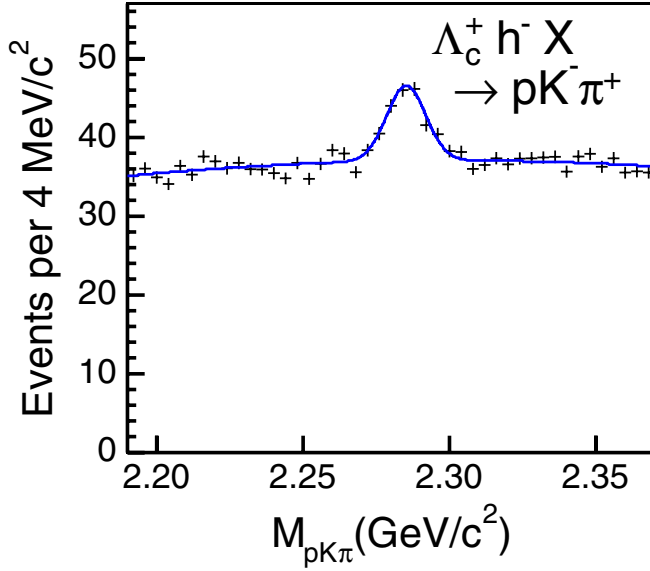
FIG. 7 (color online). Distribution of $M_{pK\pi}$ produced from data with a hadron track (h^-) and a Λ_c^+ candidate in the final state, after weighting the hadron track with an average muon-misidentification probability ($\mathcal{P}_{avg}$). The curve indicates the result of the χ^2 fit.

displaced from the beam line (see Sec. III). In addition, the PYTHIA simulation indicates that the background where a false muon and a Λ_c^+ signal originate from decays of two different b or c hadrons is less than 0.1% of the inclusive semileptonic signal and can be ignored. Therefore, F_p, F_K, and F_π are obtained from the $H_b \to \Lambda_c^+ h^- X$ full simulation.

Table IV shows values obtained for F_p, F_K, F_π, and $N_{\text{false}\mu}$. The uncertainty on $N_{\text{false}\mu}$ includes the statistical uncertainty from the χ^2 fit, the uncertainties on F_p, F_K, and F_π, and the uncertainties on the measured muon-misidentification probabilities. The $N_{\text{false}\mu}$ is approximately 3.2% of the number of $\Lambda_c^+ \mu^- X$ events.

B. Feed-in backgrounds

The feed-in backgrounds to the $\Lambda_b^+ \to \Lambda_c^+ \mu^- \bar{\nu}_\mu$ signal fall into three categories:

(1) $N_{\text{feed}}^{\text{meson}}$: Baryonic, semileptonic decays of $\bar{B}^0/B^-/\bar{B}_s^0$, which decay into Λ_c^+, an antinucleon and leptons (e.g., $B^- \to \Lambda_c^+ \bar{p} \mu^- \bar{\nu}_\mu$).

TABLE IV. The fractions of p, K, and π in the h^- (F_p, F_K, and F_π), the estimated number of false-muon events to the $\Lambda_b^0 \to \Lambda_c^+ \mu^- \bar{\nu}_\mu$ signal, and for comparison, the number of the inclusive semileptonic events in data.

F_p	0.24 ± 0.16
F_K	0.05 ± 0.08
F_π	0.71 ± 0.16
$N_{\text{false}\mu}$	40 ± 9
N_{inclsemi}	1237 ± 97

(2) $N_{\text{feed}}^{b-\text{baryon}}$: Semileptonic decays of other b baryons (e.g., $\Xi_b^0 \to \Lambda_c^+ \bar{K}^0 \mu^- \bar{\nu}_\mu$).

(3) $N_{\text{feed}}^{\text{other}\Lambda_b^0}$: Other semileptonic decays of Λ_b^0, which include either additional particles (e.g., $\Lambda_b^0 \to \Lambda_c^+ \pi^+ \pi^- \mu^- \bar{\nu}_\mu$) or a higher mass c baryon with subsequent decay into the Λ_c^+ signal (e.g., $\Lambda_b^0 \to \Lambda_c(2595)^+ \mu^- \bar{\nu}_\mu$, $\Lambda_c(2595)^+ \to \Lambda_c^+ \gamma$),

and the ratio $N_{\text{feed}}/N_{\text{had}}$ is expressed as

$$\frac{N_{\text{feed}}}{N_{\text{had}}} = \frac{N_{\text{feed}}^{\text{meson}} + N_{\text{feed}}^{b-\text{baryon}} + N_{\text{feed}}^{\text{other}\Lambda_b^0}}{N_{\text{had}}}. \quad (8)$$

The $N_{\text{feed}}^{\text{meson}}$ and $N_{\text{feed}}^{b-\text{baryon}}$ have been estimated to be very small and contribute $\leq 1\%$ to the $\Lambda_b^0 \to \Lambda_c^+ \mu^- \bar{\nu}_\mu$ signal. Details of these estimates are found in Appendices A and B. The contributions from other Λ_b^0 semileptonic decays are estimated below.

The ratio $N_{\text{feed}}^{\text{other}\Lambda_b^0}/N_{\text{had}}$ is given by

$$\frac{N_{\text{feed}}^{\text{other}\Lambda_b^0}}{N_{\text{had}}} = \frac{\sum_i \mathcal{B}_i \epsilon_i}{\mathcal{B}(\Lambda_b^0 \to \Lambda_c^+ \pi^-) \epsilon_{\Lambda_b^0 \to \Lambda_c^+ \pi^-}}, \quad (9)$$

where $\mathcal{B}_i$ and ϵ_i are the branching fraction of Λ_b^0 semileptonic decay mode i and the efficiency of partially reconstructing the decay i as the semileptonic signal, respectively. The estimate of $N_{\text{feed}}^{\text{other}\Lambda_b^0}$ starts by identifying the dominant background decay modes that enter Eq. (9). The observation of spin-1/2 $\Lambda_c(2595)^+$ and spin-3/2
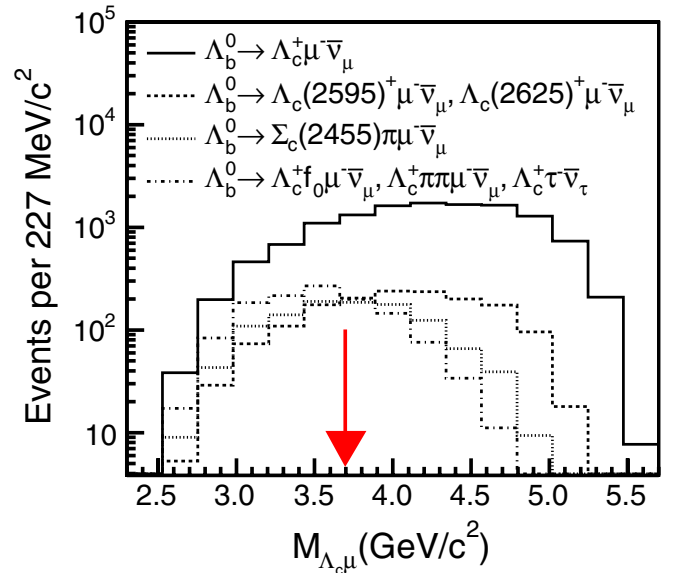

FIG. 8 (color online). The fully simulated $M_{\Lambda_c\mu}$ distributions of the signal and backgrounds from other semileptonic decays of Λ_b^0, on a log scale. The arrow indicates the minimum analysis requirement at 3.7 GeV/c^2. Note that the backgrounds tend to be at the lower mass region.

$\Lambda_c(2625)^+$ [41,42] indicates the existence of $\Lambda_b^0 \to \Lambda_c(2595)^+ \mu^- \bar{\nu}_\mu$ and $\Lambda_b^0 \to \Lambda_c(2625)^+ \mu^- \bar{\nu}_\mu$ decays. In addition, the following decays may contribute to the $\Lambda_c^+ \mu^- X$ final state:

$$\Lambda_b^0 \to \Sigma_c(2455)^0 \pi^+ \mu^- \bar{\nu}_\mu,$$

$$\Lambda_b^0 \to \Sigma_c(2455)^+ \pi^0 \mu^- \bar{\nu}_\mu,$$

$$\Lambda_b^0 \to \Sigma_c(2455)^{++} \pi^- \mu^- \bar{\nu}_\mu,$$

$$\Lambda_b^0 \to \Lambda_c^+ f_0(980) \mu^- \bar{\nu}_\mu,$$

$$\Lambda_b^0 \to \Lambda_c^+ \pi^+ \pi^- \mu^- \bar{\nu}_\mu \text{(non-resonant)},$$

$$\Lambda_b^0 \to \Lambda_c^+ \pi^0 \pi^0 \mu^- \bar{\nu}_\mu \text{(non-resonant)}.$$

The decay in the tau channel, $\Lambda_b^0 \to \Lambda_c^+ \tau^- \bar{\nu}_\tau$, where $\tau^- \to \mu^- \bar{\nu}_\mu \nu_\tau$, also makes a small contribution. Equation (9)

requires knowledge of the branching fractions of $\Lambda_b^0 \to \Lambda_c^+ \pi^-$ and these background decays. In order to reduce systematic uncertainties from theoretical predictions, the dominant background decays $\Lambda_b^0 \to \Lambda_c(2595)^+ \mu^- \bar{\nu}_\mu$, $\Lambda_b^0 \to \Lambda_c(2625)^+ \mu^- \bar{\nu}_\mu$, $\Lambda_b^0 \to \Sigma_c(2455)^0 \pi^+ \mu^- \bar{\nu}_\mu$, and $\Lambda_b^0 \to \Sigma_c(2455)^{++} \pi^- \mu^- \bar{\nu}_\mu$ have been reconstructed in the data. Measurements of their branching fractions relative to the branching fraction of the $\Lambda_b^0 \to \Lambda_c^+ \mu^- \bar{\nu}_\mu$ decay and estimates of the branching fractions of $\Lambda_b^0 \to \Lambda_c^+ \pi^-$ and the other Λ_b^0 semileptonic decays are found in Sec. VII. Once the list of background decay modes is established and their branching fractions are estimated, the acceptances and efficiencies of these backgrounds relative to that of the hadronic mode ($\epsilon_i/\epsilon_{\Lambda_b^0 \to \Lambda_c^+ \pi^-}$) are obtained from the full simulation as described in Sec. IV. Figure 8 shows that

TABLE V.   Feed-in backgrounds to $\Lambda_b^0 \to \Lambda_c^+ \mu^- \bar{\nu}_\mu$ from other Λ_b^0 semileptonic decays. The "*" indicates decays, which have been reconstructed for this measurement and seen in data for the first time (Sec. VII A). The second column lists the estimated branching fractions from Sec. VII. Numbers in parentheses are estimated uncertainties [43,44]. The third column lists $\epsilon_i/\epsilon_{\Lambda_b^0 \to \Lambda_c^+ \pi^-}$ with statistical uncertainty. All efficiencies are determined from the full simulation as described in Sec. IV. The fourth and the fifth columns list the normalization for each background relative to the hadronic and the exclusive semileptonic signals, respectively. The last column lists the number of events for each background after multiplying $(N_{\text{feed}}^{\text{other}\Lambda_b^0}/N_{\text{had}})^i$ by N_{had}, and the uncertainty includes only the statistical uncertainty on N_{had}. Note that while the numbers listed in the fourth column are used in the final measurement, the last two columns are shown only for a comparison with the $\Lambda_b^0 \to \Lambda_c^+ \mu^- \bar{\nu}_\mu$ signal.

Mode	$\mathcal{B}$ (%)	$\dfrac{\epsilon_i}{\epsilon_{\Lambda_b^0 \to \Lambda_c^+ \pi^-}}$	$\left(\dfrac{N_{\text{feed}}^{\text{other}\Lambda_b^0}}{N_{\text{had}}}\right)^i$	$\left(\dfrac{N_{\text{feed}}^{\text{other}\Lambda_b^0}}{N_{\text{exclsemi}}}\right)^i$	N_{event}
$\Lambda_b^0 \to \Lambda_c^+ \pi^-$	$0.36 ^{+(0.24)}_{-(0.18)}$	1.000	–	–	179 ± 19
$\Lambda_c^+ \mu^- X$	–	–	–	–	1237 ± 97
$\Lambda_b^0 \to \Lambda_c^+ \mu^- \bar{\nu}_\mu$	$7.3 \pm (1.4)$	0.303 ± 0.004	6.118	1.000	–
*$\Lambda_b^0 \to \Lambda_c(2595)^+ \mu^- \bar{\nu}_\mu$	$0.9 \pm (0.4)$	0.198 ± 0.003	0.503	0.082	90 ± 10
$\hookrightarrow \Sigma_c(2455)^{++}\pi^-$	24 ± 7				
$\hookrightarrow \Lambda_c^+ \pi^+$	$100 \pm (5)$				
$\hookrightarrow \Sigma_c(2455)^0 \pi^+$	24 ± 7				
$\hookrightarrow \Lambda_c^+ \pi^-$	$100 \pm (5)$				
$\hookrightarrow \Sigma_c(2455)^+ \pi^0$	$24 \pm (1.2)$				
$\hookrightarrow \Lambda_c^+ \pi^0$	$100 \pm (5)$				
$\hookrightarrow \Lambda_c^+ \pi^+ \pi^-$	18 ± 10				
$\hookrightarrow \Lambda_c^+ \pi^0 \pi^0$	$9 \pm (0.45)$				
$\hookrightarrow \Lambda_c^+ \gamma$	$1 \pm (0.05)$				
*$\Lambda_b^0 \to \Lambda_c(2625)^+ \mu^- \bar{\nu}_\mu$	$1.5 \pm (0.6)$	0.192 ± 0.003	0.815	0.133	146 ± 15
$\hookrightarrow \Lambda_c^+ \pi^+ \pi^-$	$66 \pm (3.3)$				
$\hookrightarrow \Lambda_c^+ \pi^0 \pi^0$	$33 \pm (1.7)$				
$\hookrightarrow \Lambda_c^+ \gamma$	$1 \pm (0.05)$				
*$\Lambda_b^0 \to \Sigma_c(2455)^0 \pi^+ \mu^- \bar{\nu}_\mu$	$0.39 \pm (0.23)$	0.082 ± 0.004	0.089	0.015	16 ± 2
$\hookrightarrow \Lambda_c^+ \pi^-$	$100 \pm (5)$				
$\Lambda_b^0 \to \Sigma_c(2455)^+ \pi^0 \mu^- \bar{\nu}_\mu$	$0.39 \pm (0.23)$	0.073 ± 0.004	0.080	0.013	14 ± 2
$\hookrightarrow \Lambda_c^+ \pi^0$	$100 \pm (5)$				
*$\Lambda_b^0 \to \Sigma_c(2455)^{++} \pi^- \mu^- \bar{\nu}_\mu$	$0.39 \pm (0.23)$	0.077 ± 0.004	0.084	0.014	15 ± 2
$\hookrightarrow \Lambda_c^+ \pi^+$	$100 \pm (5)$				
$\Lambda_b^0 \to \Lambda_c^+ \tau^- \bar{\nu}_\tau$	$2.0 \pm (2.0)$	0.041 ± 0.003	0.040	0.006	7 ± 1
$\hookrightarrow \mu^- \bar{\nu}_\mu \nu_\tau$	17.36 ± 0.05				
$\Lambda_b^0 \to \Lambda_c^+ f_0(980) \mu^- \bar{\nu}_\mu$	$0.00 \pm (0.32)$	0.023 ± 0.002	0.000	0.000	0
$\Lambda_b^0 \to \Lambda_c^+ \pi^+ \pi^- \mu^- \bar{\nu}_\mu$	$0.00 \pm (0.64)$	0.032 ± 0.002	0.000	0.000	0
$\Lambda_b^0 \to \Lambda_c^+ \pi^0 \pi^0 \mu^- \bar{\nu}_\mu$	$0.00 \pm (0.32)$	0.033 ± 0.002	0.000	0.000	0

TABLE VI.   The values of background variables in Eq. (6) and the composition of the $\Lambda_c^+ \mu^- X$ sample. Uncertainties on the $b\bar{b}/c\bar{c}$ and feed-in backgrounds to the $\Lambda_b^0 \to \Lambda_c^+ \mu^- \bar{\nu}_\mu$ decay are statistical only. The values of N_{had}, N_{inclsemi}, and $\epsilon_{\text{had}}/\epsilon_{\text{exclsemi}}$ in Eq. (6) are 179 ± 19, 1237 ± 97, and 0.303 ± 0.004, respectively.

Source	N	N/N_{had}	N/N_{inclsemi} (%)
Signal	–	–	72.5
False muon	40 ± 9	–	3.2
$b\bar{b}/c\bar{c}$	–	0.017 ± 0.009	0.3
Feed-in	–	1.660 ± 0.018	24.0

a minimum requirement on $M_{\Lambda_c \mu}$ of 3.7 GeV/c^2 reduces the backgrounds from other Λ_b^0 semileptonic decays, which have more particles in the final state.

Table V summarizes the feed-in backgrounds from the Λ_b^0 semileptonic decays discussed above and lists the hadronic and inclusive semileptonic yields observed in data. The two leading backgrounds after all selections are $\Lambda_b^0 \to \Lambda_c(2595)^+ \mu^- \bar{\nu}_\mu$ and $\Lambda_b^0 \to \Lambda_c(2625)^+ \mu^- \bar{\nu}_\mu$. The total contribution from feed-in backgrounds has been estimated to be 24.0% of the number of $\Lambda_c^+ \mu^- X$ events.

C. Summary

Table VI lists the values of all the background variables that enter Eq. (9) and summarizes the composition of the inclusive $\Lambda_c^+ \mu^-$ sample. The dominant signal contamination is from the feed-in background. The second largest background arises from false muons. The smallest background source is $b\bar{b}/c\bar{c}$. The estimate of $N_{\text{feed}}^{\text{other}\Lambda_b^0}/N_{\text{had}}$ requires knowledge of the branching fraction of each feed-in decay and also the hadronic decay $\Lambda_b^0 \to \Lambda_c^+ \pi^-$. The next section details the measurements and assumptions used to estimate these branching fractions.

VII. OBSERVATIONS OF FOUR NEW Λ_b^0 SEMILEPTONIC DECAYS AND ESTIMATES OF Λ_b^0 SEMILEPTONIC AND HADRONIC BRANCHING FRACTIONS

The size of the background contribution from the feed-in of other semileptonic decays of Λ_b^0, $N_{\text{feed}}^{\text{other}\Lambda_b^0}$ is normalized

to the observed hadronic signal yield in data, with corrections for the relative acceptance times efficiency for each decay mode [see Eq. (9)]. This procedure requires estimates of the branching fractions for each background decay and also for the hadronic signal. In order to reduce systematic uncertainties from these branching fractions, resonant Λ_b^0 semileptonic decays expected to contribute to the $\Lambda_c^+ \mu^-$ sample have been reconstructed in data. These reconstructed decays are then used to estimate the branching fractions of nonresonant Λ_b^0 semileptonic decays with a constraint of the world average of $\mathcal{B}(\Lambda_b^0 \to \Lambda_c^+ \ell^- \bar{\nu}_\ell \text{anything})$ and an estimate of $\mathcal{B}(\Lambda_b^0 \to \Lambda_c^+ \mu^- \bar{\nu}_\mu)$. Note that the estimate of the $\Lambda_b^0 \to \Lambda_c^+ \pi^-$ and $\Lambda_b^0 \to \Lambda_c^+ \mu^- \bar{\nu}_\mu$ branching fractions appear in the estimate of the backgrounds (Sec. VI B). It must be pointed out here that from Table VI, the total contribution of feed-in background is 24.0% and contributes at most this amount to the total uncertainty for this measurement. Furthermore, the ratio of the estimated $\mathcal{B}(\Lambda_b^0 \to \Lambda_c^+ \mu^- \bar{\nu}_\mu)$ to $\mathcal{B}(\Lambda_b^0 \to \Lambda_c^+ \pi^-)$ need not be the same as the final measured result.

Section VII A first presents measurements of the branching fractions of four new Λ_b^0 semileptonic decays relative to that of the $\Lambda_b^0 \to \Lambda_c^+ \mu^- \bar{\nu}_\mu$ decay: $\Lambda_b^0 \to \Lambda_c(2595)^+ \mu^- \bar{\nu}_\mu$, $\Lambda_b^0 \to \Lambda_c(2625)^+ \mu^- \bar{\nu}_\mu$, $\Lambda_b^0 \to \Sigma_c(2455)^0 \pi^+ \mu^- \bar{\nu}_\mu$, and $\Lambda_b^0 \to \Sigma_c(2455)^{++} \pi^- \mu^- \bar{\nu}_\mu$ and then describes the estimation of $\mathcal{B}(\Lambda_b^0 \to \Lambda_c^+ \mu^- \bar{\nu}_\mu)$ and branching fractions of several nonresonant Λ_b^0 semileptonic decays. Section VII B shows that how the p_T distribution of the Λ_b^0 baryon produced from $p\bar{p}$ collisions is significantly different from that of the $\bar{B}^0$ meson and gives the corresponding modification to the ratio, $\sigma_{\Lambda_b^0}/\sigma_{\bar{B}^0}$, with respect to the CDF I measurement [12]. The ratio $\sigma_{\Lambda_b^0}/\sigma_{\bar{B}^0}$ is then used to estimate $\mathcal{B}(\Lambda_b^0 \to \Lambda_c^+ \pi^-)$.

A. Observations of four new Λ_b^0 semileptonic decays and estimates of the Λ_b^0 semileptonic branching fractions

The following Λ_b^0 semileptonic decays are considered in the estimate of $N_{\text{feed}}^{\text{other}\Lambda_b^0}$ in Sec. VI B:

$$\Lambda_b^0 \to \Lambda_c(2595)^+ \mu^- \bar{\nu}_\mu, \qquad \Lambda_b^0 \to \Lambda_c(2625)^+ \mu^- \bar{\nu}_\mu, \qquad \Lambda_b^0 \to \Sigma_c(2455)^0 \pi^+ \mu^- \bar{\nu}_\mu,$$

$$\Lambda_b^0 \to \Sigma_c(2455)^+ \pi^0 \mu^- \bar{\nu}_\mu, \qquad \Lambda_b^0 \to \Sigma_c(2455)^{++} \pi^- \mu^- \bar{\nu}_\mu, \qquad \Lambda_b^0 \to \Lambda_c^+ f_0(980) \mu^- \bar{\nu}_\mu,$$

$$\Lambda_b^0 \to \Lambda_c^+ \pi^+ \pi^- \mu^- \bar{\nu}_\mu (\text{non-resonant}), \qquad \Lambda_b^0 \to \Lambda_c^+ \pi^0 \pi^0 \mu^- \bar{\nu}_\mu (\text{non-resonant}), \qquad \Lambda_b^0 \to \Lambda_c^+ \tau^- \bar{\nu}_\tau.$$

Among the nine decays above, none have been observed previously [50]; only the branching fractions for the $\Lambda_b^0 \to \Lambda_c(2595)^+ \mu^- \bar{\nu}_\mu$ and the $\Lambda_b^0 \to \Lambda_c(2625)^+ \mu^- \bar{\nu}_\mu$ decays have been predicted, but with an uncertainty as large as 100% [45].

In order to reduce the systematic uncertainty on the final measurement coming from the branching ratios of these backgrounds, the following decays are searched for in a larger $\Lambda_c^+ \mu X$ data sample (360 pb^{-1}):
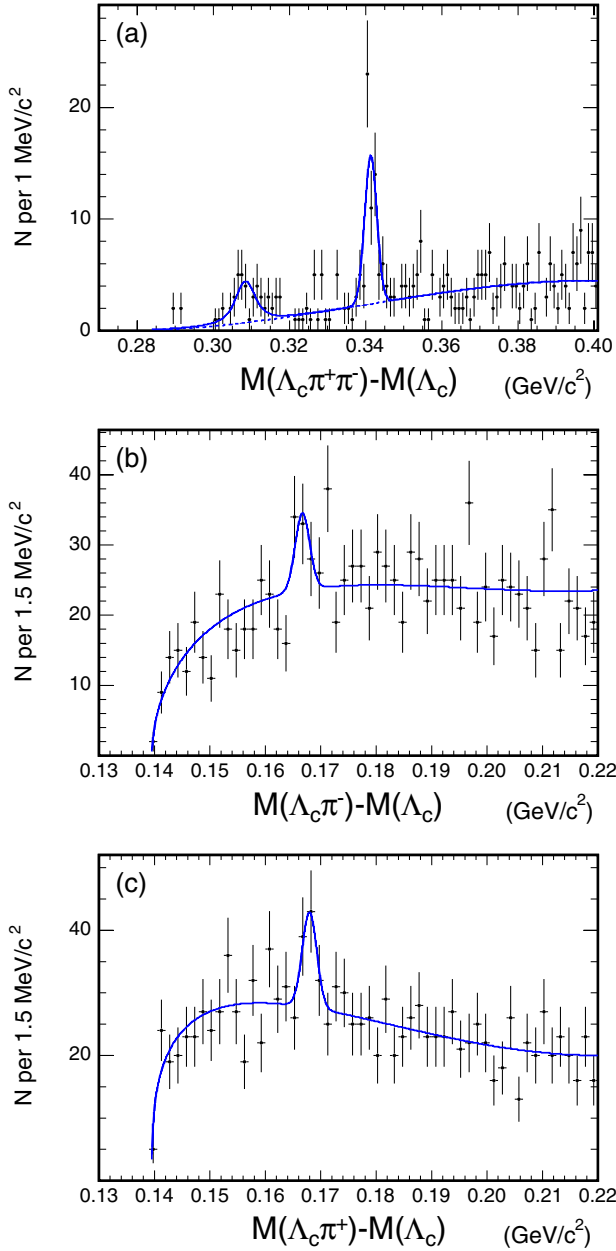
FIG. 9 (color online). The excited-c-baryon candidates that are associated with a μ^-: (a) $\Lambda_c(2595)^+$ and $\Lambda_c(2625)^+$, (b) $\Sigma_c(2455)^0$, and (c) $\Sigma_c(2455)^{++}$. The curves indicate fit results to the spectra of mass differences.

(1) $\Lambda_b^0 \to \Lambda_c(2595)^+ \mu^- \bar{\nu}_\mu X$, where $\Lambda_c(2595)^+$ $(\to \Sigma_c(2455)^{++} \pi^-$, $\to \Sigma_c(2455)^0 \pi^+) \to$ $\Lambda_c^+ \pi^+ \pi^-$.

(2) $\Lambda_b^0 \to \Lambda_c(2625)^+ \mu^- \bar{\nu}_\mu X$, where $\Lambda_c(2625)^+ \to$ $\Lambda_c^+ \pi^+ \pi^-$.

(3) $\Lambda_b^0 \to \Sigma_c(2455)^0 \pi^+ \mu^- \bar{\nu}_\mu X$, where $\Sigma_c(2455)^0 \to$ $\Lambda_c^+ \pi^-$.

(4) $\Lambda_b^0 \to \Sigma_c(2455)^{++} \pi^- \mu^- \bar{\nu}_\mu X$, where $\Sigma_c(2455)^{++} \to \Lambda_c^+ \pi^+$.

All four decays modes above contain $\Lambda_c^+ \pi^+ \pi^- \mu^-$ in the final state. The selection criteria are the same as those for the $\Lambda_c^+ \mu^- X$ sample (see Sec. III), except that two oppositely charged tracks are added to determine the secondary vertex for the $\Lambda_c(2595)^+$ and $\Lambda_c(2625)^+$ modes, and one track is added for the $\Sigma_c(2455)$ modes. In all cases, the pion mass is assumed for each additional track and each track is required to have $p_T > 0.4$ GeV/c. The available four momentum transferred to the daughters in the decays of these c baryons into Λ_c^+ is small. Therefore, the mass differences $M_{\Lambda_c \pi^+ \pi^-} - M_{\Lambda_c}$, $M_{\Lambda_c \pi^-} - M_{\Lambda_c}$, and $M_{\Lambda_c \pi^+} - M_{\Lambda_c}$ have a better resolution than the masses of the c-baryon candidates and are the figure of merit for detecting signal peaks. Figure 9 shows the mass difference distributions, where the numbers of signal events are determined by fitting the mass differences to a Gaussian for the signal and a kinematically motivated line shape for the combinatorial background. Table VII summarizes the signal yields, the corresponding significances, and the fitted mass differences. In this table, contributions of $\Lambda_c(2595)^+$ in the $\Sigma_c(2455)\pi$ modes have been subtracted from the $\Sigma_c(2455)\pi$ modes and the significances of the $\Sigma_c(2455)^0$ and $\Sigma_c(2455)^{++}$ modes are combined. Systematic uncertainties on the yields are determined by varying the functions for the combinatorial background in the fit. This is the first observation of the $\Lambda_b^0 \to \Lambda_c(2625)^+ \mu^- \bar{\nu}_\mu$ decay.

After estimating, with simulation, the acceptance times efficiency of these reconstructed decays relative to that of the $\Lambda_b^0 \to \Lambda_c^+ \mu^- \bar{\nu}_\mu$ decay, and taking into account the false-muon background [52], the relative branching ratios (R_i) are extracted:

TABLE VII. The observed number of signal events, the corresponding significance ($S/\sqrt{S+B}$), and the fitted mass difference in data for each Λ_b^0 semileptonic decay mode.

Mode	Yield	Significance (σ)	ΔM [MeV/c^2]
$\Lambda_c(2595)^+ \mu^- X$	31 ± 8(stat) ± 7(syst)	2.9	308.47 ± 0.99(stat)
$\Lambda_c(2625)^+ \mu^- X$	53 ± 9(stat) ± 5(syst)	5.2	341.39 ± 0.31(stat)
$\Sigma_c(2455)^0 \pi^+ \mu^- X$	16 ± 11(stat) ± 7(syst)		166.72 ± 0.69(stat)
$\Sigma_c(2455)^{++} \pi^- \mu^- X$	26 ± 12(stat) ± 9(syst)		168.01 ± 0.51(stat)
$\Sigma_c(2455)$ modes combined		2.1	

$$R_1 \equiv \frac{\mathcal{B}(\Lambda_b^0 \to \Lambda_c(2595)^+ \mu^- \bar{\nu}_\mu)}{\mathcal{B}(\Lambda_b^0 \to \Lambda_c^+ \mu^- \bar{\nu}_\mu)}$$

$$= 0.126 \pm 0.033(\text{stat}) {}^{+0.047}_{-0.038} (\text{syst}),$$

$$R_2 \equiv \frac{\mathcal{B}(\Lambda_b^0 \to \Lambda_c(2625)^+ \mu^- \bar{\nu}_\mu)}{\mathcal{B}(\Lambda_b^0 \to \Lambda_c^+ \mu^- \bar{\nu}_\mu)}$$

$$= 0.210 \pm 0.042(\text{stat}) {}^{+0.071}_{-0.050} (\text{syst}),$$

$$R_{3,4} \equiv \frac{1}{2}\left[\frac{\mathcal{B}(\Lambda_b^0 \to \Sigma_c(2455)^0 \pi^+ \mu^- \bar{\nu}_\mu)}{\mathcal{B}(\Lambda_b^0 \to \Lambda_c^+ \mu^- \bar{\nu}_\mu)} \right.$$

$$\left. + \frac{\mathcal{B}(\Lambda_b^0 \to \Sigma_c(2455)^{++} \pi^- \mu^- \bar{\nu}_\mu)}{\mathcal{B}(\Lambda_b^0 \to \Lambda_c^+ \mu^- \bar{\nu}_\mu)} \right]$$

$$= 0.054 \pm 0.022(\text{stat}) {}^{+0.021}_{-0.018} (\text{syst}),$$

where the two $\Sigma_c(2455)\pi$ modes are averaged. Assuming isospin symmetry leads to the estimate

$$R_5 \equiv \frac{\mathcal{B}(\Lambda_b^0 \to \Sigma_c(2455)^+ \pi^0 \mu^- \bar{\nu}_\mu)}{\mathcal{B}(\Lambda_b^0 \to \Lambda_c^+ \mu^- \bar{\nu}_\mu)} = R_{3,4} = 0.054.$$

The systematic uncertainties on the relative branching fractions come from variation of background fitting models and uncertainties on the low-momentum pion p_T spectrum and the correction to the reconstruction efficiency.

In order to convert the above measurements of the relative branching fractions into absolute branching fractions, an estimate of $\mathcal{B}(\Lambda_b^0 \to \Lambda_c^+ \mu^- \bar{\nu}_\mu)$ is required. A recent measurement by the DELPHI collaboration reported $(5.0 {}^{+1.1}_{-0.8} (\text{stat}) {}^{+1.6}_{-1.2} (\text{syst}))\%$ for this branching fraction [51]. However, from heavy quark symmetry, the semileptonic decay widths for all b hadrons are expected to be the same. Therefore, semileptonic branching fractions of the b hadrons, $\Gamma^{\text{semi}}/\Gamma^{\text{total}}$, vary only due to their lifetime differences. Since the Λ_b^0 decays to a spin-1/2 Λ_c^+,

TABLE VIII. The Λ_b^0 semileptonic branching fractions for decays that are included in the central value (middle portion) and those that are not (bottom portion). All the numbers in parentheses are estimated uncertainties.

Mode	BR (%)
$\Lambda_b^0 \to \Lambda_c^+ \mu^- \bar{\nu}_\mu$	$7.3 \pm (1.4)$
$\Lambda_b^0 \to \Lambda_c(2595)^+ \mu^- \bar{\nu}_\mu$	$0.9 \pm (0.4)$
$\Lambda_b^0 \to \Lambda_c(2625)^+ \mu^- \bar{\nu}_\mu$	$1.5 \pm (0.6)$
$\Lambda_b^0 \to \Sigma_c(2455)^0 \pi^+ \mu^- \bar{\nu}_\mu$	$0.39 \pm (0.23)$
$\Lambda_b^0 \to \Sigma_c(2455)^+ \pi^0 \mu^- \bar{\nu}_\mu$	$0.39 \pm (0.23)$
$\Lambda_b^0 \to \Sigma_c(2455)^{++} \pi^- \mu^- \bar{\nu}_\mu$	$0.39 \pm (0.23)$
$\Lambda_b^0 \to \Lambda_c^+ \tau^- \bar{\nu}_\tau$	$2.0 \pm (2.0)$
$\Lambda_b^0 \to \Lambda_c^+ f_0(980)\mu^- \bar{\nu}_\mu$	$0 \pm (0.32)$
$\Lambda_b^0 \to \Lambda_c^+ \pi^+ \pi^- \mu^- \bar{\nu}_\mu$	$0 \pm (0.64)$
$\Lambda_b^0 \to \Lambda_c^+ \pi^0 \pi^0 \mu^- \bar{\nu}_\mu$	$0 \pm (0.32)$

contributions from both S and P wave amplitudes are expected. A sum of $\mathcal{B}(\bar{B}^0 \to D^+ \ell^- \bar{\nu}_\ell) + \mathcal{B}(\bar{B}^0 \to D^*(2010)^+ \ell^- \bar{\nu}_\ell)$, where the decays to $D^+[D^*(2010)^+]$ correspond to the S(P) wave amplitudes, yield $(7.33 \pm 0.16)\%$. The number, 7.33%, is then scaled by the world average of the ratio of lifetimes, $\tau_{\Lambda_b^0}/\tau_{\bar{B}^0} = 0.99 \pm 0.10(\text{stat} + \text{syst})$ [7]. The $\mathcal{B}(\Lambda_b^0 \to \Lambda_c^+ \mu^- \bar{\nu}_\mu)$ is estimated to be $(7.3 \pm 0.8 \pm 1.1)\%$, where the first uncertainty arises from the propagation of errors and the second is half of the difference between the above estimate and the DELPHI result [53]. The $\mathcal{B}(\Lambda_b^0 \to \Lambda_c^+ \tau^- \bar{\nu}_\tau)$ can be estimated by scaling $\mathcal{B}(\Lambda_b^0 \to \Lambda_c^+ \mu^- \bar{\nu}_\mu)$ by the ratio of phase space area: $\text{Ph.Sp.}(\Lambda_b^0 \to \Lambda_c^+ \tau^- \bar{\nu}_\tau)/\text{Ph.Sp.}(\Lambda_b^0 \to \Lambda_c^+ \mu^- \bar{\nu}_\mu) = 0.277$. The middle portion of Table VIII summarizes the branching fractions of the Λ_b^0 semileptonic decays discussed above. Uncertainties on the observed Λ_b^0 semileptonic decays and the $\Lambda_b^0 \to \Sigma_c(2455)^+ \pi^0 \mu^- \bar{\nu}_\mu$ decay include uncertainties from the relative branching fraction measurement and uncertainty from the assumed $\mathcal{B}(\Lambda_b^0 \to \Lambda_c^+ \mu^- \bar{\nu}_\mu)$. A 100% systematic uncertainty is also assigned to $\mathcal{B}(\Lambda_b^0 \to \Lambda_c^+ \tau^- \bar{\nu}_\tau)$.

The sum of $\mathcal{B}(\Lambda_b^0 \to \Lambda_c^+ \mu^- \bar{\nu}_\mu)$ and the branching fractions in the middle portion of Table VIII is already larger than the inclusive Λ_b^0 semileptonic branching fraction in the 2008 Particle Data Group (PDG) summary

$$\mathcal{B}(\Lambda_b^0 \to \Lambda_c^+ \ell^- \bar{\nu}_\ell \text{anything}) = 9.9 \pm 2.6\%.$$

The following decays are, therefore, ignored in the central values but will be included in the systematic uncertainty:

$$\Lambda_b^0 \to \Lambda_c^+ f_0(980)\mu^- \bar{\nu}_\mu,$$
$$\Lambda_b^0 \to \Lambda_c^+ \pi^+ \pi^- \mu^- \bar{\nu}_\mu(\text{non-resonant}),$$
$$\Lambda_b^0 \to \Lambda_c^+ \pi^0 \pi^0 \mu^- \bar{\nu}_\mu(\text{non-resonant}).$$

An estimate of these branching fractions is obtained by moving $\mathcal{B}(\Lambda_b^0 \to \Lambda_c^+ \ell^- \bar{\nu}_\ell \text{anything})$ upward by 1σ. The remaining branching fraction is calculated to be

$$(9.9 + 2.6)\% - 7.3\% \times [1 + R_1 + R_2 + 3R_3 + 0.277$$
$$\times \mathcal{B}(\tau^- \to \mu^- \bar{\nu}_\mu \nu_\tau)] \approx 1.3\%.$$

The 1.3% is then attributed to the above decays, which are ignored in the central value. The branching fraction of $\Lambda_b^0 \to \Lambda_c^+ \pi^+ \pi^- \mu^- \bar{\nu}_\mu$ is estimated to be twice that of $\Lambda_b^0 \to \Lambda_c^+ \pi^0 \pi^0 \mu^- \bar{\nu}_\mu$ based on the isospin invariance, and the $f_0(980)$ mode is assumed to have the same branching fraction as that of the $\pi^0 \pi^0$ mode. The bottom portion of Table VIII lists zero central values for these three decays and uses their estimated branching fractions above as the systematic uncertainties on the branching fractions.

B. Modification of $\sigma_{\Lambda_b^0}(p_T > 6.0)/\sigma_{\bar{B}^0}(p_T > 6.0)$ and estimate of $\mathcal{B}(\Lambda_b^0 \to \Lambda_c^+ \pi^-)$

Equation (9) requires $\mathcal{B}(\Lambda_b^0 \to \Lambda_c^+ \pi^-)$ to obtain the ratio $N_{\text{feed}}^{\text{other}\Lambda_b^0}/N_{\text{had}}$. Combining the CDF measurement $G \equiv \frac{\sigma_{\Lambda_b^0}(p_T>6.0)\mathcal{B}(\Lambda_b^0 \to \Lambda_c^+ \pi^-)}{\sigma_{\bar{B}^0}(p_T>6.0)\mathcal{B}(\bar{B}^0 \to D^+ \pi^-)}$ [37], the world average of $\mathcal{B}(\bar{B}^0 \to D^+ \pi^-)$, and the ratio of production cross sections $\rho \equiv \frac{\sigma_{\Lambda_b^0}(p_T>6.0)}{\sigma_{\bar{B}^0}(p_T>6.0)}$, one may express

$$\mathcal{B}(\Lambda_b^0 \to \Lambda_c^+ \pi^-) = \frac{G}{\rho} \mathcal{B}(\bar{B}^0 \to D^+ \pi^-). \quad (10)$$

The ratio of cross sections ρ is calculated from the expression

$$\rho \equiv \frac{\sigma_{\Lambda_b^0}(p_T > 6\,\text{GeV}/c)}{\sigma_{\bar{B}^0}(p_T > 6\,\text{GeV}/c)} = \left(\frac{\sigma_{\Lambda_b^0}}{\sigma_{\bar{B}^0}}\right)^{\text{CDF I}} C_{\mathcal{BR}} C_\alpha C_{p_T}, \quad (11)$$

where $(\sigma_{\Lambda_b^0}/\sigma_{\bar{B}^0})^{\text{CDFI}}$ is the CDF I result 0.236 ± 0.084 [12]. The $C_{\mathcal{BR}}$, C_α, and C_{p_T} are the correction factors to account for differences between the CDF I result and this analysis in the assumed $\mathcal{B}(\Lambda_b^0 \to \Lambda_c^+ \ell^- \bar{\nu}_\ell)$, kinematic acceptance, and requirements on the minimum p_T of Λ_b^0 and $\bar{B}^0$. Each correction factor is explained in the text that follows.

The CDF I analysis used electron-charm final states, such as $H_b \to D^*(2010)^+ e^- X$, $H_b \to D^+ e^- X$, and $H_b \to \Lambda_c^+ e^- X$ to measure the ratio of production cross sections. The branching fraction, $\mathcal{B}(\Lambda_b^0 \to \Lambda_c^+ \ell^- \bar{\nu}_\ell)$, was needed and estimated to be $7.94 \pm 0.39\%$, while this analysis estimates the value to be $7.3 \pm 1.4\%$. The uncertainty 1.4% is dominated by the difference from the DELPHI result (see Sec. VII A). In order to be consistent within this analysis, a correction to the branching fraction $C_{\mathcal{BR}}$ is applied. The value of $C_{\mathcal{BR}}$ is the ratio of 7.94% to 7.3% and found to be 1.09 ± 0.21.

In the CDF I analysis, the Λ_b^0 and $\bar{B}^0$ p_T spectra measured with fully reconstructed decays were not available. In order to extract the signal acceptance and efficiency, the Nason-Dawson-Ellis (NDE) b-quark spectrum [54] followed by the Peterson fragmentation model [55] was used at CDF I to obtain the p_T distributions of b hadrons in simulation [56]. The two-track trigger allows CDF II to collect large samples of fully reconstructed b-hadron decays, such as $\Lambda_b^0 \to \Lambda_c^+ \pi^-$ and $\bar{B}^0 \to D^+ \pi^-$, and to compare the p_T distributions in data with those from the NDE + Peterson model. The Λ_b^0 and the $\bar{B}^0$ p_T spectra from the NDE + Peterson model are found to be harder (more b hadrons at higher p_T) than those measured in data, which indicates an over estimate of acceptance in the CDF I analysis, particularly for the Λ_b^0 decays. The acceptance correction factor C_α is the ratio of acceptances using generator-level simulations with inputs from the measured p_T spectra (identical to those described in Sec. IV A) and
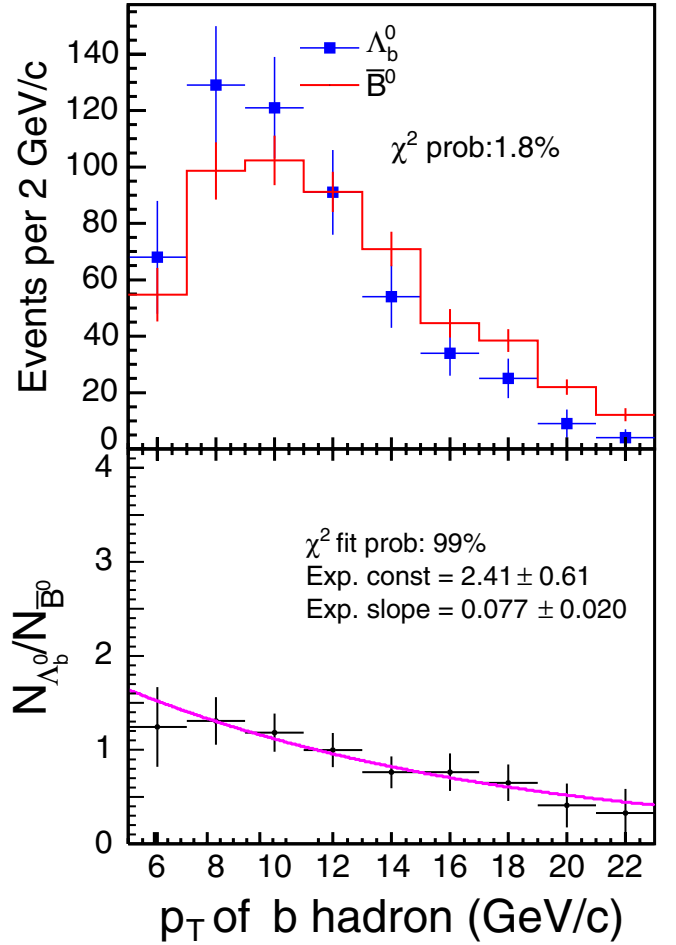

FIG. 10 (color online).   Comparison of the reconstructed Λ_b^0 and $\bar{B}^0$ p_T spectra in data. The negative slope (3–4σ away from zero) of the ratio of Λ_b^0 to $\bar{B}^0$ histograms indicates that the p_T (Λ_b^0) distribution is softer (more b hadrons at lower p_T) than the p_T ($\bar{B}^0$) distribution. In order to have a fair comparison of p_T spectra, the same requirements are applied to the $\bar{B}^0$ and Λ_b^0 candidates [58], while Fig. 3 has different selections for the $\bar{B}^0$ and Λ_b^0. Nevertheless, the p_T spectra, used as inputs for the correction factors C_α and C_{p_T}, have been corrected for acceptance and efficiency and are identical to those described in Sec. IV A.

from the NDE + Peterson model

$$C_\alpha = \alpha_R^{\text{data-based}}/\alpha_R^{\text{NDE+Peterson}}, \quad (12)$$

where α_R is the ratio of the kinematic acceptances of Λ_b^0 and $\bar{B}^0$. The value of the correction factor is found to be $C_\alpha = 1.81^{+0.42}_{-0.22}$ for the CDF I kinematic requirements [57]. The uncertainty comes from the uncertainties on the measured shapes of the Λ_b^0 and $\bar{B}^0$ p_T distributions in data.

The last correction is due to a difference in the minimum p_T requirements between the CDF I analysis $[p_T(H_b) > 10\,\text{GeV}/c]$ and this analysis $[p_T(H_b) > 6\,\text{GeV}/c]$. By applying the same requirements to the $\Lambda_b^0 \to \Lambda_c^+ \pi^-$ and $\bar{B}^0 \to D^+ \pi^-$ decays reconstructed in the two-track trigger

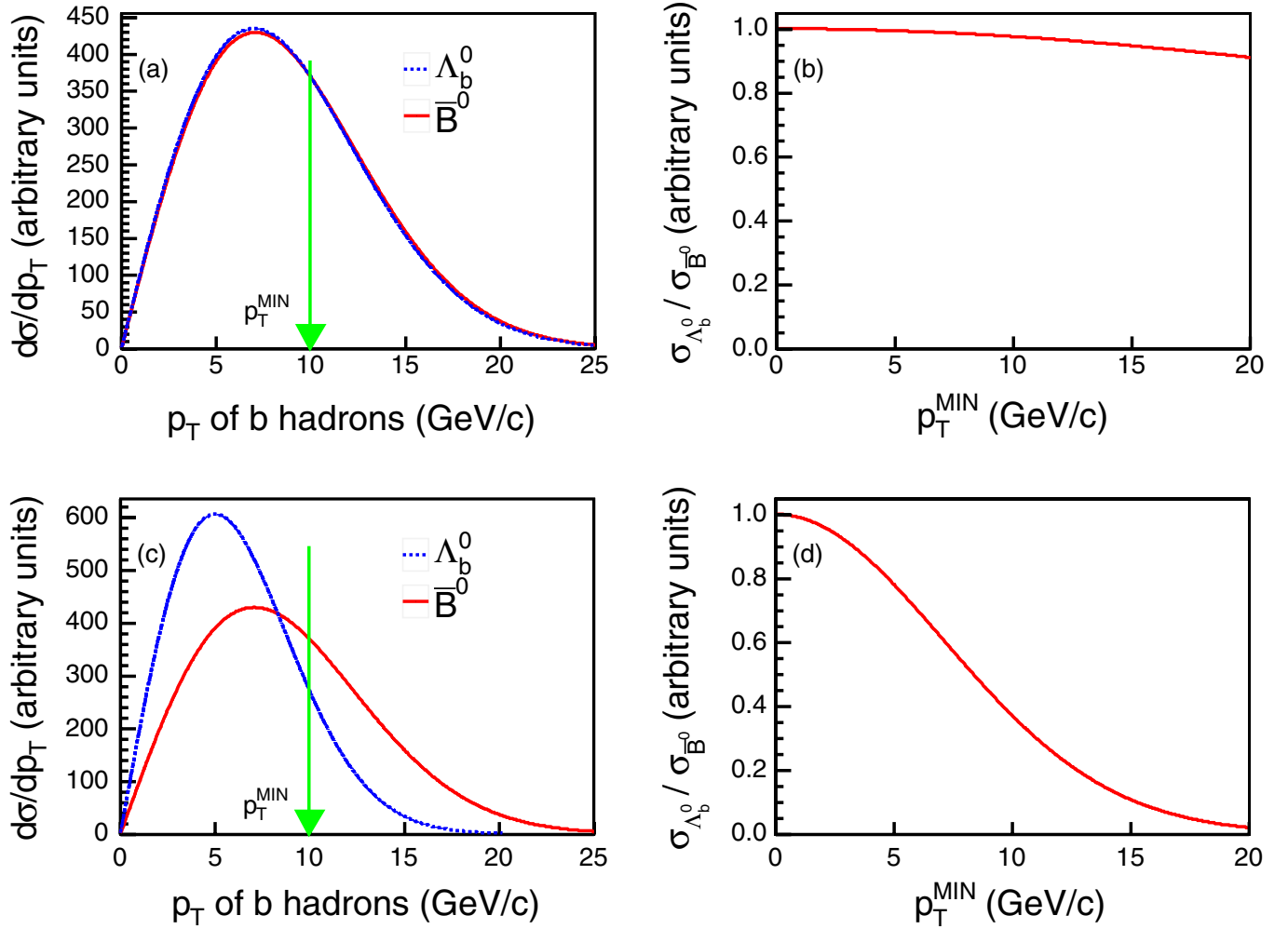FIG. 11 (color online).   Examples of the Λ_b^0 and $\bar{B}^0$ p_T spectra [(a), (c)] and the dependence of the production cross-section ratio on the minimum p_T requirements, p_T^{MIN} [(b), (d)]. Figures 11(a) and 11(b) show the case where both hadrons have similar spectra; the ratio of the integrated areas underneath the spectra, from p_T^{MIN} and above, depends little on the value of p_T^{MIN}. Figures 11(c) and 11(d) show that the Λ_b^0 p_T spectrum is significantly softer (more b hadrons at lower p_T) than the $\bar{B}^0$ p_T spectrum; the ratio of the integrated areas depends strongly on the value of p_T^{MIN}.

data, Fig. 10 shows that the Λ_b^0 p_T spectrum is significantly softer (more b hadrons at lower p_T) than that of the $\bar{B}^0$ [58]. Figure 11 illustrates the dependence of the ratio of

cross sections on the minimum p_T requirements, for a small [(a)] and a large [(c)] difference between the Λ_b^0 and $\bar{B}^0$ p_T spectra; the scenario in Fig. 11(c) is what has been observed in data. A correction factor C_{p_T} is required:

$$C_{p_T} = \frac{N_{\Lambda_b^0}(p_T > 6)}{N_{\bar{B}^0}(p_T > 6)} \bigg/ \frac{N_{\Lambda_b^0}(p_T > 10)}{N_{\bar{B}^0}(p_T > 10)}. \qquad (13)$$

The C_{p_T} is obtained using the generator-level simulation with inputs from the measured p_T spectra of Λ_b^0 and $\bar{B}^0$ (identical to those described in Sec. IVA). The value of the correction factor is found to be $C_{p_T} = 1.31 \pm 0.11$, where the uncertainty also comes from the uncertainties on the measured p_T distributions in data.

After applying corrections $C_{\mathcal{BR}}$, C_α, and C_{p_T}, ρ is calculated to be

TABLE IX.   Parameters for calculating $\mathcal{B}(\Lambda_b^0 \to \Lambda_c^+ \pi^-)$. Text in parentheses indicate the sources of uncertainty: the data sample size, general systematics, shapes of measured p_T distributions, and difference from DELPHI's $\mathcal{B}(\Lambda_b^0 \to \Lambda_c^+ \ell^- \bar{\nu}_\ell)$.

Parameter	Value
G	$0.82 \pm 0.25(\mathrm{stat} \oplus \mathrm{syst}) \pm 0.06(p_T)$
CDF I $\frac{\sigma_{\Lambda_b^0}}{\sigma_{\bar{B}^0}}$	$0.236 \pm 0.084(\mathrm{stat} \oplus \mathrm{syst})$
$C_{\mathcal{BR}}$	$1.09 \pm 0.21(\mathrm{DELPHI})$
C_α	$1.81 {}^{+0.42}_{-0.22}(p_T)$
C_{p_T}	$1.31 \pm 0.11(p_T)$
$\mathcal{B}(\bar{B}^0 \to D^+ \pi^-)$	$(0.268 \pm 0.013)\%$

$$\rho = 0.61 \pm 0.22(\text{CDF I}) \pm 0.12(\text{DELPHI}) {}^{+0.21}_{-0.12}(p_T),$$

where the uncertainties are from the uncertainty on the CDF I measurement of $\sigma_{\Lambda_b^0}/\sigma_{\bar{B}^0}$, the difference between the estimated $\mathcal{B}(\Lambda_b^0 \to \Lambda_c^+ \ell^- \bar{\nu}_\ell)$ for this analysis and that measured by DELPHI, and the uncertainties on the measured shapes of the Λ_b^0 and $\bar{B}^0$ p_T distributions. The value of ρ is also consistent with the result from [59]. The $\mathcal{B}(\Lambda_b^0 \to \Lambda_c^+ \pi^-)$ is then extracted following Eq. (10), with the input of the parameters listed in Table IX, and is found to be

$$\mathcal{B}(\Lambda_b^0 \to \Lambda_c^+ \pi^-)$$

$$= (0.36 \pm 0.07(\text{DELPHI}) {}^{+0.05}_{-0.07}(p_T) {}^{+0.23}_{-0.15}(\text{syst}^{\text{other}}))\%.$$

The "syst$^{\text{other}}$" uncertainty includes the uncertainty on the CDF I measurement, and the uncertainty on G, which is dominated by the world average of $\mathcal{B}(\Lambda_c^+ \to pK^- \pi^+)$ [60]. This evaluation of $\mathcal{B}(\Lambda_b^0 \to \Lambda_c^+ \pi^-)$ differs from that of the Particle Data Group due to the differing production spectrum of the Λ_b^0 relative to the $\bar{B}^0$ as described in the previous text [61]. The estimated value is in good agreement with the values predicted by Leibovich *et al.* [10], $(0.54 \pm 0.18)\%$, and Cheng [11], $(0.50 \pm 0.17)\%$, which gives confidence in the procedure described above. The estimated $\mathcal{B}(\Lambda_b^0 \to \Lambda_c^+ \pi^-)$ has been used in Eq. (9) to estimate $N_{\text{feed}}^{\text{other}\Lambda_b^0}/N_{\text{had}}$ (see Sec. VI B).

VIII. SYSTEMATIC UNCERTAINTIES

The Λ_b^0 relative branching fractions (R), with statistical uncertainty only, can now be extracted from Eq. (1):

$$R = \frac{\mathcal{B}(\Lambda_b^0 \to \Lambda_c^+ \mu^- \bar{\nu}_\mu)}{\mathcal{B}(\Lambda_b^0 \to \Lambda_c^+ \pi^-)} = 16.6 \pm 3.0(\text{stat}).$$

A check of internal consistency is performed by dividing the data and simulation samples into several groups of independent subsets, according to the time period, vertex position, ct and p_T of the Λ_c^+ candidate, ct^* and p_T of the Λ_b^0 candidate, etc. Figure 12 shows that the R of each subset for each group is consistent with those of the other subsets in the same group. The result of this check also proves that there is no major problem in the detector, trigger, reconstruction, or simulation, which produces bias in the measurement.

The systematic uncertainties on R may be classified as internal and external. Internal uncertainties are those that affect the final measurement through their effects on the observed yields, the numbers of false-muon and $b\bar{b}/c\bar{c}$ background events, and the modeling of acceptance times efficiency. External uncertainties are those from production fractions and branching ratios, which are used in Eqs. (9) and (A1) to determine N_{feed}. The input value for each systematic source is varied by $\pm 1\sigma$, where σ is the
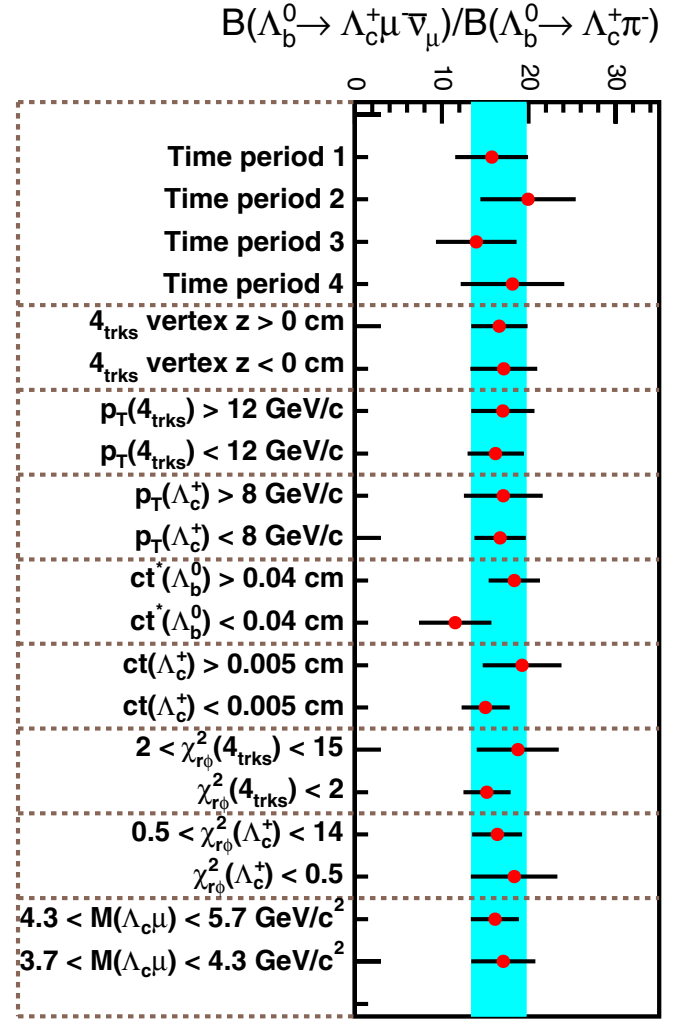

FIG. 12 (color online). Internal-consistency check of the Λ_b^0 relative branching fractions. The uncertainty on each point is statistical only. Each independent group is separated by a horizontal dashed line. The solid bands indicate the relative branching fractions with their statistical uncertainties from the complete, undivided samples.

uncertainty on the input value. The resulting difference in R from the central value is the systematic uncertainty. The following text describes how the uncertainty for each systematic source is obtained.

A. Internal systematic uncertainties

The signal yields N_{had} and N_{inclsemi} are affected by the background functions, which describe the mass spectra of misidentified or partially reconstructed decays of b hadrons. The systematic uncertainty on the $M_{\Lambda_c \pi}$ fitting model is estimated by changing the relative fraction of the contributing decays in each background function. The fragmentation fraction and the branching ratio of every contributing decay are varied independently according to their uncertainties by $\pm 1\sigma$ [62]. After combining these

contributing decays according to their modified fragmentation fractions and branching ratios and producing a new simulated mass spectrum, the parameter values for each background function are redetermined. The $M_{\Lambda_c \pi}$ spectrum in data is refit again using the new background function and the systematic uncertainty is taken from the deviation of the $\Lambda_b^0 \to \Lambda_c^+ \pi^-$ yield from the central value. Correlations between different parameters have been taken into account. For the fitting of $M_{pK\pi}$, since no branching ratio assumptions are made, no systematic uncertainty is assigned.

The uncertainty on the false-muon estimate is driven by 1) the size of the sample used to measure the false-muon probability, 2) the fit to the weighted Λ_c mass distributions, and 3) the probability of a hadron track being a p, a K, or a π, which is determined from simulation. The resulting changes in the number of false-muon events from the three sources above are added in quadrature and already listed in Table IV. The size of the $b\bar{b}/c\bar{c}$ background contribution has a 100% systematic uncertainty, due to a lack of knowledge of the relative $b\bar{b}/c\bar{c}$ production rates between different processes [63] and the 10–50% discrepancy of the inclusive hadron production cross section between PYTHIA and data (Appendix C).

The uncertainty on the modeling of acceptance times efficiency for signal and background processes arises from: the size of simulation samples, the shapes of the measured Λ_b^0 and $\bar{B}^0$ p_T spectra, the efficiency scale factors of the Λ_b^0 semileptonic decay model/muon reconstruction/XFT trigger (see Sec. IV), the amount of material in the detector simulation, the Λ_b^0 lifetime, the Λ_c^+ Dalitz structure, and the Λ_b^0 and Λ_c^+ polarizations. The Λ_b^0 and $\bar{B}^0$ p_T distributions used as inputs for BGENERATOR are varied according to the uncertainties on the exponential slopes of data-to-MC ratios (shown in Fig. 3). The uncertainties on the efficiency scale factors for the Λ_b^0 semileptonic decay model/muon reconstruction/XFT trigger are listed in Table II. The uncertainty from the detector material is obtained by switching off the hadronic interaction in the detector simulation and multiplying the efficiency difference from the central value by 25%. The 25% is a quadrature sum of the 15% underestimate in the amount of material and the 20% difference between the GHEISHA and FLUKA models [26,64]. The Λ_b^0 lifetime used as an input for BGENERATOR is varied according to the uncertainty on the world average [7]. The effect of the Λ_c^+ Dalitz structure is studied by varying branching fractions of the resonant and nonresonant $\Lambda_c^+ \to pK^-\pi^+$ decays measured by E791 [65] by their uncertainties. The unpolarized Λ_b^0 and Λ_c^+ simulation samples have been used to obtain the central values of acceptance times efficiency of Λ_b^0 decays. For the systematics study, angular distributions in simulation are reweighted according to all combinations of the Λ_b^0 and Λ_c^+ polarization states: ± 1, assuming the extreme scenario, where the Λ_b^0 and Λ_c^+

baryons are 100% polarized. The difference in the kinematic acceptances between the simulation with reweighted angular distributions and the simulation with unpolarized Λ_b^0 and Λ_c^+ is used to assign a systematic uncertainty on R.

B. External systematic uncertainties

There are two types of external systematic uncertainties. The first type is denoted as the "PDG" uncertainty and includes uncertainties on: the world average of $\mathcal{B}(\bar{B}^0 \to D^+\pi^-)$, the CDF I measurement of $\sigma_{\Lambda_b^0}/\sigma_{\bar{B}^0}$, the CDF measurement of $\frac{\sigma_{\Lambda_b^0}(p_T>6.0)\mathcal{B}(\Lambda_b^0 \to \Lambda_c^+\pi^-)}{\sigma_{\bar{B}^0}(p_T>6.0)\mathcal{B}(\bar{B}^0 \to D^+\pi^-)}$, and the measured branching fractions of the four new Λ_b^0 semileptonic decays relative to that of the $\Lambda_b^0 \to \Lambda_c^+\mu^-\bar{\nu}_\mu$ decay (see Sec. VII A). The second type is denoted as the estimated from theory ("EBR") uncertainty and comes from unmeasured branching fractions estimated from theory. A 5% uncertainty is assigned to the estimated branching fractions of the excited c-hadron decays [43]. A 100% uncertainty is assigned to the other unobserved b-hadron decays to cover the wide range of theoretical predictions [44]. Note that the uncertainty on the estimated $\mathcal{B}(\Lambda_b^0 \to \Lambda_c^+\mu^-\bar{\nu}_\mu)$ does not affect the final measurement because it affects the branching fractions of $\Lambda_b^0 \to \Lambda_c^+\pi^-$ and other Λ_b^0 semileptonic decays in the same way so that any change completely cancels.

C. Summary

The fractional systematic and statistical uncertainties on the Λ_b^0 relative branching fraction are summarized in Table X. The leading sources of internal systematic uncertainty are the mass fitting model, the shapes of the mea-

TABLE X. Summary of statistical and systematic uncertainties for the Λ_b^0 mode. The σ_R is the uncertainty on the Λ_b^0 relative branching fraction, R.

Source	$\frac{\sigma_R}{R}$ (%)
Mass fitting	$^{+3.8}_{-3.1}$
False μ	1.0
$b\bar{b}/c\bar{c}$ background	0.3
Simulation sample size	2.0
b-hadron p_T spectrum	$^{+0.0}_{-2.9}$
Λ_b^0 decay model	3.3
XFT/CMU efficiency scale factor	0.4
detector material	1.3
Λ_b^0 lifetime	0.3
Λ_c^+ Dalitz	0.4
Λ_b^0, Λ_c^+ polarizations	2.2
Sum of internal	6.3
PDG	$^{+15.6}_{-20.4}$
Estimated branching fractions	2.1
Statistical	17.8

sured p_T spectra, and the Λ_b^0 semileptonic decay model. The PDG uncertainty is dominated by the world average of $\mathcal{B}(\Lambda_c^+ \to pK^-\pi^+)$ and the CDF I measurement of $\sigma_{\Lambda_b^0}/\sigma_{\bar{B}^0}$, which have been used to extract $\mathcal{B}(\Lambda_b^0 \to \Lambda_c^+\pi^-)$ [66]. The uncertainty on $\mathcal{B}(\Lambda_c^+ \to pK^-\pi^+)$ may be reduced in the near future by more precise measurements proposed by Dunietz [67] and Migliozzi [68]. The EBR uncertainty is dominated by the branching fractions of nonresonant $\Lambda_b^0 \to \Lambda_c^+ \pi^+ \pi^- \mu^- \bar{\nu}_\mu$ and $\Lambda_b^0 \to \Lambda_c^+ \pi^0 \pi^0 \mu^- \bar{\nu}_\mu$ decays. The Λ_b^0 relative branching fraction with complete uncertainties is found to be

$$\frac{\mathcal{B}(\Lambda_b^0 \to \Lambda_c^+ \mu^- \bar{\nu}_\mu)}{\mathcal{B}(\Lambda_b^0 \to \Lambda_c^+ \pi^-)}$$

$$= 16.6 \pm 3.0(\text{stat}) \pm 1.0(\text{syst}) {}^{+2.6}_{-3.4}(\text{PDG}) \pm 0.3(\text{EBR}).$$

The uncertainties are from statistics (stat), internal systematics (syst), world averages of measurements published by the PDG or subsidiary measurements in this analysis (PDG), and unmeasured branching fractions estimated from theory (EBR), respectively.

IX. MEASUREMENTS OF THE $\bar{B}^0$ RELATIVE BRANCHING FRACTIONS

The same analysis technique used for the Λ_b^0 samples is applied to the $\bar{B}^0$ decays. This section only describes the difference in the details of event reconstruction, yield determination, and background estimation and summarizes the systematic uncertainties.

A. Reconstruction of the $\bar{B}^0$ candidates

The following decay modes are reconstructed in the data collected with the two-track trigger:
 (1) $\bar{B}^0 \to D^+\pi^-$ and $D^+\mu^-X$, where $D^+ \to K^-\pi^+\pi^+$.
 (2) $\bar{B}^0 \to D^*(2010)^+\pi^-$ and $D^*(2010)^+\mu^-X$, where $D^*(2010)^+ \to D^0\pi^+$, $D^0 \to K^-\pi^+$.

The requirements on the $\bar{B}^0$ and Λ_b^0 candidates are kept as similar as possible.

For the reconstruction of $D^+ \to K^-\pi^+\pi^+$ decays, the pion mass is assigned to the two positively charged tracks and the kaon mass to the negatively charged track. The invariant mass of the three tracks ($M_{K\pi\pi}$), as computed by a three-track kinematic fit, is required to be in the range 1.74–2.00 GeV/c^2. The $D^*(2010)^+$ signals are reconstructed by first looking for $D^0 \to K^-\pi^+$ candidates. A two-track kinematic fit determines the D^0 vertex, and the invariant mass of the two tracks ($M_{K\pi}$) is required to be within the range 1.820–1.906 GeV/c^2. Then, the pion mass is assigned to an additional positively charged track. This third track is expected to have a low p_T due to the small four-momentum transfer in the $D^*(2010)^+ \to D^0\pi^+$

TABLE XI. Optimized requirements for reconstructing the $\bar{B}^0 \to D^+\pi^-$, $D^+\mu^-X$, $\bar{B}^0 \to D^*(2010)^+\pi^-$, and $D^*(2010)^+\mu^-X$ decays.

$\bar{B}^0 \to D^+\pi^-$ $D^+\mu^-X$		$\bar{B}^0 \to D^*(2010)^+\pi^-$ $D^*(2010)^+\mu^-X$	
$p_T(\pi^-, \mu^-)$	>2 GeV/c	$p_T(\pi^-, \mu^-)$	>2 GeV/c
$p_T(D^+)$	>5 GeV/c	$p_T(D^*(2010)^+)$	>5 GeV/c
$p_T(4_{\text{trks}})$	>6 GeV/c	$p_T(4_{\text{trks}})$	>6 GeV/c
$\chi_{r\phi}^2(D^+)$	<14	$\chi_{r\phi}^2(D^0)$	<16
$\chi_{r\phi}^2(4_{\text{trks}})$	<15	$\chi_{r\phi}^2(4_{\text{trks}})$	<17
$ct(D^+)$	>-30 μm	$ct(D^0)$	>-70 μm
$ct^*(\bar{B}^0)$	>200 μm	$ct^*(\bar{B}^0)$	>200 μm

decay. However, a minimum p_T requirement of 0.5 GeV/c is imposed to ensure a good measurement of the pion track. For the $D^*(2010)^+$ candidate, the mass difference, $M_{K\pi\pi} - M_{K\pi}$, must be within the range 0.14–0.18 GeV/c^2.

In order to form a $\bar{B}^0$ candidate, the D^+ and $D^*(2010)^+$ candidates are then combined with an additional negatively charged track, which satisfies the requirements described in Sec. III. After the four-track kinematic fit, the values of $M_{K\pi\pi}$ for the D^+ and $M_{K\pi\pi} - M_{K\pi}$ for the $D^*(2010)^+$ must be in the range 1.8517–1.8837 GeV/c^2 and 0.143–0.148 GeV/c^2 for the hadronic candidates; 1.74–2.00 GeV/c^2 and 0.14–0.18 GeV/c^2 for the inclusive semileptonic candidates. The four-track invariant mass, $M_{D\mu}$ and $M_{D^*\mu}$ must be within 3.0–5.3 GeV/c^2 for the semileptonic decays. Selection criteria for the following variables: p_T of the fourth $\bar{B}^0$-candidate track $[p_T(\pi^-, \mu^-)]$, p_T of D^+, p_T of $D^*(2010)^+$, and combined p_T of the four-track system, $\chi_{r\phi}^2$ of the D^+ and D^0 vertex fits, and $\chi_{r\phi}^2$ of the four-track kinematic fits, ct of the D^+ and D^0 candidates, and ct^* of the $\bar{B}^0$ candidate, are also optimized using the simulation and data of hadronic modes, as described for the Λ_b^0 sample. Table XI lists the optimized values.

B. Determination of the $\bar{B}^0$ yields

Figure 13(a) shows the fit result for the $M_{D\pi}$ spectrum. The $\bar{B}^0 \to D^+\pi^-$ yield returned by the fit is 579 ± 30. The signal peak at $M_{D\pi} \approx 5.3$ GeV/c^2 and the combinatorial background are described by a Gaussian function and an exponential, respectively. The ratio of the number of doubly Cabibbo-suppressed decays relative to that of the signal mode $N_{DK}/N_{D\pi}$ is Gaussian constrained to the value for the relative branching ratio from the PDG, convoluted with the efficiency from the full simulation. The constrained value is 0.073 ± 0.023. Backgrounds from the other b-hadron decays consist of the following decays: The $\bar{B}_s^0 \to D_s^+\pi^-$ decays, where $D_s^+ \to \phi(1020)\pi^+$, $\phi(1020) \to K^+K^-$ and the pion mass is assigned to one of the kaons, appear as a peak at around 5.31 GeV/c^2.
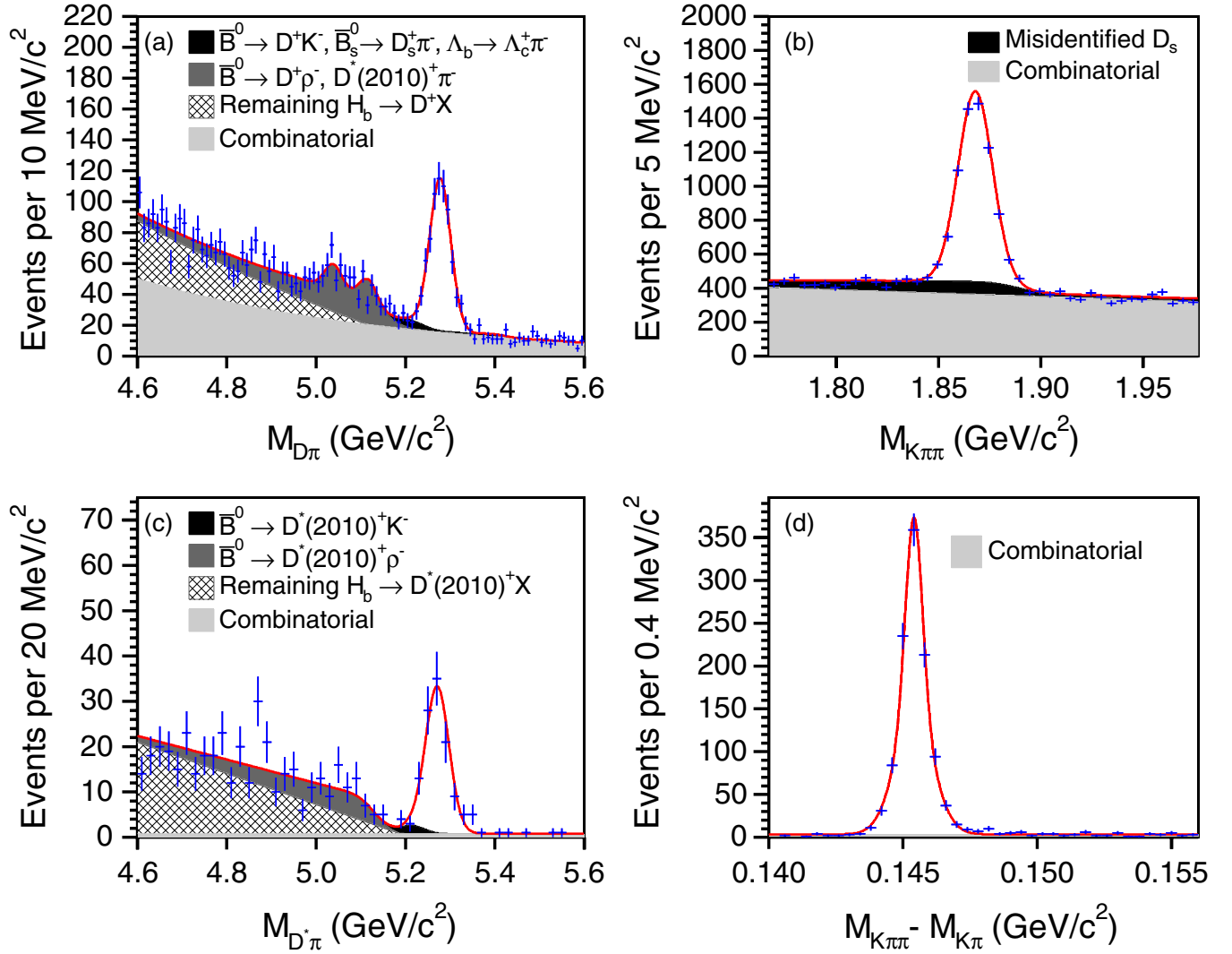
FIG. 13 (color online). Results (curve) of the unbinned, extended likelihood fits for determining the numbers of $\bar{B}^0$ candidates: the hadronic modes (a) $M_{D\pi}$ and (c) $M_{D^*\pi}$, and inclusive semileptonic modes (b) $M_{K\pi\pi}$ and (d) $M_{K\pi\pi} - M_{K\pi}$. The filled histograms indicate various backgrounds.

Misreconstructed $\Lambda_b^0 \to \Lambda_c^+ \pi^-$ decays, where $\Lambda_c^+ \to pK^-\pi^+$ and the pion mass is assigned to the proton, form a broad peak around 5.4 GeV/c^2. The backgrounds from the $\bar{B}^0 \to D^+ K^-$, $\bar{B}_s^0 \to D_s^+ \pi^-$, and $\Lambda_b^0 \to \Lambda_c^+ \pi^-$ decays are combined and indicated by the black filled region. The $\bar{B}^0 \to D^+ \rho^-$ decays, where $\rho^- \to \pi^0 \pi^-$ and the π^0 is not reconstructed in the event, have a triangular mass distribution, which peaks at ≈ 5.1 GeV/c^2. The $\bar{B}^0 \to D^*(2010)^+ \pi^-$ decays, where $D^*(2010)^+ \to D^+ \pi^0$ and the π^0 is not reconstructed, have a double-peak structure. This structure is consistent with the spin-1 $D^*(2010)^+$ being polarized. This polarization results in the π^0 from the $D^*(2010)^+$ decay having a momentum preferentially parallel or antiparallel to the momentum of $D^*(2010)^+$. The $\bar{B}^0 \to D^+ \rho^-$ and $\bar{B}^0 \to D^*(2010)^+ \pi^-$ backgrounds are combined and indicated by the dark-gray filled region. The remaining partially reconstructed decays of b hadrons

$H_b \to D^+ X$ have a monotonically falling distribution (hatched region). The determination of the background shapes and the estimation of systematic uncertainty are similar to those in the Λ_b^0 system.

Figure 13(b) shows the fit result for the $M_{K\pi\pi}$ spectrum for events with muons. The inclusive $D^+ \mu^- X$ yield returned by the fit is 4720 ± 100. The signal peak at $M_{K\pi\pi} \approx 1.9$ GeV/c^2 is described by a Gaussian function. The combinatorial background (light-gray filled region) is parameterized by a first-order polynomial. Misidentified $H_b \to D_s^+ \mu^- X$ decays (black filled region), where the mass of at least one D_s^+ daughter has been misassigned, appear in the mass window of interest. The dominant contributing D_s^+ decay modes are $D_s^+ \to \phi(1020)\pi^+$, $D_s^+ \to K^{*0} K^+$, and $D_s^+ \to$ nonresonant $K^+ K^- \pi^+$. The function parameters describing the shape of misidentified D_s^+ spectrum are obtained from the $\bar{B}_s^0 \to D_s^+ \mu^- \bar{\nu}_\mu$ simu-

lation; in this simulation, the D_s^+'s are forced to decay only to the final states, which can yield misidentified mass in the $M_{K\pi\pi}$ window. The number of the D_s^+ background events is constrained to the estimated number of $H_b \to D_s^+ \mu^- X$ events in the data ($N_{D_s\mu}$) as described below. First, the following decay mode is reconstructed in the data: $H_b \to D_s^+ \mu^- X$, where $D_s^+ \to \phi(1020)\pi^+$ and $\phi(1020) \to K^+ K^-$. The narrow $\phi(1020)$ resonance provides a good handle for removing the combinatorial background of D_s^+. Second, the fraction from the $\phi(1020)\pi^+$ mode relative to all contributing D_s^+ decays ($R_{\phi\pi}$) is extracted using the world averages of the D_s^+ branching ratios, and the acceptance times efficiency determined from the full simulation. Then, $N_{D_s\mu}$ is simply the yield of the $\phi(1020)\pi^+\mu^-$ mode in data divided by $R_{\phi\pi}$. The value of $N_{D_s\mu}$ for the constraint is 1812 ± 160. The systematic uncertainty is assigned by independently varying the ratio of the branching fraction of one specific D_s^+ decay relative to that of the $D_s^+ \to \phi(1020)\pi^+$ decay by $\pm 1\sigma$, since the branching fractions of all D_s decays have been measured relative to that of the $\phi(1020)\pi^+$ mode [7].

Figure 13(c) shows the fit result for the $M_{D^*\pi}$ spectrum. The $\bar{B}^0 \to D^*(2010)^+\pi^-$ yield returned by the fit is 106 ± 11. The analysis of the $D^*(2010)^+\pi^-$ signal and backgrounds is similar to that in the $D^+\pi^-$ mode. The only difference is that extra constraints are imposed due to the small size of the $D^*(2010)^+\pi^-$ sample. The width of the signal Gaussian $\sigma_{D^*\pi}$, the ratio $\frac{N_{D^*K}}{N_{D^*\pi}}$, and the ratio of backgrounds $N_{D^*\rho}/(N_{D^*\rho} + N_{H_b\to\text{remaining}D^*X})$, are constrained to 0.0259 ± 0.0012 GeV/c^2, 0.071 ± 0.019, and 0.242 ± 0.008, respectively. The systematic uncertainty is assessed in the same way as in the Λ_b^0 and the $D^+\pi^-$ modes.

Figure 13(d) shows the fit result for the $M_{K\pi\pi} - M_{K\pi}$ spectrum for events with muons. The likelihood fit for the $D^*(2010)^+\mu^- X$ mode is performed in the mass window $M_{K\pi\pi} - M_{K\pi} = 0.14 - 0.18$ GeV/c^2, whereas Fig. 13(d) shows a more restricted mass range near the signal peak. The inclusive $D^*(2010)^+\mu^- X$ yield returned by the fit is 1059 ± 33. The signal peak at $M_{K\pi\pi} - M_{K\pi} \approx 0.145$ GeV/c^2 is modeled by two Gaussian distributions with a common mean and different widths. The combinatorial background (light-gray filled region) is parameter-

TABLE XII. Observed number of events in each decay mode determined from the unbinned, extended likelihood fit, χ^2/NDF, and the corresponding probability computed to indicate quality of the fit.

Mode	Yield	χ^2/NDF	Prob (%)
$\bar{B}^0 \to D^+\pi^-$	579 ± 30	80/91	78.9
$D^+\mu^- X$	4720 ± 100	47/31	3.40
$\bar{B}^0 \to D^*(2010)^+\pi^-$	106 ± 11	21/12	5.40
$D^*(2010)^+\mu^- X$	1059 ± 33	108/93	14.1

ized by a constant, while the background from other b-hadron decays with misidentified c-hadron daughters is found to be negligible. The size of the combinatorial background is very small due to the requirement that $M_{K\pi}$ is consistent with the world average D^0 mass, the minimum requirement on the mass $M_{D^*\mu}$, and the minimum requirements on the p_T and the number of SVX hits for the low-momentum pion from the $D^*(2010)^+$ decay (Sec. IX A). The fitting function for this spectrum does not use any branching ratios and no systematic uncertainty is assigned.

Table XII summarizes the $\bar{B}^0$ hadronic and inclusive semileptonic yields and the χ^2 probability of corresponding fits. Each model describes the data well, as indicated by the χ^2 probability.

C. Compositions of the inclusive semileptonic data

The procedures for estimating the backgrounds to the $\bar{B}^0 \to D^+\mu^-\bar{\nu}_\mu$ and $\bar{B}^0 \to D^*(2010)^+\mu^-\bar{\nu}_\mu$ decays are similar to those described in Sec. VI. The following describes the differences when estimating the feed-in background N_{feed} in the $\bar{B}^0$ system. Unlike the Λ_b^0 system, many decays of b and c mesons have been measured by other experiments [31–34], and serve as inputs to the EVTGEN decay package. In addition, EVTGEN also includes estimates of branching fractions for decay modes that have not yet been measured. Therefore, all possible decays that may contribute to the N_{feed} in the $\bar{B}^0$ control samples are studied using the PDG summary and the default EVTGEN decay table [7,30].

The feed-in backgrounds to the $\bar{B}^0 \to D^+\mu^-\bar{\nu}_\mu$ and $\bar{B}^0 \to D^*(2010)^+\mu^-\bar{\nu}_\mu$ signals fall into two categories:

(1) Semileptonic decays of $\bar{B}^0/B^-/\bar{B}_s^0$, which include either additional particles (e.g., $\bar{B}^0 \to D^+\pi^0\mu^-\bar{\nu}_\mu$) or a higher mass c meson with subsequent decay into the c-meson signal [e.g., $\bar{B}^0 \to D^*(2010)^+\mu^-\bar{\nu}_\mu$, $D^*(2010)^+ \to D^+\pi^0$].

(2) Hadronic decays of b mesons into two c mesons: one c meson decays hadronically in a reconstructed final state, the other c meson decays semileptonically (e.g., $\bar{B}^0 \to D^+D_s^-$, $D_s^- \to \phi(1020)\mu^-\bar{\nu}_\mu$).

Branching fractions of the $\bar{B} \to D\bar{D}$ decays relative to the signal are all below 3%. A generator-level study indicates that they are further suppressed after a minimum requirement on the four-track invariant mass $M_{D(D^*)\mu}$, and therefore, contribute less than 1% to the signal. Backgrounds from b mesons decaying semileptonically to more particles or higher mass c mesons are also reduced or eliminated by the same minimum mass requirement.

Tables XIII and XIV summarize the feed-in backgrounds that contribute $\geq 1\%$ to the $\bar{B}^0 \to D^+\mu^-\bar{\nu}_\mu$ and the $\bar{B}^0 \to D^*(2010)^+\mu^-\bar{\nu}_\mu$ decays. The definition of quantities listed in each column follows Table V. Only

TABLE XIII. The feed-in backgrounds to the $\bar{B}^0 \to D^+ \mu^- \bar{\nu}_\mu$ signal. For the $\bar{B}_s^0 \to D^+ K^0 \mu^- \bar{\nu}_\mu$ decay, the $\Gamma(\bar{B}_s^0)/[\Gamma(B^-) + \Gamma(\bar{B}^0)]$ from the PDG is used to obtain $N_{\text{feed}}/N_{\text{had}}$ [69,70]. Numbers in parentheses are estimated uncertainties for the unmeasured branching fractions [71]. The definition of quantities listed in each column follows Table V.

Mode	$\mathcal{B}$ (%)	$\dfrac{\epsilon_i}{\epsilon_{\bar{B}^0 \to D^+ \pi^-}}$	$\left(\dfrac{N_{\text{feed}}}{N_{\text{had}}}\right)^i$	$\left(\dfrac{N_{\text{feed}}}{N_{\text{exclsemi}}}\right)^i$	N_{event}
$\bar{B}^0 \to D^+ \pi^-$	0.268 ± 0.013	1.000	–	–	579 ± 30
$D^+ \mu^- X$	–	–	–	–	4720 ± 100
$\bar{B}^0 \to D^+ \mu^- \bar{\nu}_\mu$	2.17 ± 0.12	0.455 ± 0.004	3.688	1.000	–
$\bar{B}^0 \to D^*(2010)^+ \mu^- \bar{\nu}_\mu$	5.16 ± 0.11	0.372 ± 0.004	2.314	0.627	1340 ± 69
$\quad \hookrightarrow D^+ \pi^0/\gamma$	32.30 ± 0.64				
$\bar{B}^0 \to D^+ \pi^0 \mu^- \bar{\nu}_\mu$	$0.30 \pm (0.30)$	0.165 ± 0.003	0.185	0.050	107 ± 6
$\bar{B}^0 \to D^+ \tau^- \bar{\nu}_\tau$	1.00 ± 0.40	0.100 ± 0.004	0.065	0.018	37 ± 2
$\quad \hookrightarrow \mu^- \bar{\nu}_\mu \nu_\tau$	17.36 ± 0.05				
$B^- \to D_1(2420)^0 \mu^- \bar{\nu}_\mu$	0.40 ± 0.07	0.278 ± 0.005	0.134	0.036	78 ± 4
$\quad \hookrightarrow D^*(2010)^+ \pi^-$					
$\quad\quad \hookrightarrow D^+ \pi^0/\gamma$	32.30 ± 0.64				
$B^- \to D_1'(2430)^0 \mu^- \bar{\nu}_\mu$	$0.37 \pm (0.37)$	0.273 ± 0.005	0.081	0.022	47 ± 2
$\quad \hookrightarrow D^*(2010)^+ \pi^-$	$66.67 \pm (3.33)$				
$\quad\quad \hookrightarrow D^+ \pi^0/\gamma$	32.30 ± 0.64				
$B^- \to D^+ \pi^- \mu^- \bar{\nu}_\mu$	0.42 ± 0.05	0.165 ± 0.003	0.259	0.070	150 ± 8
$\bar{B}_s^0 \to D^+ K^0 \mu^- \bar{\nu}_\mu$	$0.30 \pm (0.30)$	0.137 ± 0.004	0.064	0.017	37 ± 2

these decays are subtracted from the inclusive semileptonic yield. The leading background to $\bar{B}^0 \to D^+ \mu^- \bar{\nu}_\mu$ is $\bar{B}^0 \to D^*(2010)^+ \mu^- \bar{\nu}_\mu$, where $D^*(2010)^+ \to D^+ \pi^0$. The leading background to $\bar{B}^0 \to D^*(2010)^+ \mu^- \bar{\nu}_\mu$ is $B^- \to D_1(2420)^0 \mu^- \bar{\nu}_\mu$, where $D_1(2420)^0 \to D^*(2010)^+ \pi^-$. Combining information compiled in the PDG, backgrounds from $B \to D^{(*,**)} \mu^- \bar{\nu}_\mu X$, which are not considered in Tables XIII and XIV contribute less than 2% to the signal. The estimates of $N_{\text{false}\,\mu}$ and $N_{b\bar{b},c\bar{c}}$ for the $\bar{B}^0$ are identical to those for the Λ_b^0. Table XV lists the results. Figure 14 shows the $M_{K\pi\pi}$ and $M_{K\pi\pi} - M_{K\pi}$ distributions weighted with muon-misidentification probabilities and the results of the χ^2 fit.

The compositions of the inclusive $D^+ \mu^-$ and $D^*(2010)^+ \mu^-$ samples are summarized in Table XVI. The dominant signal contamination is from the feed-in background. The second largest background arises from false muons. The smallest background source is from $b\bar{b}/c\bar{c}$.

D. Systematic uncertainties

Figure 15 shows a summary of internal-consistency checks. The fractional systematic and statistical uncertainties on the $\bar{B}^0$ relative branching fractions are summarized in Table XVII. The leading sources of internal systematic uncertainties are the mass fitting models and the shape of

TABLE XIV. The feed-in backgrounds to the $\bar{B}^0 \to D^*(2010)^+ \mu^- \bar{\nu}_\mu$ signal.

| Mode	$\mathcal{B}$ (%)	$\dfrac{\epsilon_i}{\epsilon_{\bar{B}^0 \to D^*(2010)^+ \pi^-}}$	$\left(\dfrac{N_{\text{feed}}}{N_{\text{had}}}\right)^i$	$\left(\dfrac{N_{\text{feed}}}{N_{\text{exclsemi}}}\right)^i$	N_{event}
$\bar{B}^0 \to D^*(2010)^+ \pi^-$	0.276 ± 0.013	1.000	–	–	106 ± 11
$D^*(2010)^+ \mu^- X$	–	–	–	–	1059 ± 33
$\bar{B}^0 \to D^*(2010)^+ \mu^- \bar{\nu}_\mu$	5.16 ± 0.11	0.447 ± 0.006	8.361	1.000	–
$\bar{B}^0 \to D_1(2420)^+ \mu^- \bar{\nu}_\mu$	$0.81 \pm (0.32)$	0.349 ± 0.008	0.341	0.041	36 ± 4
$\quad \hookrightarrow D^*(2010)^+ \pi^0$	$33.33 \pm (1.67)$				
$\bar{B}^0 \to D_1'(2430)^+ \mu^- \bar{\nu}_\mu$	$0.37 \pm (0.37)$	0.336 ± 0.008	0.150	0.018	16 ± 2
$\quad \hookrightarrow D^*(2010)^+ \pi^0$	$33.33 \pm (1.67)$				
$\bar{B}^0 \to D^*(2010)^+ \pi^0 \mu^- \bar{\nu}_\mu$	$0.10 \pm (0.10)$	0.239 ± 0.006	0.086	0.010	9 ± 1
$\bar{B}^0 \to D^*(2010)^+ \tau^- \bar{\nu}_\tau$	1.60 ± 0.50	0.136 ± 0.005	0.137	0.016	14 ± 2
$\quad \hookrightarrow \mu^- \bar{\nu}_\mu \nu_\tau$	17.36 ± 0.05				
$B^- \to D_1(2420)^0 \mu^- \bar{\nu}_\mu$	0.40 ± 0.07	0.356 ± 0.008	0.516	0.062	55 ± 6
$\quad \hookrightarrow D^*(2010)^+ \pi^-$					
$B^- \to D_1'(2430)^0 \mu^- \bar{\nu}_\mu$	$0.37 \pm (0.37)$	0.351 ± 0.008	0.314	0.038	33 ± 3
$\quad \hookrightarrow D^*(2010)^+ \pi^-$	$66.67 \pm (3.33)$				
$B^- \to D^*(2010)^+ \pi^- \mu^- \bar{\nu}_\mu$	0.61 ± 0.06	0.242 ± 0.006	0.534	0.064	57 ± 6
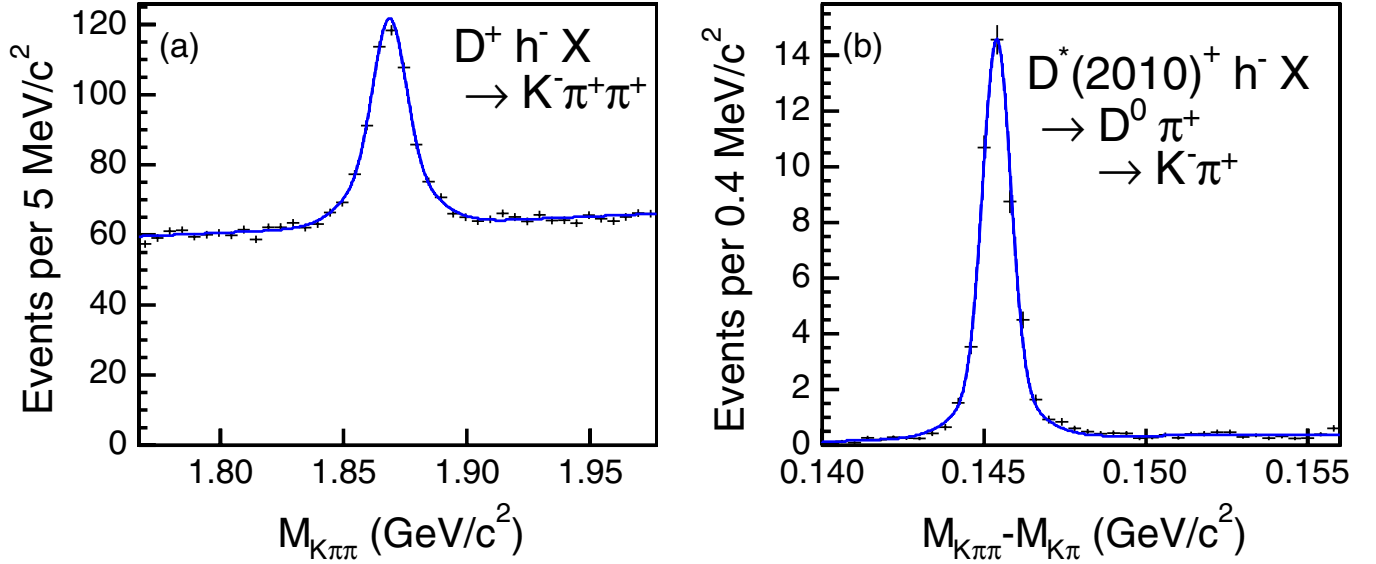
FIG. 14 (color online). The invariant mass distributions produced from data with a hadron track (h^-) and a c-meson candidate in the final state, after weighting the hadron track with an average muon-misidentification probability ($\mathcal{P}_{avg}$): (a) $M_{K\pi\pi}$ and (b) $M_{K\pi\pi} - M_{K\pi}$. The curves indicate the results of the χ^2 fit.

the measured $\bar{B}^0$ p_T spectrum. The dominant PDG uncertainties come from $\mathcal{B}(\bar{B}^0 \to D^+\pi^-)$ for the D^+ mode, and $\mathcal{B}(\bar{B}^0 \to D_1(2420)^+\mu^-\bar{\nu}_\mu)$ for the $D^*(2010)^+$ mode. The dominant uncertainties on the estimated branching fractions come from $\mathcal{B}(\bar{B}^0 \to D^+\pi^0\mu^-\bar{\nu}_\mu)$ for the D^+ mode and $\mathcal{B}(B^- \to D_1'(2430)^0\mu^-\bar{\nu}_\mu)$ for the $D^*(2010)^+$ mode. The $\bar{B}^0$ relative branching fractions with complete uncer-

tainties are found to be

$$\frac{\mathcal{B}(\bar{B}^0 \to D^+\mu^-\bar{\nu}_\mu)}{\mathcal{B}(\bar{B}^0 \to D^+\pi^-)} = 9.9 \pm 1.0(\text{stat}) \pm 0.6(\text{syst})$$
$$\pm 0.4(\text{PDG}) \pm 0.5(\text{EBR}),$$

$$\frac{\mathcal{B}(\bar{B}^0 \to D^*(2010)^+\mu^-\bar{\nu}_\mu)}{\mathcal{B}(\bar{B}^0 \to D^*(2010)^+\pi^-)} = 16.5 \pm 2.3(\text{stat}) \pm 0.6(\text{syst})$$
$$\pm 0.5(\text{PDG}) \pm 0.8(\text{EBR}).$$

The uncertainties are from stat, internal syst, world averages of measurements published by the PDG or subsidiary measurements in this analysis, and unmeasured branching fractions EBR, respectively.

TABLE XV. The estimated sizes of the false-muon, $b\bar{b}$, $c\bar{c}$, and feed-in background contribution to the $\bar{B}^0 \to D^+\mu^-\bar{\nu}_\mu$ and $\bar{B}^0 \to D^*(2010)^+\mu^-\bar{\nu}_\mu$ signals and the observed yields in data. Uncertainties on the $b\bar{b}$, $c\bar{c}$, and feed-in backgrounds are statistical only.

	$D^+\mu^-$	$D^*(2010)^+\mu^-$
$N_{\text{false}\mu}$	230 ± 19	44 ± 3
$N_{b\bar{b}}/N_{\text{had}}$	0.08 ± 0.01	0.08 ± 0.01
$N_{c\bar{c}}/N_{\text{had}}$	0.05 ± 0.01	0.05 ± 0.01
$N_{\text{feed}}/N_{\text{had}}$	3.10 ± 0.03	2.08 ± 0.02
N_{had}	579 ± 30	106 ± 11
N_{inclsemi}	4720 ± 100	1059 ± 33

X. RESULTS

The Λ_b^0 and $\bar{B}^0$ relative branching fractions are measured to be:

$$\frac{\mathcal{B}(\Lambda_b^0 \to \Lambda_c^+\mu^-\bar{\nu}_\mu)}{\mathcal{B}(\Lambda_b^0 \to \Lambda_c^+\pi^-)} = 16.6 \pm 3.0(\text{stat})$$
$$\pm 1.0(\text{syst})\,^{+2.6}_{-3.4}(\text{PDG})$$
$$\pm 0.3(\text{EBR}),$$

$$\frac{\mathcal{B}(\bar{B}^0 \to D^+\mu^-\bar{\nu}_\mu)}{\mathcal{B}(\bar{B}^0 \to D^+\pi^-)} = 9.9 \pm 1.0(\text{stat}) \pm 0.6(\text{syst})$$
$$\pm 0.4(\text{PDG}) \pm 0.5(\text{EBR}),$$

$$\frac{\mathcal{B}(\bar{B}^0 \to D^*(2010)^+\mu^-\bar{\nu}_\mu)}{\mathcal{B}(\bar{B}^0 \to D^*(2010)^+\pi^-)} = 16.5 \pm 2.3(\text{stat}) \pm 0.6(\text{syst})$$
$$\pm 0.5(\text{PDG}) \pm 0.8(\text{EBR}).$$

TABLE XVI. The composition of the inclusive $D^+\mu^-$ and $D^*(2010)^+\mu^-$ data samples.

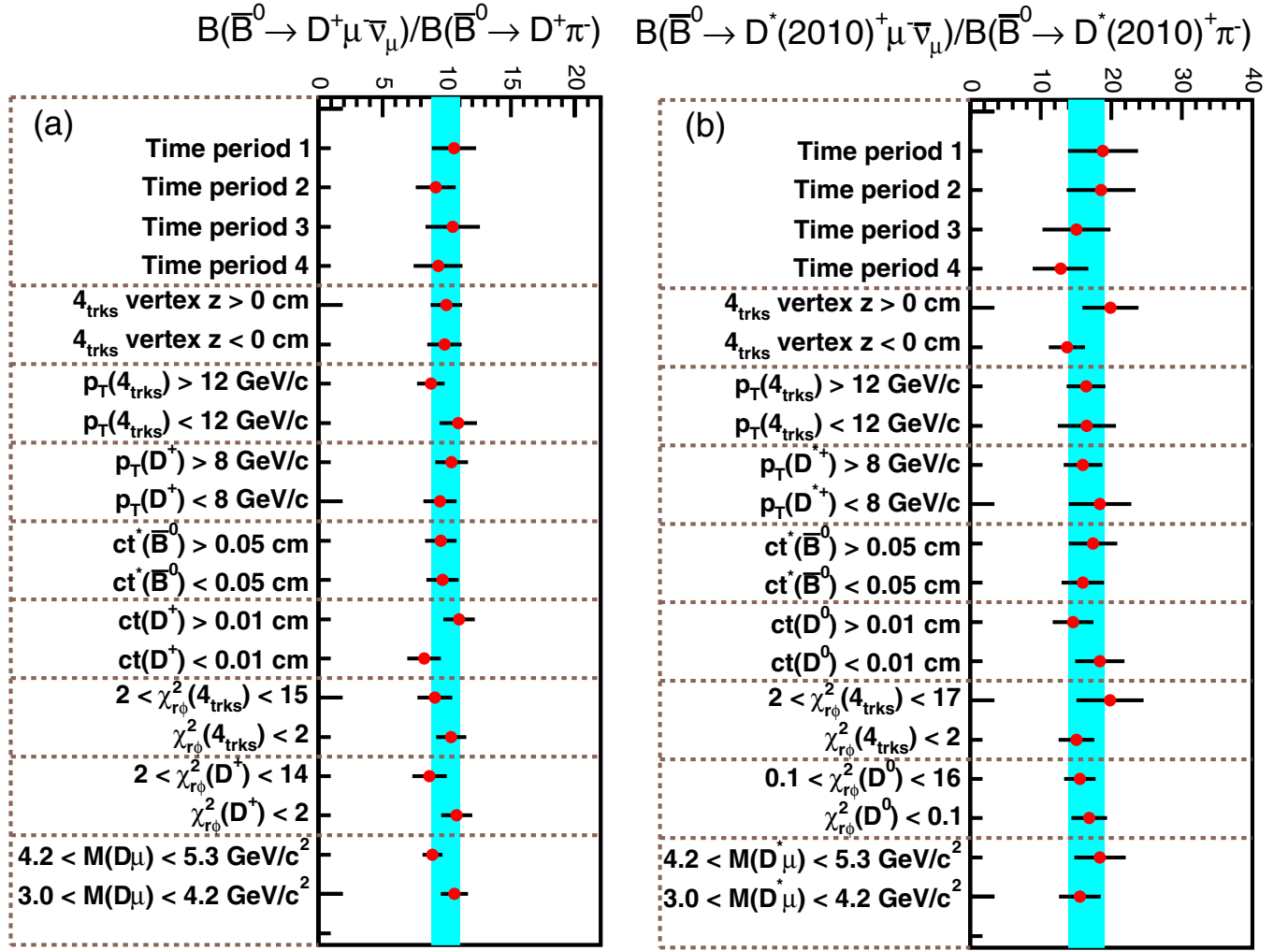|	N/N_{inclsemi} (%)	
	$D^+\mu^-$	$D^*(2010)^+\mu^-$
Signal	55.5	73.7
False muon	4.9	4.2
$b\bar{b}/c\bar{c}$	1.6	1.3
Feed-in	38.0	20.8

FIG. 15 (color online). Internal-consistency checks of the relative branching fractions measured in the two $\bar{B}^0$ control samples: (a) $\bar{B}^0 \to D^+$ decays and (b) $\bar{B}^0 \to D^*(2010)^+$ decays. The uncertainty on each point is a statistical only. Each independent group is separated by a horizontal dashed line. The solid bands indicate the relative branching fractions with their statistical uncertainties from the complete, undivided samples.

TABLE XVII. Summary of statistical and systematic uncertainties for the $\bar{B}^0$ modes. The σ_R is uncertainty on the $\bar{B}^0$ relative branching fraction, R.

Source	$\frac{\sigma_R}{R}$ (%)	
	$\frac{\mathcal{B}(\bar{B}^0 \to D^+ \mu^- \bar{\nu}_\mu)}{\mathcal{B}(\bar{B}^0 \to D^+ \pi^-)}$	$\frac{\mathcal{B}(\bar{B}^0 \to D^*(2010)^+ \mu^- \bar{\nu}_\mu)}{\mathcal{B}(\bar{B}^0 \to D^*(2010)^+ \pi^-)}$
Mass fitting	4.1	<0.1
False μ	0.7	0.4
$b\bar{b}/c\bar{c}$ background	2.9	1.7
Simulation sample size	1.6	1.7
$\bar{B}^0$ p_T spectrum	3.0	2.4
XFT/CMU efficiency scale factor	0.5	0.4
Detector material	1.7	1.3
Sum of internal	6.3	3.7
PDG	4.1	2.8
Estimated branching fractions	4.7	4.9
Statistical	9.7	14.1

The uncertainties are from statistics (stat), internal systematics (syst), world averages of measurements published by the Particle Data Group or subsidiary measurements in this analysis (PDG), and unmeasured branching fractions estimated from theory (EBR), respectively. The control sample results are consistent with the ratios published by the

TABLE XVIII. The $\bar{B}^0$ relative branching fractions measured in this analysis and those published in the 2008 PDG [7]. The measurements of this analysis include both the statistical and the systematic uncertainties.

Mode	PDG	This Analysis
$\frac{\mathcal{B}(\bar{B}^0 \to D^+ \mu^- \bar{\nu}_\mu)}{\mathcal{B}(\bar{B}^0 \to D^+ \pi^-)}$	8.1 ± 0.6	9.9 ± 1.3
$\frac{\mathcal{B}(\bar{B}^0 \to D^*(2010)^+ \mu^- \bar{\nu}_\mu)}{\mathcal{B}(\bar{B}^0 \to D^*(2010)^+ \pi^-)}$	18.7 ± 1.0	16.5 ± 2.6

2008 PDG [7] at the 1.3σ and 0.8σ level, respectively, (see Table XVIII). The measured ratio of Λ_b^0 branching fractions is compared with the predicted value based on HQET. The prediction has a $\approx 30\%$ uncertainty and is obtained by combining the results of Huang *et al.* [9] and Leibovich *et al.* [10,72]. Figure 16 shows the consis-

tency between this measurement and the theoretical prediction.

The branching fractions of the four new Λ_b^0 semileptonic decays relative to that of $\Lambda_b^0 \to \Lambda_c^+ \mu^- \bar{\nu}_\mu$ are measured to be

$$\frac{\mathcal{B}(\Lambda_b^0 \to \Lambda_c(2595)^+ \mu^- \bar{\nu}_\mu)}{\mathcal{B}(\Lambda_b^0 \to \Lambda_c^+ \mu^- \bar{\nu}_\mu)} = 0.126 \pm 0.033(\text{stat})^{+0.047}_{-0.038}(\text{syst}),$$

$$\frac{\mathcal{B}(\Lambda_b^0 \to \Lambda_c(2625)^+ \mu^- \bar{\nu}_\mu)}{\mathcal{B}(\Lambda_b^0 \to \Lambda_c^+ \mu^- \bar{\nu}_\mu)} = 0.210 \pm 0.042(\text{stat})^{+0.071}_{-0.050}(\text{syst}),$$

$$\frac{1}{2}\left[\frac{\mathcal{B}(\Lambda_b^0 \to \Sigma_c(2455)^0 \pi^+ \mu^- \bar{\nu}_\mu)}{\mathcal{B}(\Lambda_b^0 \to \Lambda_c^+ \mu^- \bar{\nu}_\mu)} + \frac{\mathcal{B}(\Lambda_b^0 \to \Sigma_c(2455)^{++} \pi^- \mu^- \bar{\nu}_\mu)}{\mathcal{B}(\Lambda_b^0 \to \Lambda_c^+ \mu^- \bar{\nu}_\mu)}\right] = 0.054 \pm 0.022(\text{stat})^{+0.021}_{-0.018}(\text{syst}).$$

XI. CONCLUSION

Using data from an integrated luminosity of ≈ 172 pb^{-1} collected with the CDF II detector, 1237 ± 97 $\Lambda_c^+ \mu^- X$ and 179 ± 19 $\Lambda_b^0 \to \Lambda_c^+ \pi^-$ signal events are reconstructed. The large Λ_b^0 sample enables the measurement of $\mathcal{B}(\Lambda_b^0 \to \Lambda_c^+ \mu^- \bar{\nu}_\mu)/\mathcal{B}(\Lambda_b^0 \to \Lambda_c^+ \pi^-)$ and the com-
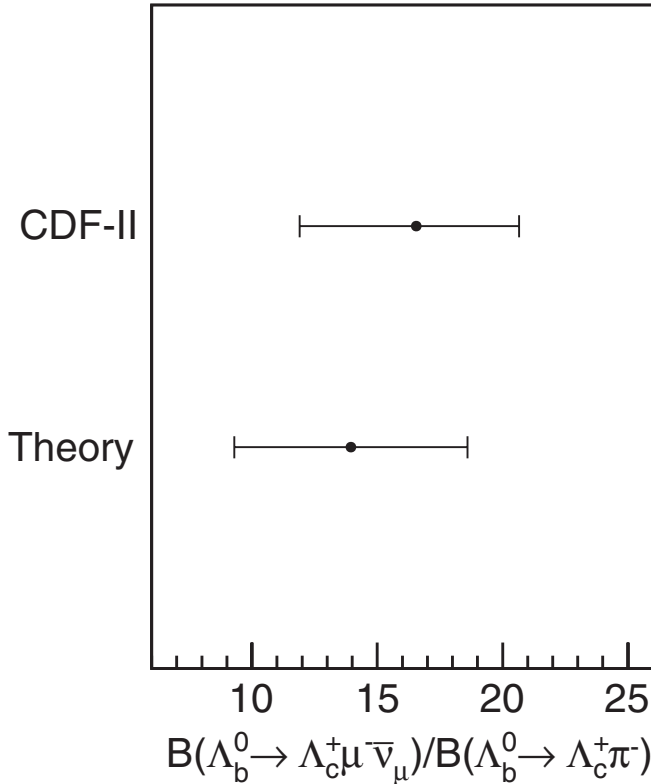

FIG. 16. Comparison of the measured $\mathcal{B}(\Lambda_b^0 \to \Lambda_c^+ \mu^- \bar{\nu}_\mu)/\mathcal{B}(\Lambda_b^0 \to \Lambda_c^+ \pi^-)$ with the theoretical prediction based on HQET by Huang *et al.* [9] and Leibovich *et al.* [10]. The measurement includes both the statistical and the systematic uncertainties.

parison to the predictions of heavy quark effective theory. The uncertainty is dominated by the size of the data sample, the world average of $\mathcal{B}(\Lambda_c^+ \to pK^- \pi^+)$, and the CDF I measurement of $\sigma_{\Lambda_b^0}/\sigma_{\bar{B}^0}$. Ratios for the control modes $\mathcal{B}(\bar{B}^0 \to D^+ \mu^- \bar{\nu}_\mu)/\mathcal{B}(\bar{B}^0 \to D^+ \pi^-)$ and $\mathcal{B}(\bar{B}^0 \to D^*(2010)^+ \mu^- \bar{\nu}_\mu)/\mathcal{B}(\bar{B}^0 \to D^*(2010)^+ \pi^-)$ are found to be in good agreement with the world averages [7]. For the first time, the semileptonic decay $\Lambda_b^0 \to \Lambda_c(2625)^+ \mu^- \bar{\nu}_\mu$ has been observed, and three other semileptonic decays $\Lambda_b^0 \to \Lambda_c(2595)^+ \mu^- \bar{\nu}_\mu$, $\Lambda_b^0 \to \Sigma_c(2455)^0 \pi^+ \mu^- \bar{\nu}_\mu$, $\Lambda_b^0 \to \Sigma_c(2455)^{++} \pi^- \mu^- \bar{\nu}_\mu$ have been reconstructed, using data from an integrated luminosity of ≈ 360 pb^{-1}. Measurements of the ratios of their branching fractions to the branching fraction of $\Lambda_b^0 \to \Lambda_c^+ \mu^- \bar{\nu}_\mu$ have been performed. Finally, the transverse-momentum distribution of the Λ_b^0 baryon produced in $p\bar{p}$ collisions is found to be softer (more b hadrons at lower p_T) than that of the $\bar{B}^0$ meson; this results in a new estimate for $\mathcal{B}(\Lambda_b^0 \to \Lambda_c^+ \pi^-)$ in better agreement with the theory than the PDG evaluation.

ACKNOWLEDGMENTS

APPENDIX A: SEMILEPTONIC DECAYS OF *b* MESONS TO BARYONS

The number of feed-in events from semileptonic decays of *b* mesons to baryons ($N_{\text{feed}}^{\text{meson}}$) is also normalized to the $\Lambda_b^0 \to \Lambda_c^+ \pi^-$ yield in data (N_{had}) and has an expression similar to that of Eq. (9):

$$\frac{N_{\text{feed}}^{\text{meson}}}{N_{\text{had}}} = \frac{\sigma_{B_{u,d,s}}(p_T > 6.0)}{\sigma_{\Lambda_b^0}(p_T > 6.0)} \frac{\sum_i \mathcal{B}_i \epsilon_i}{\mathcal{B}(\Lambda_b^0 \to \Lambda_c^+ \pi^-)\epsilon_{\Lambda_b^0 \to \Lambda_c^+ \pi^-}},$$

(A1)

where $\sigma_{B_{u,d,s}}(p_T > 6.0)$ and $\sigma_{\Lambda_b^0}(p_T > 6.0)$ are the production cross sections of *b* mesons and Λ_b^0 baryons for p_T greater than 6 GeV/c.

A list of *b*-meson decays that may contribute to the $\Lambda_c^+ \mu^- X$ sample is obtained from an inclusive sample of *b*-meson semimuonic decays generated using PYTHIA. After applying the trigger and analysis requirements to the PYTHIA generated events, the maximum contributing decays are found to be $\bar{B}^0 \to \Lambda_c^+ \bar{n} \mu^- \bar{\nu}_\mu$ and $B^- \to \Lambda_c^+ \bar{p} \mu^- \bar{\nu}_\mu$. While there are measurements of branching ratios of the *b*-meson hadronic decays to baryons, e.g., $\bar{B}^0 \to \Lambda_c^+ \bar{p} \pi^+ \pi^-$, there is only an upper limit for the semileptonic decay of B^-

$$\mathcal{B}(B^- \to \Lambda_c^+ \bar{p} e^- \bar{\nu}_e) < 0.15\%.$$

Assuming the branching fractions of the muon-neutron and muon-proton final states are the same as that of the proton-electron final state, the value of this upper limit is then taken for the branching fraction of the $\bar{B}^0 \to \Lambda_c^+ \bar{n} \mu^- \bar{\nu}_\mu$ and the $B^- \to \Lambda_c^+ \bar{p} \mu^- \bar{\nu}_\mu$ decays. The ratio $N_{\bar{B}^0 \to \Lambda_c^+ \bar{n} \mu^- \bar{\nu}_\mu}/N_{\Lambda_b^0 \to \Lambda_c^+ \pi^-}$, for example, is then given by

$$\frac{N_{\bar{B}^0 \to \Lambda_c^+ \bar{n} \mu^- \bar{\nu}_\mu}}{N_{\Lambda_b^0 \to \Lambda_c^+ \pi^-}} = \frac{\sigma_{\bar{B}^0}(p_T > 6.0)}{\sigma_{\Lambda_b^0}(p_T > 6.0)}$$

$$\times \frac{\mathcal{B}(\bar{B}^0 \to \Lambda_c^+ \bar{n} \mu^- \bar{\nu}_\mu)\epsilon_{\bar{B}^0 \to \Lambda_c^+ \bar{n} \mu^- \bar{\nu}_\mu}}{\mathcal{B}(\Lambda_b^0 \to \Lambda_c^+ \pi^-)\epsilon_{\Lambda_b^0 \to \Lambda_c^+ \pi^-}}$$

$$= \frac{1}{G} \times \frac{0.15\%\epsilon_{\bar{B}^0 \to \Lambda_c^+ \bar{n} \mu^- \bar{\nu}_\mu}}{\mathcal{B}(\bar{B}^0 \to D^+ \pi^-)\epsilon_{\Lambda_b^0 \to \Lambda_c^+ \pi^-}},$$

(A2)

where *G* is the CDF measurement [37]

$$G \equiv \frac{\sigma_{\Lambda_b^0}(p_T > 6.0)\mathcal{B}(\Lambda_b^0 \to \Lambda_c^+ \pi^-)}{\sigma_{\bar{B}^0}(p_T > 6.0)\mathcal{B}(\bar{B}^0 \to D^+ \pi^-)}. \quad \text{(A3)}$$

The ratio $N_{B^- \to \Lambda_c^+ \bar{p} \mu^- \bar{\nu}_\mu}/N_{\Lambda_b^0 \to \Lambda_c^+ \pi^-}$ follows Eq. (A2), assuming the production fractions are the same for the $\bar{B}^0$ and B^- mesons [70]. Table XIX lists the estimated size of the feed-in background contribution from semileptonic decays of *b* mesons to baryons.

APPENDIX B: SEMILEPTONIC DECAYS OF OTHER *b* BARYONS

In addition to the feed-in backgrounds from the semileptonic decays of *b* mesons to baryons, contributions are also expected from the semileptonic decays of other *b* baryons. Until recently [73,74], the Λ_b^0 was the only *b* baryon that had been observed unambiguously. Therefore, in order to estimate the number of feed-in background events, the production cross section of the other *b* baryons and the branching ratio of the feed-in channel must be estimated. The first step in the estimation is to identify possible contributions to the feed-in.

Of the lowest lying *b* baryons, the members of Σ_b triplet are expected to decay to $\Lambda_b^0 \pi$ via the strong interaction and contribute to the Λ_b^0 signal. This leaves Ξ_b^-, Ξ_b^0, and Ω_b^-, and they are expected to decay predominantly to Ξ_c^+ and Ω_c^0. However, by vacuum production of one or more $q\bar{q}$ pairs, these *b* baryons can decay into a Λ_c^+, specifically,

$$\Xi_b^0 \to \Lambda_c^+ \bar{K}^0 \mu^- \bar{\nu}_\mu, \qquad \Xi_b^- \to \Lambda_c^+ K^- \mu^- \bar{\nu}_\mu,$$

$$\Omega_b^- \to \Lambda_c^+ K^- \bar{K}^0 \mu^- \bar{\nu}_\mu.$$

Since the Ξ_b decays have a decay topology similar to

TABLE XIX.   Feed-in backgrounds to $\Lambda_b^0 \to \Lambda_c^+ \mu^- \bar{\nu}_\mu$ from *b* mesons. All the numbers in parentheses are estimated uncertainties. The definition of quantities listed in each column follows Table V.

Mode	$\mathcal{B}$ (%)	$\frac{\epsilon_i}{\epsilon_{\Lambda_b^0 \to \Lambda_c^+ \pi^-}}$	$\left(\frac{N_{\text{feed}}^{\text{meson}}}{N_{\text{had}}}\right)^i$	$\left(\frac{N_{\text{feed}}^{\text{meson}}}{N_{\text{exclsemi}}}\right)^i$	N_{event}
$\Lambda_b^0 \to \Lambda_c^+ \pi^-$	$0.36\,^{+(0.24)}_{-(0.18)}$	1.000	–	–	179 ± 19
$\Lambda_c^+ \mu^- X$	–	–	–	–	1237 ± 97
$\Lambda_b^0 \to \Lambda_c^+ \mu^- \bar{\nu}_\mu$	$7.3 \pm (1.4)$	0.303 ± 0.004	6.118	1.000	–
$B^- \to \Lambda_c^+ \bar{p} \mu^- \bar{\nu}_\mu$	$0.15 \pm (0.15)$	0.035 ± 0.002	0.024	0.004	4.3 ± 0.5
$\bar{B}^0 \to \Lambda_c^+ \bar{n} \mu^- \bar{\nu}_\mu$	$0.15 \pm (0.15)$	0.037 ± 0.002	0.025	0.004	4.5 ± 0.5

$\Lambda_b^0 \to \Sigma_c(2455)\pi\mu^-\bar{\nu}_\mu$ and the Ω_b^- decay topology is similar to that of $\Lambda_b^0 \to \Lambda_c^+ \pi^+ \pi^- \mu^- \bar{\nu}_\mu$, a branching fraction of 0.39%, 0.39%, and 0.64% (given in Table VIII) are assigned to these three decays, respectively. CDF reports observing 17 $\Xi_b^- \to J/\psi \Xi^-$ events in data from an integrated luminosity of approximately 1900 pb^{-1} [74]. Assuming that the branching fraction for $\Xi_b^- \to J/\psi \Xi^-$ is similar to that reported by the Particle Data Group for $\Lambda_b^0 \to J/\psi \Lambda$ [7], using a generator-level simulation to estimate the ratio of acceptances of $\Xi_b \to \Lambda_c^+ K \mu^- \bar{\nu}_\mu$ relative to that of $\Xi_b^- \to J/\psi \Xi^-$ (0.2), and scaling by the ratio of luminosities for this analysis and the Ξ_b^- analysis (172/1900), each of the Ξ_b decays is found to contribute approximately 0.2% to the signal. For the Ω_b^- decays, a similar calculation is performed assuming the same production rate as for the Ξ_b. However, because of the larger number of particles in the Ω_b^- decay, the acceptance for the Ω_b^- is an order of magnitude smaller than that of the Ξ_b. For the Ω_b^-, the contribution is 0.03%. These three decays are found to contribute $\leq 1\%$ to the signal and may be ignored [75].

APPENDIX C: THE $b\bar{b}/c\bar{c}$ BACKGROUND

The $b\bar{b}/c\bar{c}$ background refers to the pairing of a Λ_c^+ and a real muon from the decays of two different heavy-flavor hadrons produced by the fragmentation of $b\bar{b}$ or $c\bar{c}$ pairs. In $p\bar{p}$ collisions, the b and c quarks are primarily pair produced via the strong interaction; the single-quark production cross section via the electroweak process, $p\bar{p} \to W^+$ anything $\to \bar{b}$ anything or c anything, is more than 20 000 times smaller [76,77]. Figure 17 shows the Feynman diagrams up to α_s^3 for the three processes that contribute to the $b\bar{b}/c\bar{c}$ production [78,79]: flavor creation, flavor excitation, and gluon splitting. Flavor creation, referring to gluon fusion and quark antiquark annihilation, tends to produce $b\bar{b}/c\bar{c}$ pairs with an azimuthal angle

distribution ($\Delta\phi$) between the two quarks, which peaks at 180°. In contrast, the $\Delta\phi$ distribution is more evenly distributed for the flavor excitation and the low-momentum gluon splitting and peaks at small angles for the high-momentum gluon splitting. When $\Delta\phi$ is small, daughters of the two heavy-flavor hadrons from the fragmentation of $b\bar{b}/c\bar{c}$ may appear to come from the same decay vertex, as shown in Fig. 18. If one hadron decays semileptonically, and the other hadron decays into a final state including a $\Lambda_c^+ \to pK^-\pi^+$ decay, the muon from the semileptonic decay together with the Λ_c^+ may be misidentified as the exclusive semileptonic signal, $\Lambda_b^0 \to \Lambda_c^+ \mu^- \bar{\nu}_\mu$. An estimate using PYTHIA has shown that this measurement is most sensitive to the $b\bar{b}/c\bar{c}$ background from high-momentum gluon splitting.

In the following, the determination of the $b\bar{b}$ background contribution is described. The same procedure is followed for the $c\bar{c}$ background. The ratio $N_{b\bar{b}}/N_{\text{had}}$ is given by

$$\frac{N_{b\bar{b}}}{N_{\text{had}}} = \frac{\sigma_{b\bar{b}}\mathcal{P}(b \to \Lambda_c^+ X)\mathcal{P}(\bar{b} \to \mu^- X)\epsilon_{b\bar{b} \to \Lambda_c^+ \mu^- X}}{\sigma_{\Lambda_b^0}\mathcal{B}(\Lambda_b^0 \to \Lambda_c^+ \pi^-)\epsilon_{\Lambda_b^0 \to \Lambda_c^+ \pi^-}}.$$

(C1)

The $\sigma_{b\bar{b}}$ is the production cross section of $b\bar{b}$ pairs; $\mathcal{P}(b \to \Lambda_c^+ X)$ and $\mathcal{P}(\bar{b} \to \mu^- X)$ are the probabilities for a b and a $\bar{b}$ quark to fragment into a b hadron and a $\bar{b}$ hadron and to decay to a final state including a Λ_c^+ and a μ^-, respectively. The $\epsilon_{b\bar{b} \to \Lambda_c^+ \mu^- X}$ is the acceptance times efficiency for reconstructing the background as the $\Lambda_b^0 \to \Lambda_c^+ \mu^- \bar{\nu}_\mu$ signal. The denominator of Eq. (C1) can be rewritten using the CDF measurement [37] defined in Eq. (A3), the CDF measurement of σ_{B^+} [80] assuming $\sigma_{B^+} = \sigma_{\bar{B}^0}$ [70], and the world average of $\mathcal{B}(\bar{B}^0 \to D^+ \pi^-)$
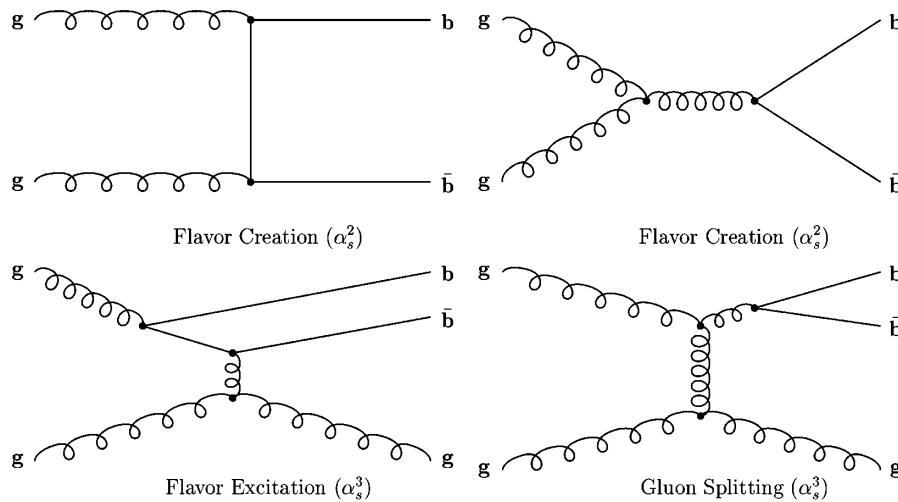

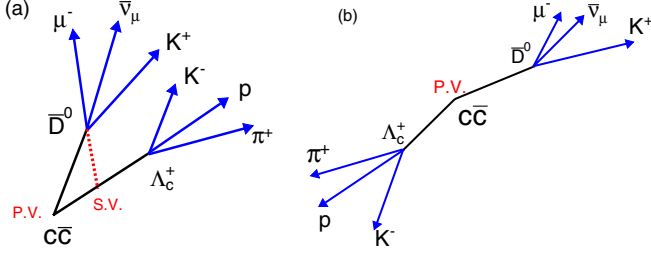FIG. 17. Representative lowest-order Feynman diagrams that contribute to the pair production of b quarks [78,79].

FIG. 18 (color online). The c hadrons from $c\bar{c}$ with (a) small and (b) large $\Delta\phi$. Unlike Fig. 18(b), Fig. 18(a) shows that the Λ_c^+ and the muon from the semileptonic decay of $\bar{D}^0$ form a secondary vertex and are misidentified as the $\Lambda_b^0 \to \Lambda_c^+ \mu^- \bar{\nu}_\mu$ signal.

$$\frac{N_{b\bar{b}}}{N_{\text{had}}} = \frac{1}{G} \frac{\sigma_{b\bar{b}} \mathcal{P}(b \to \Lambda_c^+ X)\mathcal{P}(\bar{b} \to \mu^- X)\epsilon_{b\bar{b} \to \Lambda_c^+ \mu^- X}}{\sigma_{\bar{B}^0} \mathcal{B}(\bar{B}^0 \to D^+ \pi^-)\epsilon_{\Lambda_b^0 \to \Lambda_c^+ \pi^-}}.$$

$$\text{(C2)}$$

The $\epsilon_{\Lambda_b^0 \to \Lambda_c^+ \pi^-}$ is determined from a signal simulation generated with the BGENERATOR program [81,82] and Table XX lists the parameters for calculating the denominator of Eq. (C2). In order to determine the numerator of Eq. (C2), inclusive $b\bar{b}$ events are first generated with PYTHIA. The p_T of the hard scattering, i.e., the part of the interaction with the largest momentum scale, is required to be greater than 5 GeV/c. At least one b quark must have a p_T greater than 4 GeV/c and $|\eta|$ less than 1.5. The value of

$\sigma_{b\bar{b}}$, after applying the kinematic requirements above, is obtained from PYTHIA, since the status of the $\sigma_{b\bar{b}}$ measurements at the Tevatron is still inconclusive [83–85]. Then, the gluon-splitting events are filtered, and the decays are simulated with EVTGEN. Only events with a μ^- and a Λ_c^+, which pass the generator-level trigger and analysis requirements, are considered further. Ancestors of the μ^- and the Λ_c^+ determine whether they originate from $b\bar{b}$ pairs or single b hadrons, and are retrieved by tracing the information from the generator. The number of events satisfying these criteria divided by the number of generated events gives the product $\mathcal{P}(b \to \Lambda_c^+ X)\mathcal{P}(\bar{b} \to \mu^- X)\epsilon_{b\bar{b} \to \Lambda_c^+ \mu^- X}$. Table XXI lists the parameters for the determination of the numerator of Eq. (C2).

Table XXII lists the estimated ratios, $N_{b\bar{b}}/N_{\text{had}}$ and $N_{c\bar{c}}/N_{\text{had}}$, based on the values in Tables XX and XXI. The $N_{b\bar{b},c\bar{c}}$ is found to be only 0.3% of the number of inclusive $\Lambda_c^+ \mu^- X$ events. The production of $b\bar{b}$ and $c\bar{c}$ pairs in $p\bar{p}$ collisions has not yet been completely understood [63,83–85]. In order to understand how well PYTHIA predicts $\sigma_{b\bar{b}}$ and $\sigma_{c\bar{c}}$, an indirect cross-check was performed by comparing the differential cross sections of inclusive b hadrons, B^+, and D^0 in PYTHIA with the CDF measurements [13,80,86] (see Appendix C 1). The discrepancy between PYTHIA and the data cross sections is generally within 10% for c hadrons and 50% for b hadrons, which will be included in the systematic uncertainty in Sec. VIII. Another cross-check using the signed

TABLE XX. Parameters used to calculate the denominator of Eq. (C2).

CDF σ_{B^+} (μb)	2.78 ± 0.24
$\dfrac{\sigma_{\Lambda_b^0}(p_T>6.0)B(\Lambda_b^0 \to \Lambda_c^+ \pi^-)}{\sigma_{\bar{B}^0}(p_T>6.0)B(\bar{B}^0 \to D^+ \pi^-)}(G)$	0.82 ± 0.26
$\mathcal{B}(\bar{B}^0 \to D^+ \pi^-)$	$(0.268 \pm 0.013)\%$
$\epsilon_{\Lambda_b^0 \to \Lambda_c^+ \pi^-}$	$(2.109 \pm 0.002) \times 10^{-2}$
$\sigma_{\Lambda_b^0} \mathcal{B}(\Lambda_b^0 \to \Lambda_c^+ \pi^-)\epsilon_{\Lambda_b^0 \to \Lambda_c^+ \pi^-}$ $(10^{-4}$ $\mu b)$	1.3 ± 0.4

TABLE XXI. Parameters used to determine the numerator of Eq. (C2). The uncertainties are statistical only.

PYTHIA $\sigma_{b\bar{b}}$ (μb)	49.6
$\mathcal{P}(b \to \Lambda_c^+ X)\mathcal{P}(\bar{b} \to \mu^- X)\epsilon_{b\bar{b} \to \Lambda_c^+ \mu^- X}$	$(4.1 \pm 1.4) \times 10^{-8}$
PYTHIA $\sigma_{c\bar{c}}$ (μb)	198.4
$\mathcal{P}(c \to \Lambda_c^+ X)\mathcal{P}(\bar{c} \to \mu^- X)\epsilon_{c\bar{c} \to \Lambda_c^+ \mu^- X}$	$(1.2 \pm 0.5) \times 10^{-9}$

TABLE XXII. The estimated size of the $b\bar{b}$ and $c\bar{c}$ background contribution to the $\Lambda_b^0 \to \Lambda_c^+ \mu^- \bar{\nu}_\mu$ signal and the observed yields in data.

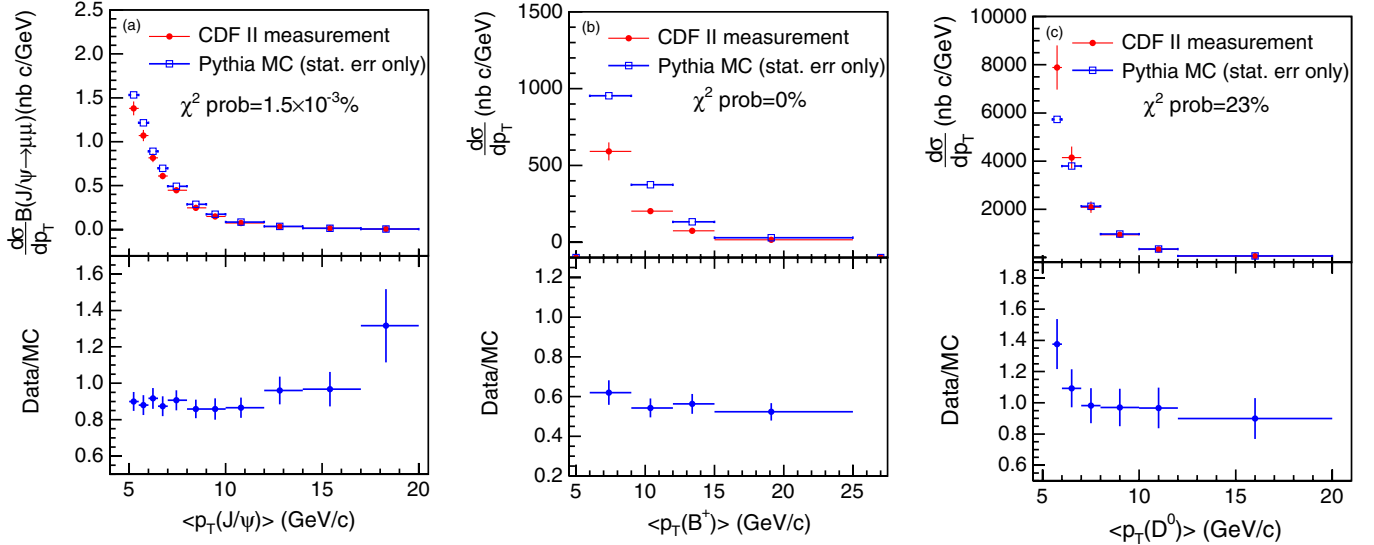|	
$N_{b\bar{b}}/N_{\text{had}}$	0.016 ± 0.008
$N_{c\bar{c}}/N_{\text{had}}$	0.0018 ± 0.0009
N_{had}	179 ± 19
$N_{\text{incl semi}}$	1237 ± 97

FIG. 19 (color online). The differential cross sections of (a) inclusive b hadrons, (b) B^+, and (c) D^0. The upper plot in each figure shows the differential cross section for data (closed circles) [13,80,86] and PYTHIA (open squares). The lower plot in each figure shows the data to PYTHIA ratio.

impact parameter distributions of the Λ_c^+ baryons (see Appendix C 2) indicates a negligible contribution of promptly produced Λ_c^+ from $c\bar{c}$, which is consistent with the above estimate using PYTHIA.

1. Cross-check of the inclusive b hadron, B^+, and D^0 cross sections

In order to understand how well PYTHIA predicts $\sigma_{b\bar{b}}$ and $\sigma_{c\bar{c}}$, a cross-check was performed indirectly by comparing

the differential cross sections of inclusive b hadrons, B^+, and $D^0(d\sigma(p\bar{p} \to D^0X)/dp_T$ etc.) in PYTHIA with the CDF measurements [13,80,86]. The differential cross section of D^0 in PYTHIA (see Fig. 19), for instance, is defined as: $d\sigma(p\bar{p} \to D^0X)^{\text{PYTHIA}}/dp_T \equiv \sigma_{c\bar{c}}(N_{D^0}/N_{\text{gen}})/\Delta p_T$, where N_{D^0} is the number of D^0 in each p_T bin, and N_{gen} is the total number of generated $c\bar{c}$ events. The Δp_T corresponds to the bin width of each p_T bin, which is the same as that in [13,80,86]. The discrepancy between the PYTHIA and the
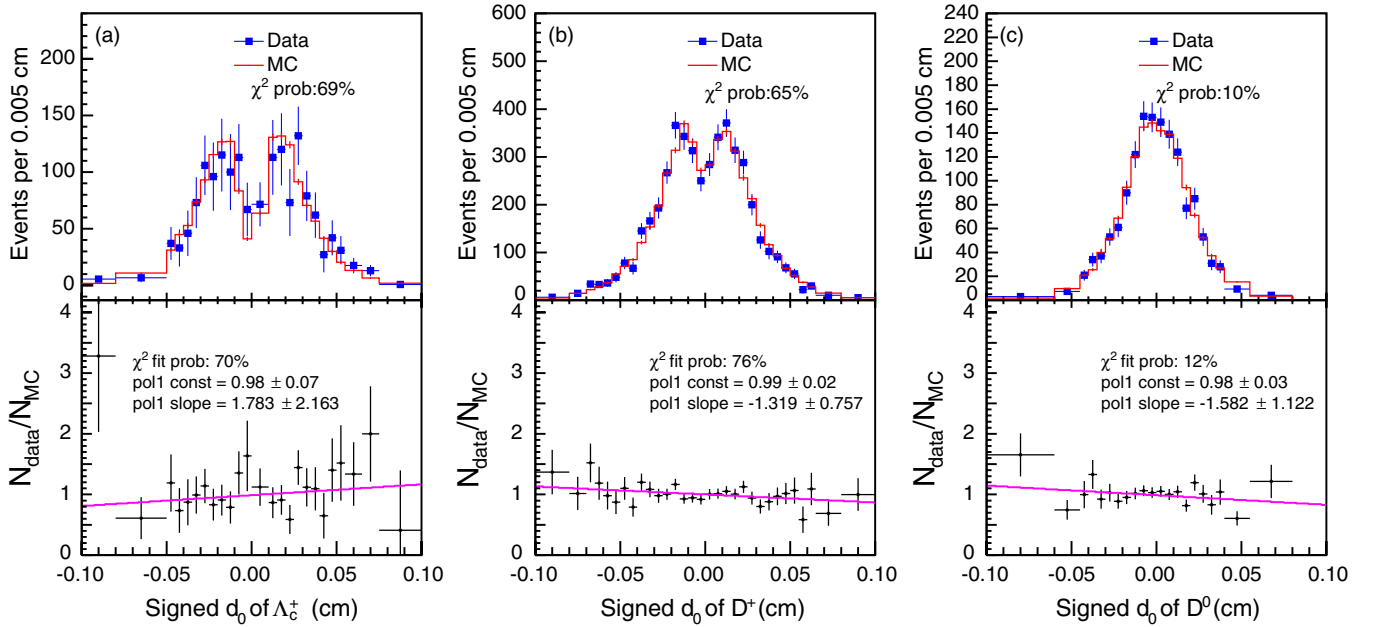

FIG. 20 (color online). Comparison of the signed impact parameters between the full simulation and data for c hadrons, which are associated with a μ^-: (a) Λ_c^+, (b) D^+, and (c) D^0 from the $D^*(2010)^+$. The good agreement of the full simulation with data indicates that backgrounds from the promptly produced Λ_c^+, D^+, and D^0 ($c\bar{c}$) are negligible.

data cross sections is generally within 10% for *c* hadrons and 50% for *b* hadrons, which is included in the systematic uncertainty in Sec. VIII.

2. Cross-check using the signed impact parameter distributions

As an additional cross-check, the signed impact parameter distributions (signed d_0) of the Λ_c^+ baryons with respect to the primary vertex, in data and the full simulation, are also compared. The signed impact parameter is defined as $d_0 = Q(r_0 - \rho)$, where Q is the charge of the particle and r_0 is the distance between the beam line and the center of

the helix describing the track in the transverse plane. The parameter ρ is the radius of the track helix. The full simulation includes the $\Lambda_b^0 \to \Lambda_c^+ \mu^- \bar{\nu}_\mu$ signal and feed-in backgrounds, with relative fractions following the estimates in Sec. VI B. An excess of the signed d_0 distribution in the region close to zero would indicate a significant contribution of the $c\bar{c}$ background in the $\Lambda_c^+ \mu^- X$ sample. Figure 20 shows good agreement between data and simulation, proving that the promptly produced Λ_c^+ from $c\bar{c}$ is a negligible contribution to the inclusive semileptonic signals. Figure 20 also shows the signed d_0 distributions of D^+ and D^0.

[1] N. Cabibbo, Phys. Rev. Lett. **10**, 531 (1963).
[2] M. Kobayashi and T. Maskawa, Prog. Theor. Phys. **49**, 652 (1973).
[3] A. V. Manohar and M. B. Wise, *Heavy Quark Physics*, Cambridge Monographs on Particle Physics and Cosmology Vol. 10, (Cambridge University Press, Cambridge, England, 2000).
[4] S. Godfrey and N. Isgur, Phys. Rev. D **32**, 189 (1985).
[5] N. Isgur, D. Scora, B. Grinstein, and M. B. Wise, Phys. Rev. D **39**, 799 (1989).
[6] H. Georgi, B. Grinstein, and M. B. Wise, Phys. Lett. B **252**, 456 (1990).
[7] C. Amsler *et al.* (Particle Data Group), Phys. Lett. B **667**, 1 (2008).
[8] Predictions of $\mathcal{B}(\Lambda_b^0 \to \Lambda_c^+ \ell^- \bar{\nu}_\ell)$ and $\mathcal{B}(\Lambda_b^0 \to \Lambda_c^+ \pi^-)$ are both obtained by combining the predicted decay widths with the world averages of $|V_{cb}| = (41.2 \pm 1.1) \times 10^{-3}$ and Λ_b^0 lifetime $\tau_{\Lambda_b^0} = 1.383^{+0.049}_{-0.048}$ ps from the PDG [7].
[9] M. Q. Huang, H. Y. Jin, J. G. Korner, and C. Liu, Phys. Lett. B **629**, 27 (2005). In this reference, the authors calculated $\Gamma(\Lambda_b^0 \to \Lambda_c^+ \ell^- \bar{\nu}_\ell) = 2.12 \times 10^{-11}|V_{cb}|^2$ GeV.
[10] A. K. Leibovich, Z. Ligeti, I. W. Stewart, and M. B. Wise, Phys. Lett. B **586**, 337 (2004). In this reference, the authors calculated $\Gamma(\Lambda_b^0 \to \Lambda_c^+ \pi^-) = 1.52 \times 10^{-12}|V_{cb}|^2$ GeV.
[11] H. Y. Cheng, Phys. Rev. D **56**, 2799 (1997). In this reference, the author calculated $\Gamma(\Lambda_b^0 \to \Lambda_c^+ \pi^-) = 1.41 \times 10^{-12}|V_{cb}|^2$ GeV.
[12] T. Affolder *et al.* (CDF Collaboration), Phys. Rev. Lett. **84**, 1663 (2000).
[13] D. Acosta *et al.* (CDF Collaboration), Phys. Rev. D **71**, 032001 (2005).
[14] The CDF II detector uses a cylindrical coordinate system in which ϕ is the azimuthal angle, r is the radius from the nominal beam line, and z points in the proton beam direction, with the origin at the center of the detector. The transverse $r - \phi$, or x-y plane, is the plane perpendicular to the z axis.
[15] A. Sill *et al.*, Nucl. Instrum. Methods Phys. Res., Sect. A **447**, 1 (2000).
[16] T. Affolder *et al.*, Nucl. Instrum. Methods Phys. Res., Sect. A **526**, 249 (2004).
[17] The pseudorapidity, η, is defined as $-\ln[\tan(\theta/2)]$, where θ is the polar angle to the proton beam.
[18] G. Ascoli *et al.*, Nucl. Instrum. Methods Phys. Res., Sect. A **268**, 33 (1988).
[19] E. J. Thomson *et al.*, IEEE Trans. Nucl. Sci. **49**, 1063 (2002).
[20] B. Ashmanskas *et al.*, Nucl. Instrum. Methods Phys. Res., Sect. A **518**, 532 (2004).
[21] The z position of the beam line at the second trigger level is obtained by averaging the detector z positions of all the tracks found by the silicon vertex trigger. The x and y positions are obtained by fitting the track impact parameter, d, with respect to the detector origin, as a function of the track azimuthal angle, ϕ: $d = -x\sin(\phi) + y\cos(\phi)$. The fitting is done for each event.
[22] G. Gomez-Ceballos *et al.*, Nucl. Instrum. Methods Phys. Res., Sect. A **518**, 522 (2004).
[23] The COT has 48 axial and 48 stereo sense wire layers.
[24] A displaced track found by the SVT has a transverse impact parameter within 120 μm–1000 μm and a transverse momentum greater than 2 GeV/c. The transverse impact parameter is computed at the trigger level using information from the SVX II, while the transverse momentum is computed by combining the information reconstructed in the SVX II and in the COT.
[25] The matching χ^2 has one degree of freedom. It is calculated from the difference between the track and the muon stub positions in the $r - \phi$ plane and the expected amount of multiple scattering for a track of given p_T obtained from the GEANT [26] simulation of CDF detector material.
[26] R. Brun, R. Hagelberg, M. Hansroul, and J. C. Lassalle, CERN Report No. CERN-DD-78-2-REV, 1978 (unpublished).
[27] The smallness of $c\bar{c}$ background is confirmed independently from the cross-check using the signed impact parameter distributions of the c hadrons (Appendix C 2). The uncertainty on the scale factor for the Λ_b^0 semileptonic decay model, C_{model}, is $\approx 2.5\%$ and only affects the relative branching fraction at the same order of magnitude. The uncertainties on the Λ_b^0 lifetime, Λ_b^0 and Λ_c^+ polar-

izations, and Λ_c^+ Dalitz structure are expected to change the numerator and the denominator of the Λ_b^0 relative branching fraction in a similar way and mostly cancel in the ratio. The CDF I $\sigma_{\Lambda_b^0}/\sigma_{\bar{B}^0}$ result already has $\approx 35\%$ uncertainty [12]; the 3% uncertainty from the generator-level MC is relatively insignificant.

[28] T. Sjostrand *et al.*, Comput. Phys. Commun. **135**, 238 (2001).

[29] The BGENERATOR is a CDF program that generates a single *b* hadron according to the input p_T and rapidity spectra.

[30] D. J. Lange, Nucl. Instrum. Methods Phys. Res., Sect. A **462**, 152 (2001).

[31] D. Boutigny *et al.* (BABAR Collaboration), SLAC Report No. SLAC-R-0457, 1995 (unpublished).

[32] K. Abe *et al.* (BELLE Collaboration),Nucl. Instrum. Methods Phys. Res., Sect. A **479**, 117 (2002).

[33] D. Andrews *et al.* (CLEO Collaboration), Nucl. Instrum. Methods **211**, 47 (1983).

[34] H. Albrecht *et al.* (ARGUS Collaboration), Nucl. Instrum. Methods Phys. Res., Sect. A **275**, 1 (1989).

[35] The bin-by-bin ratios are derived by taking the ratio of generator-level $M_{\Lambda_c \mu}$ histograms from the FF and PHSP simulation samples.

[36] D. Acosta *et al.* (CDF Collaboration), Phys. Rev. Lett. **94**, 122001 (2005).

[37] A. Abulencia *et al.* (CDF Collaboration), Phys. Rev. Lett. **98**, 122002 (2007); Y. Le, Ph.D. thesis, Johns Hopkins University, 2003.

[38] S.-S. Yu, Ph.D. thesis, University of Pennsylvania, 2005, arXiv:hep-ex/0504059.

[39] G. Cowan, *Statistical Data Analysis*, (Oxford University Press, New York, 1998) ISBN 0198501552.

[40] D. Acosta *et al.* (CDF Collaboration), Phys. Rev. D **68**, 091101 (2003).

[41] K. W. Edwards *et al.* (CLEO Collaboration), Phys. Rev. Lett. **74**, 3331 (1995).

[42] H. Albrecht *et al.* (ARGUS Collaboration), Phys. Lett. B **402**, 207 (1997).

[43] The uncertainties on the measured branching fractions of *c*-baryon decays are obtained from the PDG [7]. A 5% uncertainty is assigned to the estimated branching fractions of those unmeasured decays. Because the excited *c* baryons decay mainly via the isospin-conserving strong interaction, their branching fractions can be inferred from Clebsch-Gordan coefficients. An example of the deviation from the isospin invariance, in the *c*-meson system, due to additional electromagnetic decay, $D^*(2010)^+ \to D^+ \gamma$, is found to be $\approx 5\%$ of the branching fraction of the $D^*(2010)^+ \to D^+ \pi^0$ decay.

[44] The uncertainties on the branching fractions of $\Lambda_b^0 \to \Lambda_c^+ \pi^-$, $\Lambda_b^0 \to \Lambda_c^+ \mu^- \bar{\nu}_\mu$, $\Lambda_b^0 \to \Lambda_c(2595)^+ \mu^- \bar{\nu}_\mu$, $\Lambda_b^0 \to \Lambda_c(2625)^+ \mu^- \bar{\nu}_\mu$, and $\Lambda_b^0 \to \Sigma_c(2455)\pi\mu^- \bar{\nu}_\mu$ include the uncertainties on the estimated $\mathcal{B}(\Lambda_b^0 \to \Lambda_c^+ \mu^- \bar{\nu}_\mu)$ and the measured ratios of branching fractions. See Sec. VII for more details. A 100% uncertainty is assigned to the branching fractions of $\Lambda_b^0 \to \Lambda_c^+ \tau^- \bar{\nu}_\tau$, $\Lambda_b^0 \to \Lambda_c^+ f_0(980)\mu^- \bar{\nu}_\mu$, $\Lambda_b^0 \to \Lambda_c^+ \pi^+ \pi^- \mu^- \bar{\nu}_\mu$, and $\Lambda_b^0 \to \Lambda_c^+ \pi^0 \pi^0 \mu^- \bar{\nu}_\mu$ decays to cover the large branching fraction uncertainty that arises from the theoretical predictions using various quantum chromodynamics models [45–49].

[45] A. K. Leibovich and I. W. Stewart, Phys. Rev. D **57**, 5620 (1998).

[46] D. Chakraverty, T. De, B. Dutta-Roy, and K. S. Gupta, Mod. Phys. Lett. A **12**, 195 (1997).

[47] H. G. Dosch, E. Ferreira, M. Nielsen, and R. Rosenfeld, Phys. Lett. B **431**, 173 (1998).

[48] F. Cardarelli and S. Simula, Phys. Rev. D **60**, 074018 (1999).

[49] P. Guo, H. W. Ke, X. Q. Li, C. D. Lu, and Y. M. Wang, Phys. Rev. D **75**, 054017 (2007).

[50] The branching fraction of the $\Lambda_b^0 \to \Lambda_c^+ \pi^+ \pi^- \mu^- \bar{\nu}_\mu$ decay was measured to be $5.6 \pm 3.1\%$ by the DELPHI Collaboration [51]. However, given that the uncertainty is large, the branching fraction is not used in this analysis.

[51] J. Abdallah *et al.* (DELPHI Collaboration), Phys. Lett. B **585**, 63 (2004).

[52] The contribution of $b\bar{b}/c\bar{c}$ background may be inferred from Appendix C; it is expected to be tiny and may be ignored. The false-muon background is considered. However, this background occurs at the level of $\approx 4\%$ in both the numerator and denominator and cancels to first order. If the contribution is ignored in the numerator or denominator, a 4% fractional uncertainty is still small compared with the statistical and other systematic uncertainties.

[53] The second uncertainty is conservative since the estimated $\mathcal{B}(\Lambda_b^0 \to \Lambda_c^+ \mu^- \bar{\nu}_\mu)$ is consistent with the result from Ref. [51].

[54] P. Nason, S. Dawson, and R. K. Ellis, Nucl. Phys. **B327**, 49 (1989).

[55] C. Peterson, D. Schlatter, I. Schmitt, and P. M. Zerwas, Phys. Rev. D **27**, 105 (1983).

[56] W. J. Taylor, Ph.D. thesis, University of Toronto, 1999.

[57] Here, the denominator of kinematic acceptance is the number of events in which the *b* hadrons have $p_T > 10$ GeV/*c* [$p_T(H_b) > 10$ GeV/*c*]. The kinematic requirements include requirements on the η, p_T, and transverse energy of electron, p_T of each daughter track of the *c* hadron, significance of the decay length and impact parameter of the *c* hadron, and the four-track invariant mass.

[58] The ratio of Λ_b^0 to $\bar{B}^0$ efficiencies is found to be independent of p_T when the same requirements are made for both *b* hadrons [37]. Therefore, a comparison of the shapes of reconstructed p_T distributions is equivalent to a comparison of the shapes of differential cross sections ($d\sigma/dp_T$).

[59] T. Aaltonen *et al.* (CDF Collaboration), Phys. Rev. D **77**, 072003 (2008).

[60] In Ref. [37], the Λ_c^+ is reconstructed using the three-body decay $\Lambda_c^+ \to pK^- \pi^+$. Therefore, the branching fraction $\mathcal{B}(\Lambda_c^+ \to pK^- \pi^+)$ is required to extract $\frac{\sigma_{\Lambda_b^0}(p_T>6.0)\mathcal{B}(\Lambda_b^0 \to \Lambda_c^+ \pi^-)}{\sigma_{\bar{B}^0}(p_T>6.0)\mathcal{B}(\bar{B}^0 \to D^+ \pi^-)}$.

[61] The PDG calculates $\mathcal{B}(\Lambda_b^0 \to \Lambda_c^+ \pi^-)$ using the ratio of production cross sections $\sigma_{\Lambda_b^0}/\sigma_{\bar{B}^0} = 0.25 \pm 0.04$, with the assumption that the p_T dependence of the Λ_b^0 and $\bar{B}^0$ production is the same. This analysis measures the Λ_b^0 p_T spectrum to be softer (more *b* hadrons at lower p_T) than that of the $\bar{B}^0$ and estimates the $\sigma_{\Lambda_b^0}/\sigma_{\bar{B}^0}$ to be 2.5 times larger than that used by the PDG.

[62] The uncertainties on the fragmentation fraction and the measured *b*-meson branching ratios are obtained from the

PDG [7], while the uncertainties on the unmeasured *b*-meson branching ratios are assumed to be 3 times the uncertainties on the closest equivalent measured decays [37]. The unmeasured branching ratios of Λ_b^0 decays have asymmetric systematic uncertainties of $+100\%$, -50% [37].

[63] D. E. Acosta *et al.* (CDF Collaboration), Phys. Rev. D **71**, 092001 (2005).

[64] D. Michael, Report No. NuMI-NOTE-BEAM-0019, 1994 (unpublished).

[65] E. M. Aitala *et al.* (E791 Collaboration), Phys. Lett. B **471**, 449 (2000).

[66] The PDG uncertainty on the Λ_b^0 relative branching fraction is dominated by the following two sources. The uncertainty from the world average of $\mathcal{B}(\Lambda_c^+ \to pK^-\pi^+)$, which is used in the CDF measurement of $\frac{\sigma_{\Lambda_b^0}(p_T>6.0)\mathcal{B}(\Lambda_b^0 \to \Lambda_c^+ \pi^-)}{\sigma_{B^0}(p_T>6.0)\mathcal{B}(\bar{B}^0 \to D^+\pi^-)}$ [37], is $^{+1.2}_{-2.0}$. The uncertainty from the CDF I measurement of $\sigma_{\Lambda_b^0}/\sigma_{\bar{B}^0}$ is ± 1.9.

[67] I. Dunietz, Phys. Rev. D **58**, 094010 (1998).

[68] P. Migliozzi, G. D'Ambrosio, G. Miele, and P. Santorelli (CHORUS Collaboration), Phys. Lett. B **462**, 217 (1999).

[69] The value 0.21 ± 0.04 is used and $\Gamma(\bar{B}_s^0)/\Gamma(\bar{B}^0)$ is derived assuming $\Gamma(\bar{B}^0) = \Gamma(B^-)$.

[70] Ref. [59] reported $\Gamma(B^-)/\Gamma(\bar{B}^0) = 1.054 \pm 0.018(\text{stat})^{+0.025}_{-0.045}(\text{syst}) \pm 0.058(\mathcal{B})$, which is consistent with unity. Ref. [59] also reported $\Gamma(\bar{B}_s^0)/[\Gamma(B^-) + \Gamma(\bar{B}^0)] = 0.160 \pm 0.005(\text{stat})^{+0.011}_{-0.010}(\text{syst})^{+0.057}_{-0.034}(\mathcal{B})$, which is consistent with 0.21 ± 0.04.

[71] A 5% uncertainty is assigned to the estimated branching fractions of the excited *c*-hadron decays, while a 100% uncertainty is assigned to the unobserved *b*-hadron decays to cover the wide range of theoretical predictions.

[72] Cheng's prediction of $\mathcal{B}(\Lambda_b^0 \to \Lambda_c^+ \pi^-)$ [11] is not included for comparison because he uses a nonrelativistic quark model (instead of HQET). If his prediction is included, this measurement is still consistent with the results from theory.

[73] T. Aaltonen *et al.* (CDF Collaboration), Phys. Rev. Lett. **99**, 202001 (2007).

[74] T. Aaltonen *et al.* (CDF Collaboration), Phys. Rev. Lett. **99**, 052002 (2007).

[75] The Ξ_b contribution could be cross-checked by using the D0 measurement of $\sigma(\Xi_b)\mathcal{B}(\Xi_b^- \to J/\psi\,\Xi^-)/\sigma(\Lambda_b^0)\mathcal{B}(\Lambda_b^0 \to J/\psi\,\Lambda)$. Assuming $\mathcal{B}(\Xi_b^- \to J/\psi\,\Xi^-) = \mathcal{B}(\Lambda_b^0 \to J/\psi\,\Lambda)$, and that the branching fraction and efficiency of $\Xi_b \to \Lambda_c^+ K\mu^- \bar{\nu}_\mu$ are the same as those of $\Lambda_b^0 \to \Sigma_c(2455)\pi\mu^- \bar{\nu}_\mu$, the contribution of Ξ_b is estimated to be $\approx 0.35\%$.

[76] D. Acosta *et al.* (CDF Collaboration), Phys. Rev. Lett. **94**, 091803 (2005).

[77] CDF measured $\sigma_W \times \mathcal{B}(W^+ \to e^+\nu_e) = 2780 \pm 14 \pm 60$ pb [76]. Combining the world averages of $\mathcal{B}(W^+ \to cX)$ and $\mathcal{B}(W^+ \to e^+\nu_e)$, $\sigma_W \times \mathcal{B}(W^+ \to cX)$ is estimated to be 8600 ± 700 pb. Note that the dominant electroweak production of *b* quark from the decay $W^+ \to \bar{b}c$ will be ≈ 500 times smaller ($|V_{cb}|^2$) and $\sigma_W \times \mathcal{B}(W^+ \to \bar{b}c)$ is estimated to be 14 ± 6 pb.

[78] M. L. Mangano, P. Nason, and G. Ridolfi, Nucl. Phys. **B373**, 295 (1992).

[79] F. Halzen, W. Y. Keung, and D. M. Scott, Phys. Rev. D **27**, 1631 (1983).

[80] A. Abulencia *et al.* (CDF Collaboration), Phys. Rev. D **75**, 012010 (2007).

[81] Note that simulations for extracting the $\epsilon_{\Lambda_b^0 \to \Lambda_c^+ \pi^-}$ and the numerator of Eq. (C2) are performed at the generator level. Generator-level simulations are sufficient because this measurement is only sensitive to the ϵ of background relative to the hadronic signal, not the absolute value. The results from a generator-level simulation and from a full simulation differ by only $\approx 3\%$. Finally, the ϵ of the $b\bar{b}/c\bar{c}$ background is quite small compared with those of the feed-in and false-muon backgrounds. A large simulation sample is required to achieve reasonably small uncertainties. The full simulations are time- and CPU-intensive and are therefore not used for the estimate of the $b\bar{b}/c\bar{c}$ background.

[82] The CDF σ_{B^+} measurement [80] is restricted to the B^+ with p_T greater than 6 GeV/*c* and rapidity (*y*) less than 1.0. Therefore, the denominator of the efficiency $\epsilon_{\Lambda_b^0 \to \Lambda_c^+ \pi^-}$ is the number of events in which the Λ_b^0 baryons have $p_T > 6$ GeV/*c* and $|y| < 1.0$.

[83] F. Happacher, P. Giromini, and F. Ptohos, Phys. Rev. D **73**, 014026 (2006). The authors of this reference compare the results of different experiments as listed in Ref. [84] using R_{2b}, the ratio of the measured $\sigma_{b\bar{b}}$ to the exact next-to-leading order prediction. These five measurements yield $\langle R_{2b} \rangle = 1.8$ with a 0.8 root mean square deviation. The most recent Tevatron measurement [85] has also found inconsistency when identifying *b* quarks via secondary vertex versus via their semileptonic decays.

[84] F. Abe *et al.* (CDF Collaboration), Phys. Rev. D **53**, 1051 (1996); **55**, 2546 (1997); B. Abbott *et al.* (D0 Collaboration), Phys. Lett. B **487**, 264 (2000); D. Acosta *et al.* (CDF Collaboration), Phys. Rev. D **69**, 072004 (2004); T. Shears (CDF Collaboration), Proc. Sci., HEP2005 (2006) 072.

[85] T. Aaltonen *et al.* (CDF Collaboration), Phys. Rev. D **77**, 072004 (2008).

[86] D. Acosta *et al.* (CDF Collaboration), Phys. Rev. Lett. **91**, 241804 (2003).